University of Studies of Naples "Federico II"

International PhD on Novel Technologies for Materials, Sensors and Imaging.

XXVI Cycle

Development of radon and thoron concentrations measurement techniques with electrostatic collection

Cristina Mattone

Coordinator

prof. Luciano Lanotte

Supervisors

prof. Vincenzo Roca
dott. Giuseppe Osteria

Anno accademico 2013 - 2014

Contents

Introduction

The present work is focused on the thoron and radon concentration monitoring that has become relevant in many fields during the latest years. In particular the research topic is aimed to study and develop measurement techniques, based on electrostatic collection, in order to measure the activities of radon and thoron, radioactive gases produced in uranium and thorium decays.
It is now widely known that radon inhalation, in particular its progeny, significantly contributes to the public exposure. On the other hand, the presence of thoron (^{220}Rn) indoor was often neglected for its short half-life. Recent studies have shown that high thoron concentrations can be found in some places, like underground environments. Sources of these two isotopes are also widely distributed in our living and working environment; soil and building materials contain meaningful tracks of their sources and their exhalation rates must be determined in order to prevent human health.
Radon concentration measurements, both in air and in gas from the soil are very important. The latest ones are used in order to realize *geogenic maps*. These maps link the gas to the particular geology and lithology of the area, allowing the development of more strict criteria for assessing the risk associated with the presence of radon. The radon monitoring is important also for other essential issues, such as the Earth crust dynamics study. Currently there is no a scientific proof about any correlation with earthquakes, but certainly radon monitoring makes it possible to identify the subsurface changes.
In any field, when the radon and thoron concentration measurements are requested, a good separation of the two isotopes is important. The electrostatic collection of their daughters is the only technique able to reach this purpose. This work is focused on the development of devices based on this technique. It consists mainly of two parts: the first one is about the development of a facility for radon and thoron detectors calibration, the second one concerns RAMONA (RAdon MONitoring and Acquisition) upgrade, a device developed by the Radioactivity Laboratory of "FedericoII" University.
The development of a facility to calibrate radon and thoron detectors is

necessary to measure the detection efficiency for both radon isotopes and thus optimize the detectors performances. For this reason some reference sources, for both the radon isotopes, with different activity concentrations are required. Following the procedures of the National Metrological Institute (ENEA-INMRI), radon sources are realized [38]. There are indeed established methodologies to create atmospheres of known activity of ^{222}Rn, while for thoron samples the same cannot be applied due to the isotope short half life and the methodologies for the realization of these sources are still under investigation. A standard for internal working is developed for thoron. The development of two traceability chains for the realization of independent internal atmospheres of known specific activity and the developed method for reproducing mixed atmosphere are described in the following chapters, in addition to the calibration facility.
RAMONA upgrade arises from the need to work in environments characterized by non-standard environmental conditions. The device allows to perform the radon continuous monitoring from the measurement of the activity of radon daughters, collected via an electrostatic field by a silicon detector. Its peculiarities are worthwhile in soil radon concentration measurements when both radon isotopes are present, indeed through the alpha particles spectrometry the ^{222}Rn and ^{220}Rn separation is allowed. The RAMONA system upgrade concerns three fundamental points. The first one is the development of methods for reduction of hostile gases and humidity, which damage the electronics and the detector. Particular attention must be given to the dehumidifying system. Second and third points of the upgrade program are related to the set-up, testing and tuning of electronic components and of new detectors. The upgrade concerns the materials, which is now insulating and lighter than before, as well as the structure of the chamber. An important point is the hermetic separation between the collection chamber and the electronic board. A new improved chamber performing at the same level than the original one, and solving the problems that would arise from using the original chamber in different and non-standard environmental conditions, has been built. Another topic for the upgraded device is the costs reduction, which lead to the testing of new detectors, the PiN photodiodes, used directly or coupled to small sparkling crystals.
The upgrade in progress will allow to obtain a stable monitoring system in each environmental condition.

Chapter 1

Radon isotopes

Radioactivity is the event in which some unstable nuclei are transform themselves into others through particles emission. The discovery of radioactivity occurred at the end of $1800s$ by Henry Becquerel and Pierre and Marie Curie, who received the Nobel Prize in physics for their researches.
In the last decades, an increasing interest in the radioactivity and in its measurement, due to the reasons linked to the human health, took place. The environmental radioactivity is composed by natural and artificial components. The artificial radioactivity is due to the human activity, in particular it is linked to medical applications and to nuclear power plants. On average, the artificial component is less significant than the natural one, but in some situations it can locally take significant values.
The natural radioactivity has two contributions, the cosmic one and the environmental one; the first component is constituted by cosmic rays, the latter, caused by primordial radionuclides present in the Earth crust materials, is dominated by natural radioactive series generated by ^{235}U, ^{238}U and ^{232}Th. In this context a particular role is played by the radon isotopes.
The natural radioactivity determines most of the average dose[1] received by

[1]The *absorbed dose* D is a physical quantity defined as the amount of absorbed energy (dE) by a sample of matter, as a result of exposure to radiation, per unit mass (dm):

$$D = \frac{dE}{dm} \tag{1.1}$$

In the International System, the absorbed dose is measured in *gray* (Gy).
The *Average Absorbed Dose* in an organ or tissue is defined as:

$$D_T = \frac{1}{m_T} \int D dm \tag{1.2}$$

where m_T is the mass of the organ or tissue, and D is the absorbed dose in the element of mass dm

the world population [1]. This quantity widely depends on region and site, due to the different composition of the soil.

1.1 Radon matter

It is now well known that the radon progeny inhalation significantly contributes to the effective dose of the public. In 1988s, the World Health Organization, WHO, confirmed the dangers from radon, identifying it as a carcinogen of Group I (highest evidence of carcinogenicity).
The presence of thoron (^{220}Rn) indoor was often neglected for its short half-life. Recent studies have shown that high thoron concentrations were found in some areas, like underground environments in which some people work[2]. The sources of these two isotopes are also largely distributed in our living and working environments; indeed building materials and soils contain their precursors and their exhalation rates have to be determined for health prevention.
In addition to the measurements of radon in the air, widespread and important are the radon measurements in the soil. These are used in order to create maps of radon, *radon geogenic maps*, that link the gas to the particular geology and lithology of the area, allow the development of more effective criteria for assessing the risk associated with the presence of radon.
The radon monitoring is important also for another essential aspect: it is an indicator of the earth crust dynamics. In recent decades, many attempts to connect it to earthquakes prediction have been developed. Currently there is no confirmation about that, but, certainly, the correct radon measurement gives a valuable tool for taking information from the deeper Earth crust layers.

1.1.1 Health risk

Radon gas, exhaled into the air, becomes part of the gases mixture we breathe.
The lung is the organ the most sensitive to damage from radon radiation for radon gaseous nature. It is an inert gas with a relatively long half life, for this reason it enters and leaves the lungs with a small probability to decay inside. As previously mentioned, the gas does not directly radiate the lung tissue, but its decay products in the air do. The radon daughters, very reactive, bind to the atmospheric particulate forming voluminous conglomerates that,

once inhaled, attached themselves to external epithelium tissues, covering the respiratory interior. The bulk of the dose is due to the facts that also the radon daughters are alpha emitters. In particular, the not attached fraction of radon decay products enters in the respiratory apparatus and, due to its little size, it reaches the deepest organ parts.
Although the epidemiology of radon is very difficult, on the basis of currently available data the radon is recognized, after the cigarettes smoke, as the second universal cause of the onset of lung cancers (WHO report). The cause-effect hypothesis between radon high concentrations and lung cancer has also sensitized international organizations of radiation protection. This fact led to evaluate and to impose limits to be respected and procedures to follow, depending on the country and on the type of environment, namely underground places, workplaces, housing, etc.
In Italy, in 2000s, the Legislative Decree, $D.Lgs.241$, which integrated the previous Legislative Decree 230/95, introduced the limits to regulate the radon concentration in the potentially dangerous workplace. This Decree implemented the "Directive 96/29 EURATOM in the general public and workers health protection field against the risks of ionizing radiation"; it sets limits only for some work activities and the underground places, pointing for the houses only "attention levels": $200 Bqm^{-3}$ for new constructions and $400 Bqm^{-3}$ for houses already existing[2]. For the control of radon in the water there is a recommendation of the European Commission EURATOM (2001/928/EURATOM), notified in December 2001, which concerns the protection of people against radon exposure in drinking water. With regard to public water supply or trade, it is believed that for radon concentrations above $100 Bq/l$ a corrective action is warranted. Above $100 Bq/l$ concentration, each Member States must define a reference level for radon; it determines whether remedial action is needed to the human health protection.

1.1.2 Radon as geochemical probe

There are numerous processes in the Earth, such as earthquakes and volcanic eruptions. Seismic activity is, together with volcanism, the most evident proof of how our planet is alive.
Earthquakes are generated in the lithosphere, the external part of the earth crust. Continuously soil movements happen with different intensity; these

[2]The unit of measurement for the radioactivity is the *Becquerel*, Bq. $1 Bq$ corresponds to one disintegration per second.
The one used previously is the *Curie*, Ci. It is defined as the present amount of radioactivity in a gram of radium. This unit is larger than the Bq and the relationship between them is: $1 Ci = 37 GBq$.

phenomena are linked to a sudden stored energy release along a surface due to forces acting on it, for long time. If the seism occurs, there are different ways in which it can occur by fracture or by existing faults scrolling; in any case the stresses produce deformations. At the beginning elastic deformation, then it is able to create a breaking of the material in the rocky volume. In active seismic regions, the earthquake can be precede by low intensity foreshocks which indicate variations of strain state. The reasons of these variations can be of tectonic type, due to movement of plates, or, in volcanic regions, they can be due to magma movement caused by gasses pressure that can contribute to fracture the bordering rocks or reactivate old fractures. To these causes must be added the collapse of underground caverns, mines or the occurrence of huge faults.
Although it is not possible a deterministic forecast of an earthquake, there were and there are underway studies to define and prevent, in probabilistic terms, the seismic risk. These studies are based on two research methodologies.
The seismic zoning determines seismic risk areas through high definition maps based on chronology of past events and on reports indicating historical earthquake precursors, useful for create seismic danger papers. In this way it is possible to identify geological and geomorphological parameters, geotechnical properties, that are typical of a specific area. With this method it is possible to identify areas with different severity of foreseeable damages for a fixed intensity earthquake, but it does not define the date neither the exact location of the waiting seismic event.
The forecast based on anomalies is based on the chemical and physical phenomena studies, which have anomalous variations during stages before the seism. The anomalies may be chosen as precursors of an earthquake and predict seism promptly only if they could be confirmed with regularity. This method is still under study in order to minimize both "missed warning", namely when the event happens without parameter variations, both "wrong warning", when the precursor anomalous characteristic is present but without earthquakes [3].
Both research lines have significant limits, in particular the second one tries to reach a forecast model that, in future, would be able to correlate the sismic event with a lot of precursor phenomenons known for some time. Precursor signals of earthquakes are related to the variations study of chemical and physical parameters. Among precursor events the principal waves P analysis and the ratio variation of their velocity with the transverse waves S is very relevant; furthermore the electrical resistivity, the deformations in soils and the concentrations of different gasses, including radon, are very important.
It is well known that the radium concentration is considerably high in the

sedimentary and magmatic rocks. Moreover the areas affected by tectonic activity, where the geogas fluxes such as CH_4, H_20, H_2S and CO_2 have the property to carry with it the radon, show radon concentration increases in the air. For this reason, in the past years there have been a strong interest in the radon as a tool for estimating the seismic risk, such as earthquakes or volcanic activity. Historically the first evidence about the possible correlations between radon concentrations variations and the earthquakes close to the measurement site was shown by the obtained results in the hydrothermal basin of Tashkent, Uzbekistan, in April in 1966 [62]. The analysis of radon concentration in water, in the period between $(1956 - 1969)$, showed a significant radon concentration increase from 1964 until the earthquake in 1966, as we can see in figure 1.1.

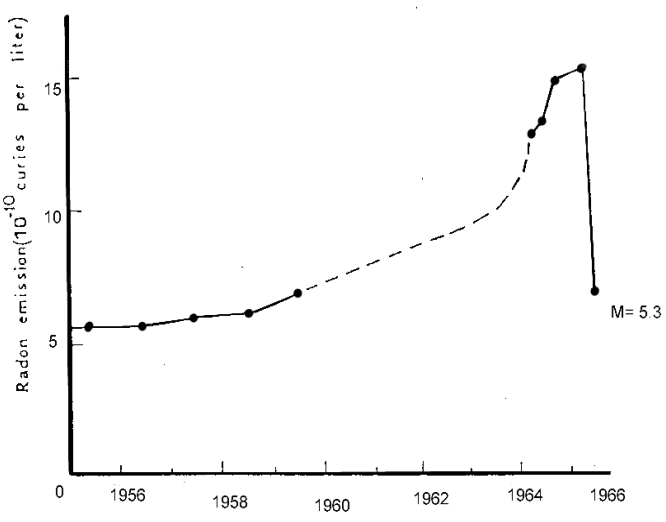

Figure 1.1: Radon concentration variations recorded before the earthquake, with magnitude $M = 5.3$, in Tashkent, 1966 (Ulo Move and Mavashev, 1971).

Using active or passive instruments of detection, many researchers have tried to develop models and theories to explain the large amount of experimental data collected during the time. But the evident and systematic lack of a causal link between the seismic and volcanic phenomena anomalies recorded and radon anomalies led to a gradual abandonment in the radon search field as geoindicator.
Today there is an increasing interest in this gas due to the new instruments that allow to obtain more interesting results. Compared to the past the approach is somewhat different, in fact it is understood that the best way for the study of the radon signal is linked to a good characterization of the site

in question. The site characterization is based on the continuous monitoring analysis of radon in conjunction with other geochemical and geophysical parameters. The parameters analysis is carried out through the simultaneous sampling in multiple sites inside the area that you have to study [**?**].

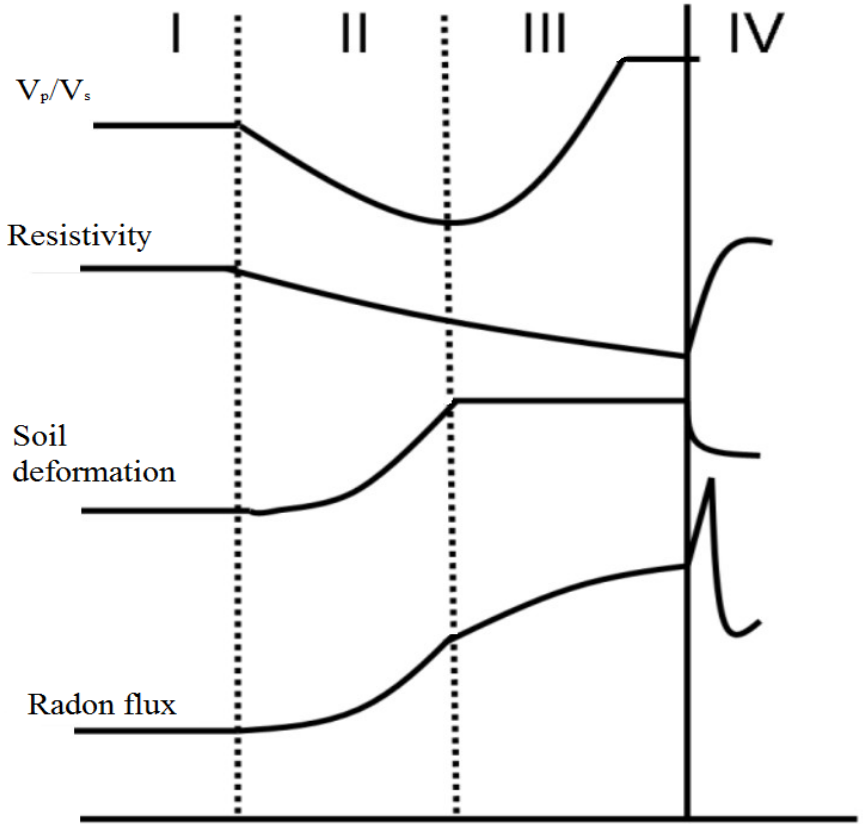

Figure 1.2: Precursory phenomena variations during the earthquake stages according to the dilatancy theory (*Scholz*, 1973).

Dilatancy theory

The correlations between the precursors variations and the earthquake stages are qualitatively explained through the *dilatancy theory* [5]. The goal is to observe some parameters and analyze the variations before and after the seismic or volcanic event in order to determine the relationship cause-effect of these changes in statistically significant way.
This theory belong to a class models based on constitutive properties materials changes inside or outside a fault area [6]. Among these models, the

most famous is the $dilatancy - diffusion\ model$ developed in 1973; it gives a qualitative explanation of precursor phenomena variations during the previous stages of the seismic events. The hypothesized scheme is subdivided in four phases in order to explain the stress effect on a rocky volume. Such model tries to define plausibility limits for a schematization but it is not scientifically valid for its lack of analytical basis.
In the time the effort on the rocks causes a series of microcracks and empty spaces (I stage); the microfractures contribute to the volume increase, dilatancy, and permeability increase (II stage); the empty spaces can be gradually filled by water and this reduces the cohesive forces between the rocks (III stage) until the stage of breaking, in which the stored energy is released, is reached (IV stage). The dilatancy therefore tends to delay the onset of the earthquake by increasing the rock elasticity. During the dilatancy phenomenon, which can last from several hours to several days, some measurable physical parameters, such as the electrical resistivity and the aquifer height and the radon emission or hydrogen gas can change. In figure 1.2, the precursor parameters expected changes, according to this theory, are represented.
The ratio between the primary and secondary waves velocity, v_p/v_s, is one of the most important observed parameters. These velocities are given by:

$$v_p = \frac{\sqrt{4/3 \cdot (\mu + \kappa)}}{\rho} \qquad v_s = \sqrt{\frac{\mu}{\rho}} \tag{1.3}$$

where $\rho(kg/m^3)$ is the material density, $\mu(N/m^2)$ is the rigidity and $\kappa(N/m^2)$ is the inverse of the compressibility coefficient. The ratio v_p/v_s is constant and equal to $\sqrt{3}$ in the cohesive and non-fractured rocks. The transverse waves are attenuated in the little hard materials, until they disappear in fluids where $\mu = 0$. Usually in a earthquakes, the waves velocities ratio decreases during the second earthquake stage, for the empty spaces formation: v_p decreases while v_s is constant. In the third phase v_p/v_s increases due to the sudden decreasing of v_s, caused by liquid in the fractures.
The electrical resistivity variation, φ is characterized by a slow but continuous decreasing before the earthquake. This behavior is probably due to the underground waters, rich of minerals, that fill the rock empty spaces.
The soil deformation, namely the soil level rise that usually precedes the seismic event, is due to the development of microfractures during the second stage.
The radon concentration grows before the earthquake and this is probably due to rock breaking; in this way the gas, at beginning trapped, is free and then spreads up to the surface. In reality, there are many parameters that affect the radon concentration in the soil gas: radium concentration, ma-

terials emanation, weather conditions and permeability porosity of the soil. Therefore to evaluate any anomaly in radon concentration, the site has to be well known. This requires long monitoring periods of radon and many other parameters, as well as a multiparametric study of all available data.

1.2 Radon isotopes properties

Except ^{40}K, the natural radionuclides belong to one of the three radioactive series known as uranium, thorium and actinium series. The respective progenitors are ^{238}U, ^{232}Th and ^{235}U. Uranium and thorium are present in the Earth crust with variable concentrations, conditioned by the rock type. From a research made on national scale, it is known that there are high uranium concentrations in volcanic tuffs and laves in Lazio and Campania, Italy regions [7].
The radon is a radioactive inert gas of natural origin. There are three natural radon isotopes: ^{222}Rn (radon), ^{220}Rn (thoron) and ^{219}Rn (actinon). The radon and thoron, the most abundant, are interesting from the point of view of radiation protection. In this work of thesis, we take in account only radon and thoron, with which are respectively indicate the two corresponding radon isotopes.
About the actinon, its half time is about $4sec$ and it comes from ^{235}U radioactive series, whose abundance is approximately 0.7% of the ^{238}U series. The principal decay scheme of this radioactive series and the radioactive elements are showed in figure 1.3 and in table 1.1.

1.2.1 Radon (^{222}Rn)

Radon, ^{222}Rn, was discovered by Dorn in 1901 in the radioactive series of ^{238}U. The term "radon" was introduced for the first time from Schimt in 1918, during the early studies of radioactivity, to indicate the element with atomic mass 222, associated to uranium-238, while William Ramsay was among the first to study the biological effects of radioactive gas radon.
Uranium is present in various concentrations in the Earth's crust and for this reason also the radon is practically everywhere in the ground. This radioactive gas is generated continuously by some rocks in the earth's crust, in some building materials and in particular by lave and plutonites, tuff, pozzolans, etc.
In figure 1.4 and in table 1.2, the sequence of the decay of the ^{238}U, nuclide more abundant in nature and responsible for most production of the radon, present in the air and in soil gas is illustrated.

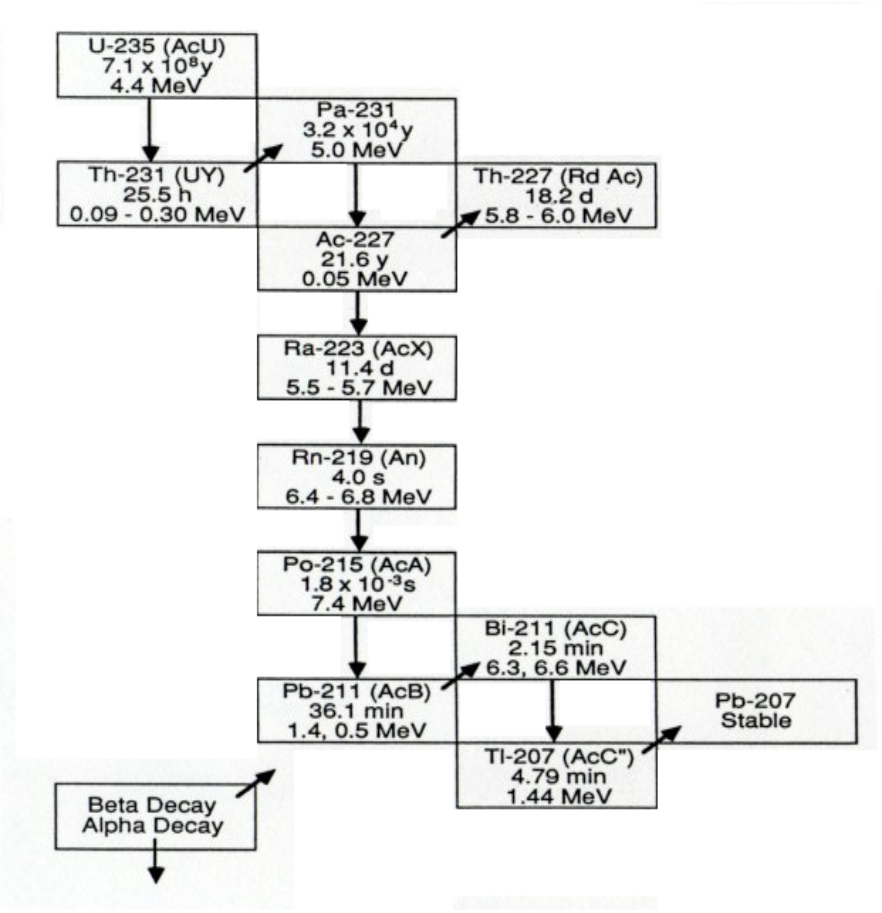

Figure 1.3: Principal decay scheme of ^{235}U

Nuclide	Decay type	half time	Energy (MeV)
${}_{95}U^{235}$	α	$7.10 * 10^8$ y	4.58
${}_{90}Th^{231}$	β	24.6 h	0.30
${}_{91}Pa^{231}$	α	$3.43 * 10^4$ y	5.042
${}_{89}Ac^{227}$	α	22.0 y	4.94
	β	22.0 y	0.04
${}_{92}Th^{227}$	α	18.6 d	6.05
${}_{87}Fr^{223}$	β	21 m	1.2
${}_{88}Ra^{223}$	α	11.2 d	5.75
${}_{86}Rn^{219}$	α	3.92 s	6.824
${}_{84}Po^{215}$	α,β	$1.83 * 10^{-1}$ s	7.365
${}_{82}Pb^{211}$	β	36.1 m	1.39
${}_{85}At^{215}$	α	10^{-4} s	8.00
${}_{83}Bi^{211}$	α,β	2.16 m	6.621
${}_{84}Po^{211}$	α	0.52 s	7.434
${}_{81}Tl^{207}$	β	4.79 m	1.44
${}_{82}Pb^{207}$	stable	–	–

Table 1.1: Actinium series

Radon is produced, for emission of an alpha particle, by ${}^{226}Ra$ whose time half-life is 1602 years. It decays via alpha with half-life of $3,82$ days. ${}^{222}Rn$ is the radon isotope with the longest half-time, long enough that most of the gas, formed in construction materials or within one meter of soil, can reach the external environment. Three radon daughters, as we can see in figure 1.4, are alpha emitters: ${}^{218}Po$ ($E_\alpha \approx 6MeV$), ${}^{214}Po$ ($E_\alpha \approx 7,7MeV$) and ${}^{210}Po$ ($E_\alpha \approx 5,3MeV$) that decays in stable ${}^{206}Pb$. The main features of the radon decay products are listed in the table 1.3.

From a chemical point of view, radon is a noble gas, colorless, odorless and chemically inert. From the physical point of view, it appears to be the noble gas heavier, with the boiling point, melting point, critical temperature and critical pressure the highest among all gasses.
Radon properties are summarized in table 1.4, while the table 1.5 shows the coefficients of solubility in water at atmospheric pressure as a function of temperature changes.

As noble gas, once it is created in material with radium, a radon atom is relatively free to move. Once in the pore space, macroscopic transport of

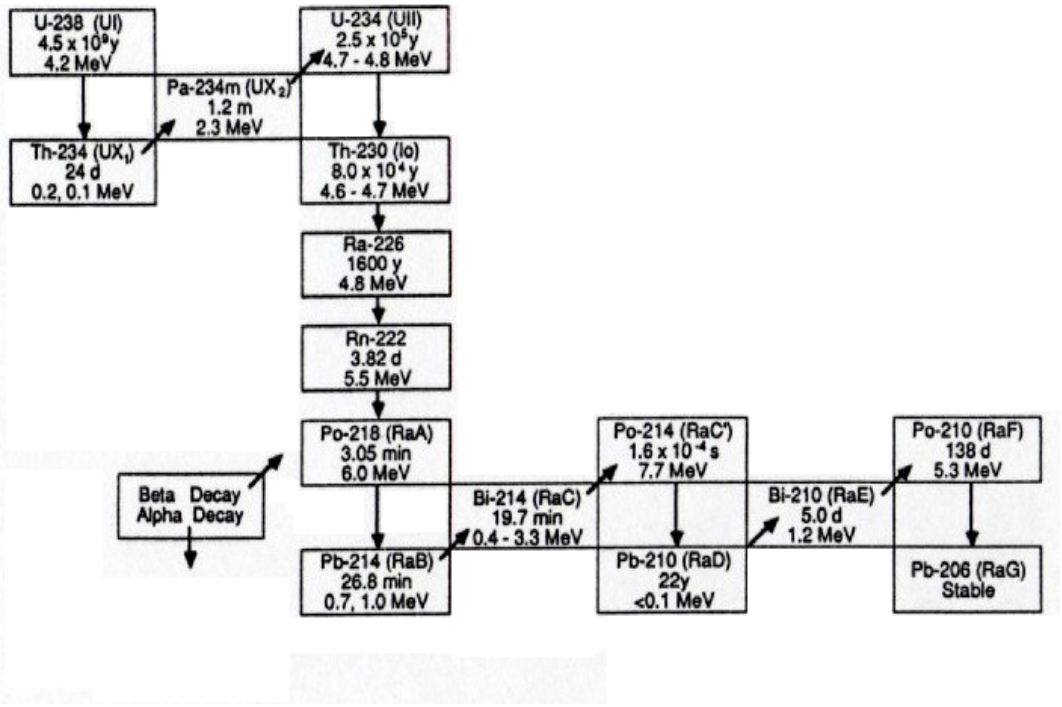

Figure 1.4: Decay chain of ^{238}U

Nuclide	Decay type	half time	Energy (MeV)
${}_{92}U^{238}$	α	$4.50 * 10^9$ y	4.20
${}_{90}Th^{234}$	β	24.1 d	0.20
${}_{91}Pa^{234}$	β	1.18 m	2.32
${}_{91}Pa^{234}$	β	6.7 h	1.2
${}_{92}U^{234}$	α	$2.50 * 10^5$ y	4.763
${}_{90}Th^{230}$	α	$8.0 * 10^4$ y	4.68
${}_{88}Ra^{226}$	α	1602 y	4.777
${}_{86}Rn^{222}$	α	3.82 d	5.486
${}_{84}Po^{218}$	α,β	3.05 m	$\alpha : 6.003$
${}_{82}Pb^{214}$	β	26.8 m	0.7
${}_{85}At^{218}$	α	$1.5 - 2.0$ s	6.63
${}_{83}Bi^{214}$	α	19.7 m	5.51
	β	19.7 m	3.17
${}_{84}Po^{214}$	α	$1.64 * 10^{-4}$ s	7.68
${}_{82}Tl^{210}$	β	1.32 m	1.9
${}_{82}Pb^{210}$	β	22 y	0.018
${}_{83}Bi^{210}$	β	5.0 d	1.17
${}_{84}Po^{210}$	α	138.3 d	5.30
${}_{84}Tl^{206}$	β	42 m	1.51
${}_{82}Pb^{206}$	stable	–	–

Table 1.2: Uranium series

Nuclide	Decay type	half time	Decay constant (h^{-1})	Energy (MeV)	Brancing (%)
^{222}Rn	α	3.82 d	0.0076	5.4897	
^{218}Po	α	3.05 m	13.6	6.0026	
^{214}Pb	β	26.8 m	1.54	0.67,0.73	
	γ			0.35192	38.9
				0.29522	19.7
				0.24192	9.0
^{214}Bi	β	19.7 m	2.10	1.54,3.27,1.51	
	γ			0.60932	43.3
				1.7645	17.0
				1.12028	15.7
				1.2381	5.94
				1.3778	5.00
				0.7684	5.04
				2.2042	4.98
^{214}Po	α	$1.64 * 10^{-4}$ s	$1.52 * 10^{7}$	7.6871	
^{210}Pb	β	22.3 y	$3.5 * 10^{-6}$	0.018,0.061	
^{210}Bi	β	5.01 d	$8.3 * 10^{-3}$	1.161	
^{210}Po	α	22.3 y	$3.01 * 10^{-4}$	5.305	

Table 1.3: Main radiations emitted by radon and its decay products.

Atomic number	86
Density at $1atm$ pressure and 0^oC	$9,73gL^{-1}$
Boiling point at $1atm$ pressure	-62^oC
Density of liquid at normal boiling point	$4,4gcm^{-3}$
Diffusion coefficient in air	$0,1cm^2s^{-1}$
Diffusion coefficient in water	$10^{-5}cm^2s^{-1}$
Viscosity at $1atm$ pressure and 20^oC	$0,229poise$
Solubility in water at $1atm$ pressure and 20^oC	$230cm^3kg^{-1}$

Table 1.4: Radon properties

Temperature	Solubility coefficient
0^oC	$0,57$
20^oC	$0,250$
37^oC	$0,167$
100^oC	$0,106$

Table 1.5: Solubility coefficient in water. The solubility coefficient is the ratio of radon concentrations between gas phase and liquid phase.

radon is possible, either by molecular diffusion or by flow of the fluid in the pore space [8]. The solubility in water is very important because the radon is partially soluble in it, so once released from the soil, some part mixes air and the other is transported through groundwater faults at great distances from the point of production.
The gas transport mechanisms from the soil will be discussed in detail in the next section.

1.2.2 Thoron (^{220}Rn)

The other important radioactive radon isotope, ^{220}Rn, also known as thoron, is created by the decay of ^{224}Ra, member of the ^{232}Th series. The series of ^{232}Th decay, listed in table 1.6, was discovered by Rutherford and Owens in 1889. It has approximately the same (activity) concentration in the Earth's crust as the ^{238}U series, about $25Bq/kg$ [8].
It has a very short half-life, $55,6sec$; as the figure 1.5 shows, it produces alpha radiation. Before decaying into stable ^{208}Pb, thoron generates three alpha emitters: ^{216}Po ($E_\alpha \approx 6,8MeV$), ^{212}Bi ($E_\alpha \approx 6,1MeV$) and ^{212}Po ($E_\alpha \approx 8,8MeV$).

Thoron has a half-time much smaller than radon, so the spread at greater distances both in the process of exhalation from the materials both in the diffusion in the air and water is dominated by radon. For this reason, the ^{222}Rn is the isotope with the higher concentration and contributes largely to the radon dose. Thoron contributes to the mean dose only for about 8%. Nevertheless, in particular environments, as mines and cellars, the concentrations of both radon isotopes are comparable and so in this case also thoron is a source of risk for the human health.
The half-lives ratio between ^{220}Rn and ^{222}Rn yields 1/77 as diffusion length ratio. Because the activity concentration in soil is similar for ^{232}Th and ^{238}U

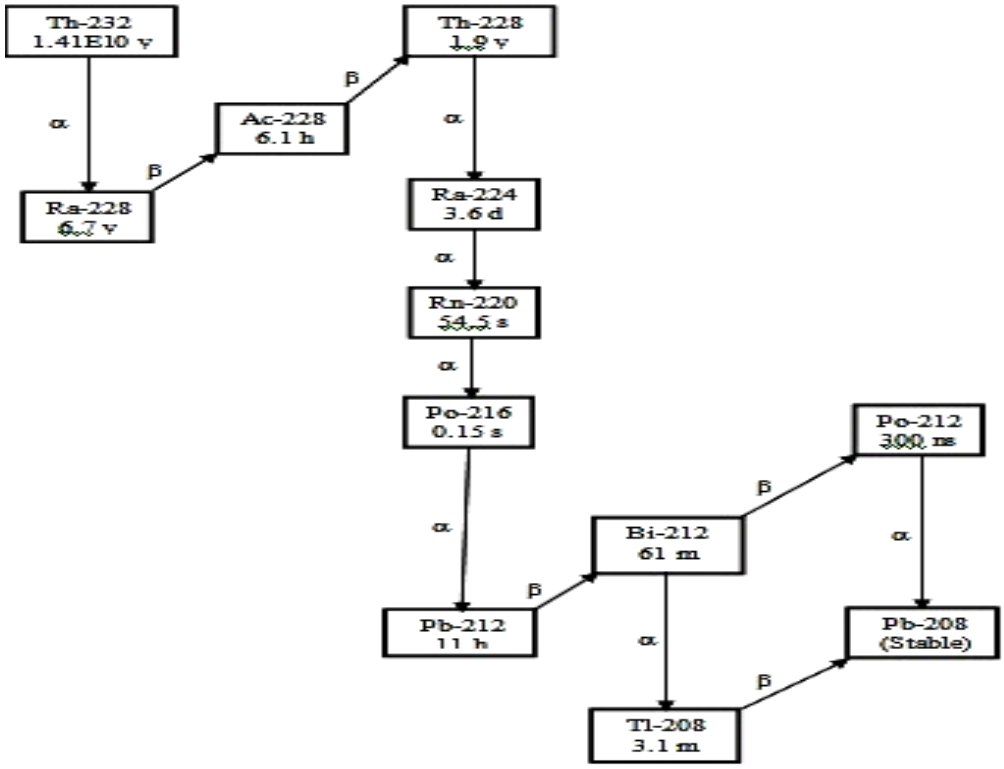

Figure 1.5: Decay chain of ^{232}Th

Nuclide	Decay type	half time	Energy (MeV)
${}_{90}Th^{232}$	α	$1.39 * 10^{10}$ y	3.98
${}_{88}Ra^{228}$	β	6.7 y	0.04
${}_{89}Ac^{228}$	β	6.13 h	2.18
${}_{90}Th^{228}$	α	1.90 d	5.423
${}_{88}Ra^{224}$	α	3.64 d	5.681
${}_{86}Rn^{220}$	α	54.5 s	6.282
${}_{84}Po^{216}$	α,β	0.16 s	6.774
${}_{82}Pb^{212}$	β	$3 * 10^{-4}$ s	0.58
${}_{85}At^{216}$	α	$3 * 10^{-4}$ s	7.79
${}_{85}Bi^{212}$	α	47 m	6.086
	β		2.25
${}_{84}Po^{212}$	α	$3.0 * 10^{-7}$ s	8.776
${}_{84}Tl^{208}$	β	2.1 m	7.79
${}_{82}Pb^{208}$	stable	–	–

Table 1.6: Thorium series

series, the activity rate from soil surface, given by the diffusion length ratio divided by half-lives ratio, yields a factor ≈ 77; in other words much more thoron activity is expected to escape than radon one. On the other hand, if the transport mechanism is due to pressure-driven air flow through the source material or into the open air, the activity rate from the surface is the same for the two isotopes.
Although the only isotope that can be traced back to the deep zones of the terrestrial crust is the radon, the study of thoron is very important for the characterization of measurement sites. Whit this measurement it is possible to discriminate changes of the gas emanation occurred in surface areas from the ones occurred in the deep zones of the terrestrial crust. Due to the different mean life of the isotopes, a emission variation of both gases can be registered only if it is originated in surface areas , while only changes in radon are connect to deep zones, from which only radon comes out.

1.3 Gas transport: soil physical characteristics

The first studies about the gas migrations in soil started in the 30s, driven by the interest for the oil exploration. In the 60s, the research increase in uranium field entailed studies on gas behavior into lithosphere, especially about the radon because linked to the uranium sources. The first physical models about the gases transport were developed for geothermal exploration, uranium studies and environmental radioprotection [9].
All the rocks, at ordinary pressure, contain some empty interstices, sometimes linked between them, through which the gas can migrate. The gas migration is strictly linked to the source existence and to the presence of gas escape route from the lithosphere deeper stages to the surface, such as faults, fractures series, high permeability, etc. The features of gas production areas are function of temperature, pressure, mechanical stress, precipitation and chemical reactions. So many parameters have to be taken into account to develop gas migration models.
In order to create the models must be analysed the soil physical characteristics, like grain size, porosity, permeability, etc.. The soil are classified according to the solid grains size; the major divisions are clay, silt and sand, as shown in table 1.7.

Type	Grain size (μm)	Porosity	Permeability (cm/s)	Field capacity, saturation (%)
Sand	$60 - 2000$	0.4	$10^{-2} - 10^{-4}$	15
Silt	$2 - 60$	0.5	$10^{-4} - 10^{-5}$	58
Clay	$<$	0.6	$\leq 10^{-6}$	68

Table 1.7: Physical characteristics of soil.

Grains larger than sand, up to $15mm$ in diameter, are classified as gravel. Clays are formed by chemical processes, while the larger particles by mechanical weathering.
The field capacity refers to the water volume fraction in soil after it has been wetted and drained for about two days. It can be expressed in terms of the saturation percent, determined with respect to the pore volume; this parameter increases with decreasing particle size.
The porosity is conditioned by the grains size and shapes and it can be divided in primary and secondary porosity; the first one is originates from the sediment and is then linked to the way in which the pore is created, the second

one is determined by factors which occur subsequently as recrystallization, fracturing, etc.. The media porosity (ϕ) is defined as the ratio between the empty spaces volume, V_d, and the media total volume, $V_d + V_s$, where V_s is the full spaces volume.

$$\phi = \frac{V_d}{V_d + V_s} \tag{1.4}$$

The gas volume inside the rock depends on its porosity, while the motion in the media interstices is proportional to the rock permeability.
The permeability is the soil property to be crossed by a fluid. It depends on the medium nature, on the fluid and on the environmental parameters. The medium nature influences the permeability for the pores size and their continuity. The intrinsic permeability K_i $(mdarcy)$[3] is a ease measure of fluid motion through the empty interstices of the solid matrix under a pressure gradient. It is derived from the Darcy law,

$$\nabla P = -\eta \frac{v}{K_i} \tag{1.5}$$

that describes the fluid motion in a porous medium, with mean velocity v, proportional to pressure gradient applied to the interstice extremity and inversely proportional to the medium viscosity. K varies in a range between $10^{-5}$and 10^{-8} [10]. K_i is connected to the total permeability through the relationship:

$$K = K_i \frac{\rho g}{\eta} \tag{1.6}$$

where ρ is medium density (kg/m^3), g is the gravity acceleration and η is the viscosity (Ns/m^2). In general the intrinsic permeability depends on the medium structure, the fractures type, the dimension, the percentage and continuity of the pores. For this reason, it is a constant dependent only by the medium structure and it is independent from the fluid nature. In a given medium, the permeability to the water and to the gas is the same.
In case of a biphasic system, liquid and gas, the gas permeability decreases when the water content increases, because the available space for the gas infiltration is reduced due to incompressibility of water than of gas one [11]. The importance of the pore size or of the fractures appears clear if we consider the Poiseuille law, namely the analogy between the gas in the pore and the

[3]The *darcy*, $1darcy = 9.87 * 10^{-13} m^2$, is the permeability measurement units. It is defined as the medium permeability in which the flow rate of a liquid with a dynamic viscosity equal to $1g * cm^{-1} * s^{-1}$ in normal direction to a straight section of a $1cm^2$ is $1cm^3 * s^{-1}$, under a pressure gradient equal to $1atm * cm^{-1}$

fluid through a capillary tube. Considering the resulting flux from every interconnected pores as a stationary flow of a viscous fluid across a circular tube with radius r, then the flow rate Q is given by:

$$Q = \frac{\pi r^4 (p_0 - p_1)}{8\eta l} \tag{1.7}$$

where p_0 and p_1 are the pressures at the start and at the end of the tube, l is the tube length and η is the fluid viscosity. The gas volume that flows in the pore in time unit is proportional to the radius fourth power [12]. The secondary permeability is determined by the faults and fractures presences, that are the fluid transport preferential routes. This fact entails a speed increase of the fluid.
Very important is also the water content in soil due to its high stopping power.

1.4 Radon emanation

The radon produced by radium alpha decay has a different concentrations inside the earth crust. However only a fraction of the radon generated in soil leaves the solid grains and enters the pore volume of the soil. This fraction, called the "$emanation\ coefficient$", e, is given by the ratio between the emanated radon activity in the air present in the free interstices of material and the total activity produced by radium decay in the material.
While the radium, both ^{226}Ra both ^{224}Ra, is bonded to the crystal lattice, the radon isotopes are free to move and migrate outside the solid due to their gaseous nature. There are two phenomena that influence the probability to exit from grain up to reach free interstices: the gas diffusion in solids and the recoil process. The gases diffusion coefficient in solid grains is very low, therefore we can say that the phenomenon is only controlled by radon atoms recoil after the alpha particle emission. The kinetic energy of ^{222}Rn and ^{220}Rn, after the decay, are respectively $86KeV$ and $103KeV$. The traveled average distances from the radon nuclei vary in the range of $(20 \div 70)nm$; in table 1.8, the radon recoil mean ranges in some materials is reported. It follows that only the gas atoms originated at a distance lower than $70nm$, can exit from the grain [13].

In figure 1.6 the different ways in which radon atom can be generated in the grain surface are shown. It can be trapped in the surface area (A), it can penetrate in an adjacent grain (B), it can stop in the interstice (C) or it can cross the interstitial space without energy loss and enter in another grain surface area (D). The case (C) is called *direct collection*, while in the

Material	Recoil average range
SiO_2	$26nm$
H_2O	$100nm$
Air	$63\mu m$
$Rocks$	$(20-70)nm$

Table 1.8: Recoil average range of ^{222}Rn nucleus with kinetic energy equal to $86KeV$ in different materials.

cases (B) and (D), being in the grain surface regions, the atom can again spread outside the grain; this last process is called *indirect collection*. A radon atom can also leave the grain easily for diffusion through the material [14].
The emanation coefficient gives the possibility to analyze some material characteristics such as pore internal surface, fractures and the soil gas fluxes.

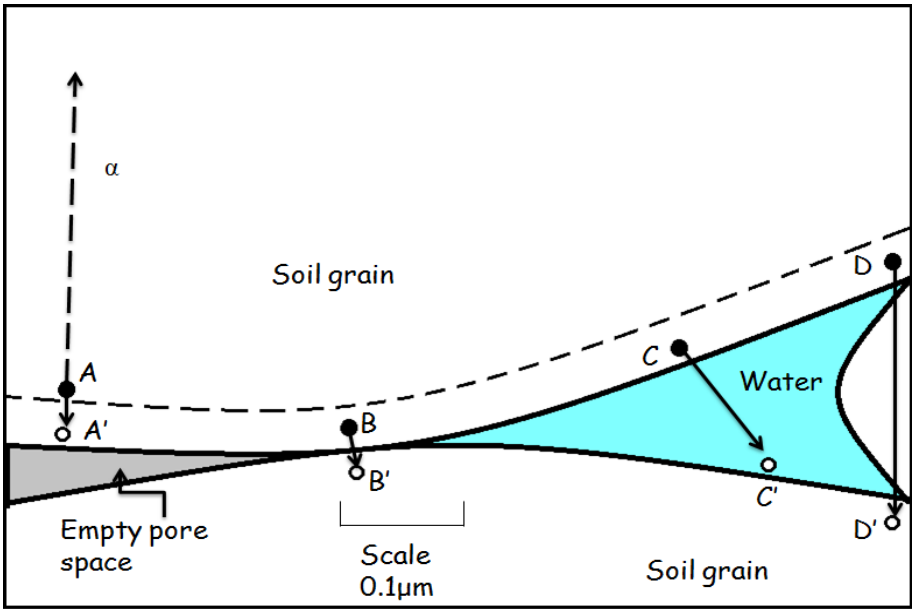

Figure 1.6: Scheme of the different ways in which it can be a radon atom generated in the grain surface. The grains size is about $2\mu m$; the dashed line describes the recoil range of radon, the black circles represent the radium atoms and the clear circles the radon atoms.

1.4.1 Parameters affecting the emanation

The emanation coefficient depends both on the material intrinsic features, like the radium distribution in the pores, the nature and the size of the grains and the porosity, both on the physical conditions, in particular on the temperature, on the pressure and on the water content in the pore. Due to these many parameters, the emanation coefficient value can vary in significant way also in the same material, as we can observe in the table 1.9 [8].

Material	Emanation coefficient
$Reinforced\ cement$	$0.1 - 0.4$
$Gypsum$	$0.02 - 0.10$
$Bricks$	$0.03 - 0.20$
$Cement$	$0.02 - 0.05$
$Sand$	$0.06 - 0.36$
$Uraniumore$	$0.06 - 0.55$

Table 1.9: Emanation coefficient of ^{222}Rn in some materials.

The temperature influences the emanation power in minimal part. Some studies in granite samples, with humidity about 30%, showed an increase of about 20% only in correspondence of temperature variations from -20^oC to 265^oC [15].
Contrarily, the emanation has a big dependence from the humidity variations, namely from the water content in the material. The reason of this behavior is due to the fact that the recoiled radon atoms reduce their speed more in water than in air because of the different viscosity. The particles path inside the pores, at least partially filled with water, is lower than the path in dry air. An atom, that after the recoil enters in a water filled pore, has an high probability to be trapped inside and so moved outside the grain, increasing the emanation phenomenon. When the air is in the grain interstices, the most part of radon atoms does not stop there and enters in another grain, reducing in this way the radon emanation fraction. Up to humidity values of about 10%, the emanation coefficient value can become four times larger than in the dry materials [16]. Over this humidity value, the material emanation speed decreases because the diffusion coefficient is low in a material saturated with water. The emanation coefficient behavior as a function of the variations humidity is shown in figure1.7.

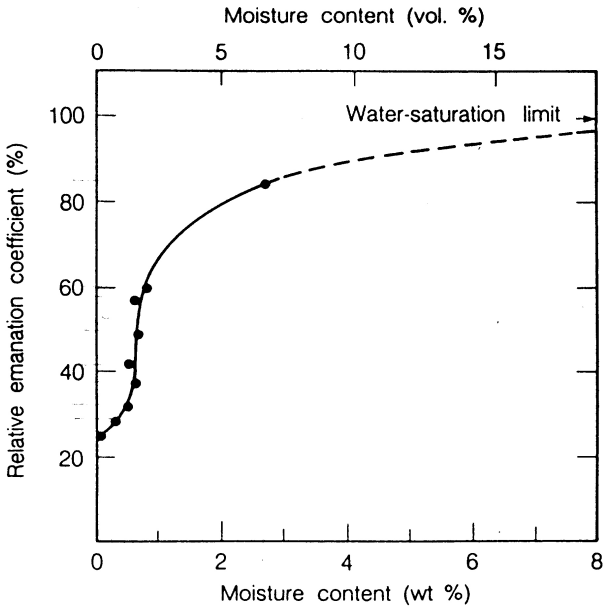

Figure 1.7: Emanation coefficient variations of the material versus the humidity (Morawska,1991).

1.4.2 Radon transport through the pores

After its production, the radon isotopes can leave the solid matrix for molecular diffusion or for convection and then they can reach the atmosphere. Generally, the mechanisms that regulate the gas movements depend on the gas quantity in a fixed volume and on its chemical reactivity. The gas relocation is due to the pressure gradient and to the concentration gradient. If a concentration gradient is present, the gas molecules tend to move to equalize the concentration throughout the rock. This diffusion phenomenon is regulated by the *Fick law*:

$$\vec{J_d} = -D \cdot \vec{\nabla} C \tag{1.8}$$

where D (m^2/s) is the diffusion coefficient, C is the gas (radon) concentration per volume unit (Bq/m^3) and J_d is the flux density in $Bq/m^2 s$. From the equation, it is obvious that the flux is directly proportional to the concentration gradient, through the diffusion concentration that changes with temperature, pressure and material type [8].
Generally the diffusion in the pores happens in air or water, so it is important to consider two diffusion coefficients, D_{air} and D_w. In particular the different diffusion processes, associated to diffusion coefficient D_i, are three

[17]:

- the gas "molecular" diffusion (D_m) in a fluid;
- the gas "interstitial" diffusion in a medium;
- the gas "global" diffusion in a medium.

The gas "molecular" diffusion considers only the interaction between the gas and the crossed fluid, the interstitial one is defined by the effective diffusion coefficient (D_e) through the relation: $D_e = \phi D_m$, where ϕ is the medium porosity. D_e describes the diffusion considering the gas molecular motion across the porous structure. The global diffusion is given by the apparent diffusion coefficient (D), which includes porosity and deviousness effects of the material. In the soils, D is defined as:

$$D = \phi D_e = \phi^2 D_m = \frac{\phi}{\tau} D_m \tag{1.9}$$

where the medium deviousness τ is the percentage of the straight compared to curvilinear. This equation implies that $D_m > D_e > D$. The diffusion coefficients for the different gases are shown in the table 1.10.

Gas	$D_m(25^oC)$ (cm^2/s)	$D_w(25^oC)$ (cm^2/s)	D_e (cm^2/s)	D (cm^2/s)
Rn	0.12	$1.37 * 10^{-5}$	$0.03 - 0.05$	0.007
CO_2	0.15	$1.95 * 10^{-5}$	$0.02 - 0.03$	0.007
He	0.70	$2.12 * 10^{-5}$		

Table 1.10: Values of the diffusion coefficients for the different gases at temperature equal to 25^oC.

The diffusion is not the only parameter for the radon motion, if it were that radon could travel a distance equal to $Z_d = (Dt)^{1/2}$ in a fixed time t. In particular, for the radon diffusion in the water, it could cross $1cm$ in one day, $6cm$ in one month, $21cm$ in one year and so on [18]. The radon concentration for a diffusion process in a isotropic medium, obtained by the Fick law, is given by:

$$C_x = C_o e^{-x/L} \tag{1.10}$$

where C_o is the gas concentration in the source, C_x is the radon concentration at distance x from the source, L is the radon diffusion length, expressed

in centimeters and defined as: $L = (D/\lambda)^{1/2}$. The equation implies that only the 3% of radon exceeds a distance of $3L$ from the source and this fact shows that the diffusive factor to the radon motion can be neglected for large distances [19].
In addition to diffusion, it is important to take into account the pressure gradient contribution. In this case, for a radioactive gas, the flux is given by *Darcy law*:

$$\vec{J_a} = \vec{v}C \tag{1.11}$$

where v (m/s) is the gas velocity. It is linked to the pressure gradient ∇p, to the medium permeability coefficient K and to the viscosity η by the formula (only for the laminar flows[4]):

$$v = \frac{-K \cdot \nabla p}{\eta}. \tag{1.13}$$

The gas total flux is given by the sum of the diffusion contribution and the convection one:

$$\vec{J} = -D\vec{\nabla}C + \vec{v}C \tag{1.14}$$

The gas transport is studied along the vertical direction, with z axis orthogonal to the earth surface and pointed downwards. It is fundamental to take into account the radon decay and the radon continuous production due to the radium, aside from the contributions already analyzed. Considering the continuity equation corrected for this affect, we obtain:

$$\vec{\nabla} \cdot \vec{J} - \lambda_{Rn}C_{Rn} + \lambda_{Ra}C_{Ra} = \frac{\delta C_{Rn}}{\delta t} \tag{1.15}$$

where λ_{Rn}, C_{Rn}, λ_{Ra} and C_{Ra} are respectively the radon and radium decay constants and concentrations.
From the equations (1.14) and (1.15), we get the equation:

$$\frac{\delta C_{Rn}}{\delta t} = D\frac{\delta^2 C_{Rn}}{\delta z^2} + v\frac{\delta C_{Rn}}{\delta z} - \lambda_{Rn}C_{Rn} + \lambda_{Ra}C_{Ra} \tag{1.16}$$

[4]A flux is laminar if the Rynolds number R is:

$$R = d \cdot v \cdot \rho/\eta \leq 4 \tag{1.12}$$

where v is the velocity in the porous material, ρ is the medium density, η is the fluid viscosity and d are the transverse dimensions of the material [6].

Furthermore if a source placed under a layer h without radon in stationary case is considered, it becomes a function of depth only:

$$\frac{d^2C_{Rn}}{dz^2} + \frac{v}{D}\frac{dC_{Rn}}{dz} - \frac{\lambda_{Rn}C_{Rn}}{D} = 0 \tag{1.17}$$

where D, z and v are the diffusion coefficient, the depth and the flux velocity. This equation describes the radon transport in the soil layer above the source in the stationary case, and its solution is:

$$C(z) = C_o \exp[v \cdot (h-z)/2D] \frac{\sinh[(\sqrt{(\frac{v}{2D})^2 + \frac{\lambda}{D}}) \cdot z]}{\sinh[(\sqrt{(\frac{v}{2D})^2 + \frac{\lambda}{D}}) \cdot h]} \tag{1.18}$$

where C_o is the radon concentration at the source. Considering a constant diffusion and an homogeneously radioactive soil, this solution becomes:

$$C(z) = C_o[1 - \exp(-z\sqrt{\lambda/D})] \tag{1.19}$$

There are some changes of the boundary conditions, such as seismic events, that can affect the source concentration C_o and/or the velocity v. For this reason, we must always keep in mind that when these changes take place, they influence the more concentration at shallow depths. In fact, as shown in figure 1.8, the velocity variation, defined as λD, in the case $h = 20m$ and $D = 0.036cm^2/s$, influence the more concentration at $50cm$ depth than at $100cm$.

This phenomenon must be evaluated when the chosen depth for the radon concentration measurement helps to reduce the meteorological parameters effects in the soil surface [20].

1.5 Radon exhalation

The *exhalation* is the process by which the radon issued in the soil manages to escape from the solid matrix and reaches the atmosphere. The radon exhalation rate from soil is one of the most important factors for the evaluation of the environmental radon level.
The radon gas concentrations in soil are much higher than in the atmosphere. This means that there is a high concentration gradient between the two media, kept constant by the continuous production by radium.
The mechanisms that contribute to this process are the diffusion and the convective transport, explained in the previous section. In the air, mainly radon behavior depends on the meteorological parameters. Indeed there are

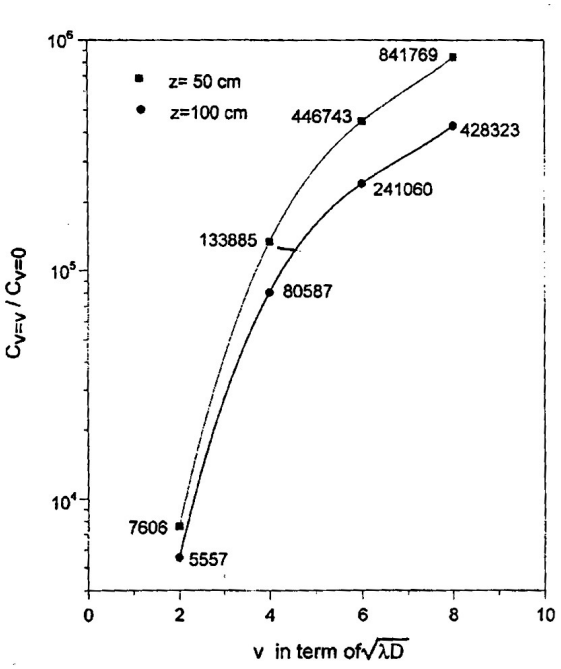

Figure 1.8: Variations of the radon relative concentrations as a function of the gas velocity in the soil air [20].

many factors that influence the exhalation, such as changes in temperature or speed wind, plenty of rain precipitation or snow and changes in atmospheric pressure. Although the high humidity facilitates the emanation process, it reduces the radon exhalation rate because the diffusion coefficient in the water ($\approx 10^{-}5 cm^2 s^{-1}$) is lower than in the air one ($\approx 10^{-}2 cm^2 s^{-1}$). This implies that the exhalation rate is greatly reduced in the materials saturated by water. From experimental data, it is known that the exhalation rate increases proportionally to the humidity content up to a maximum value. After that value it decreases reaching a minimum value in the materials saturated by water.
When the dependence on the convection is negligible compared to factors related to the diffusion, the exhalation rate is expressed by the formula, related to radon isotope ^{222}Rn [21]:

$$E_{Rn222} = \sqrt{\lambda_{Rn222} D_e} \rho_b e_{Rn222} C_{Ra} \tag{1.20}$$

where λ_{Rn222} is the radon decay constant (s^{-1}), D_e is the effective diffusion coefficient ($m^2 s^{-1}$), ρ_b is the bulk density in dry condition (kgm^{-3}), e_{Rn222} is the radon emanation coefficient and C_{Ra} is the radium concentration (Bqm^{-3}).
Similarly for the thoron exhalation:

$$E_{Rn220} = \sqrt{\lambda_{Rn220} D_e} \rho_b e_{Rn220} C_{Th} \tag{1.21}$$

where C_{Th} is the thorium concentration.
In the hypothesis that the concentrations of ^{238}U and ^{232}Th in the soil are equal, it is possible estimate the relationship between the exhalation rate E_{Rn222} and E_{Rn220} via the relation:

$$\frac{E_{Rn220}}{E_{Rn222}} = \frac{\lambda_{Rn220} L_{Rn220}}{\lambda_{Rn222} L_{Rn222}} \tag{1.22}$$

where L_{Rn220} and L_{Rn222} are the radon isotopes diffusion lengths, obtained via:

$$L = \sqrt{\frac{D_{ei}}{\lambda_i}} \tag{1.23}$$

In conclusion, for a dry ground with a value $D_e = 3.0 \cdot 10^{-6} m^2 s^{-1}$, the exhalation rate of ^{220}Rn is 76 times larger than that of ^{222}Rn.

Chapter 2

Electrostatic collection and RAMONA system

The radon concentrations are measured through different techniques depending on the field applications. In this chapter various measurement techniques are briefly described, with particular attention to that based on the electrostatic collection. Its last part of the chapter is dedicated to the device used in the work presented in this thesis: the *RAMONA* system (*RAdon MONitoring and Acquisition*) and its upgrade to allow the device operation in environments characterized by non-standard weather and environmental conditions.

2.1 Radon measurement techniques

The increasing interest for the radon concentrations measurements has encouraged the development of detection methods. Over the years, these methods have been improved and made more suitable to different situations. All the techniques are based on detection of α and γ radiations which are emitted by the radon decay products. The main detection techniques and their features are listed in the table 2.1.

These detection methodologies are characterized by different observed radiations, sensitivity, efficiency, speed of response and time resolution. Depending on the last characteristic, the detection techniques can be divided in three categories:

- integrating;
- grab-sample;

Detection method	Radiation	Measure time	Detection threshold (Bq/m^3)	Spectroscopic analysis analysis
Scintillation cells	α from Rn and its daughters	$2-60(min)$	3.7	No
Double filters method	α from Rn daughters	$2-60(min)$	3.7	Yes
Electrostatic collection with $ZnS(Ag)$	α from Rn daughters	$\geq 40(min)$	7.4	No
Electrostatic collection with LiF	α from Rn daughters	$\geq 40(min)$	1.1	No
Electrostatic collection with Si	α from ^{218}Po	$\geq 10(min)$	0.7	Yes
Electret ion chamber	α from Rn daughters	$3-5(h)$	1.1	No
Activated carbons	γ from Rn daughters	$1-7(d)$	11	Yes
Tracks method with electrostatic integrator	α from ^{218}Po	$7-60(d)$	0.7	No
Tracks method with diffusion chamber	α from Rn and its daughters	$1-12(min)$	3.7	No

Table 2.1: Main techniques for the measurements of radon concentrations.

- continuous.

The integrating techniques determine the mean value of the concentration in a fixed exposure time that can be varied between few days up to several months: these methods are used to evaluate the effective dose. Among the detectors belonging to this category there are LR-115, CR-39, electrets and activated charcoal canisters.
The grab-sample techniques rely on short integration time: the gas sampled in a short time is subsequently analysed.
The continuous techniques perform the measurement in real time and follow the variation of concentration with time. This methods are very useful to obtain data on sudden variations of radon concentration. Among the detectors belonging to the latter category there are the double filters device, the scintillation cells and the electrostatic collection chambers.
The detection method is chosen depending on the aim of the investigation. The research purposes for these measurements are:

- measurements to test the effectiveness of remediation actions;
- evaluation of human exposure to indoor radon;
- geological areas identifications with high radon levels (geogenic maps);
- study of the gas diffusion in soils and exhalation in the air.

Among the fundamental parameters affecting the detector choice there are the sensibility, the smallest and biggest measurable value. The radon concentration and its variations are also factors linked to this choice. As an example, in home environments a device sensitive to concentrations of $\sim Bq/m^3$ is required, whilst devices suitable for concentrations up to $\sim kBq/m^3$ are needed in soil.

2.2 Electrostatic collection chamber

The electrostatic collection technique is among the most used methods to analyze the radon fluxes and it is the only one able to distinguish radon and thoron daughters. The device is based on the electrostatic collection of the polonium ionized isotopes on a silicon detector. The radon gas, mixed with air, enters in the collection chamber where the polonium ions are produced by radon decay and then collected by the electrostatic field. The radon gas may enter in diffusive way, as it happens for the indoor measurements, or by pumping gas from the soil. In the former case the mainly detectable radon

isotope is the ^{222}Rn, due to its rather long half time, while in the latter case it is possible to observe also the ^{220}Rn products decay, despite its short half time.
The polonium ions drift towards the detector surface due to the electrostatic field generated by an applied voltage between the chamber wall and the grounded detector, as it is shown in figure 2.1. Once on the detector surface, the ions decay through the α emission, providing a good resolution spectra due to degradation lack in flight.

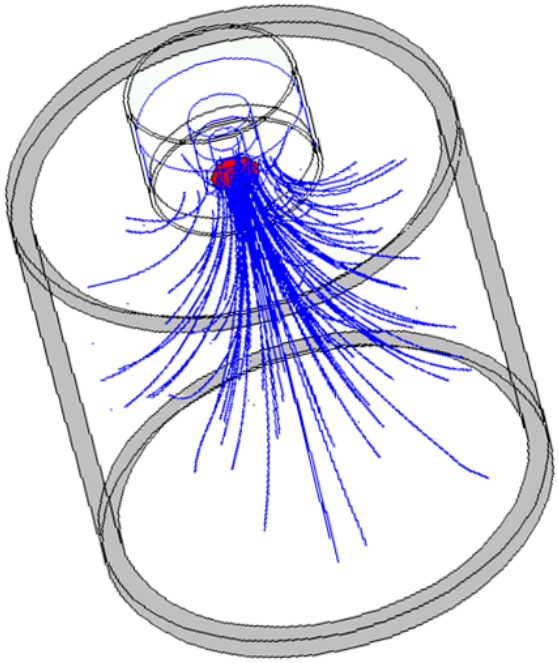

Figure 2.1: Representation of the electrostatic field force lines applied to the chamber.

A short response time is important in order to observe radon concentration variations. The device promptness is linked to the time required to reach the equilibrium between the radon isotopes and their decay products. In the scintillation cells, there is no a separation among the alpha particles emitted by ^{218}Po or ^{214}Po. So the time required to reach the equilibrium between ^{222}Rn and ^{214}Po, last element at short half time of the radioactive series, is about $200min$. In the solid state detectors it is possible to distinguish the alpha individual lines, thus also the different isotopes. With such a characteristic is possible to discriminate the ^{218}Po line that reaches the equilibrium with radon in less than half hour, due to its half time ($\approx 3.06min$); this fact

optimizes the response time and thus the time resolution [23].

2.3 The $^{218}Po^{+}$ electrostatic collection

It is very interesting to understand the physical mechanisms regulating the fraction of ^{218}Po ions in the cell volume and that are available to be collected by the electric field (ion production and ion neutralization). Initially, ^{218}Po is known to be positively charged due to the stripping of orbital electrons by the departing alpha particles in the recoil motion. About 88% of the polonium atoms are single charged and the remaining are neutral [24] [29]. This feature allows the polonium detection through electrostatic collection technique; since the ^{218}Po is an alpha emitter nucleus, the high resolution alpha spectroscopy can be performed, at better than 1%. The ion slows down toward thermal velocity at the end of the recoil path and it can capture electrons such that at the end of its path. After thermalization, the polonium mean velocity is about $1.4 \cdot 10^4 cm/s$ and its collision frequency is of the order of $10^9 collisions/s$. Nevertheless, some alternative processes take place and they reduce the collection efficiency:

- $^{218}Po^{+}$ ions decay-in-flight;
- recombination with negative ions in the air;
- neutralization after interaction with the aerosol particles (*attachment*);
- deposition on the internal walls of the chamber ($plate - out$).

The electrical charge of ^{218}Po atoms has influence on its mobility, characterized by the diffusion coefficient, which controls the formation of the radioactive aerosol and the plateau process on surfaces. Therefore the deposition and the attachment processes are linked to it. Radon progeny interactions can be further complicated by the polar molecules clustering around polonium ions to form stable complexes; this process is strongly influenced by air humidity, which modifies the cluster diameter, and thus its diffusion coefficient [30].
Neutralized ^{218}Po atoms either decay directly to ^{214}Pb, or interact with aerosol particles, or are lost to the walls by collision. Neutralization mechanism can be described with the following processes [27]:

- charged polonium recombination with negative airborne ions;
- charge transfer with present neutral molecules;

- electron scavenging through the OH radical formed by the water vapor radiolysis.

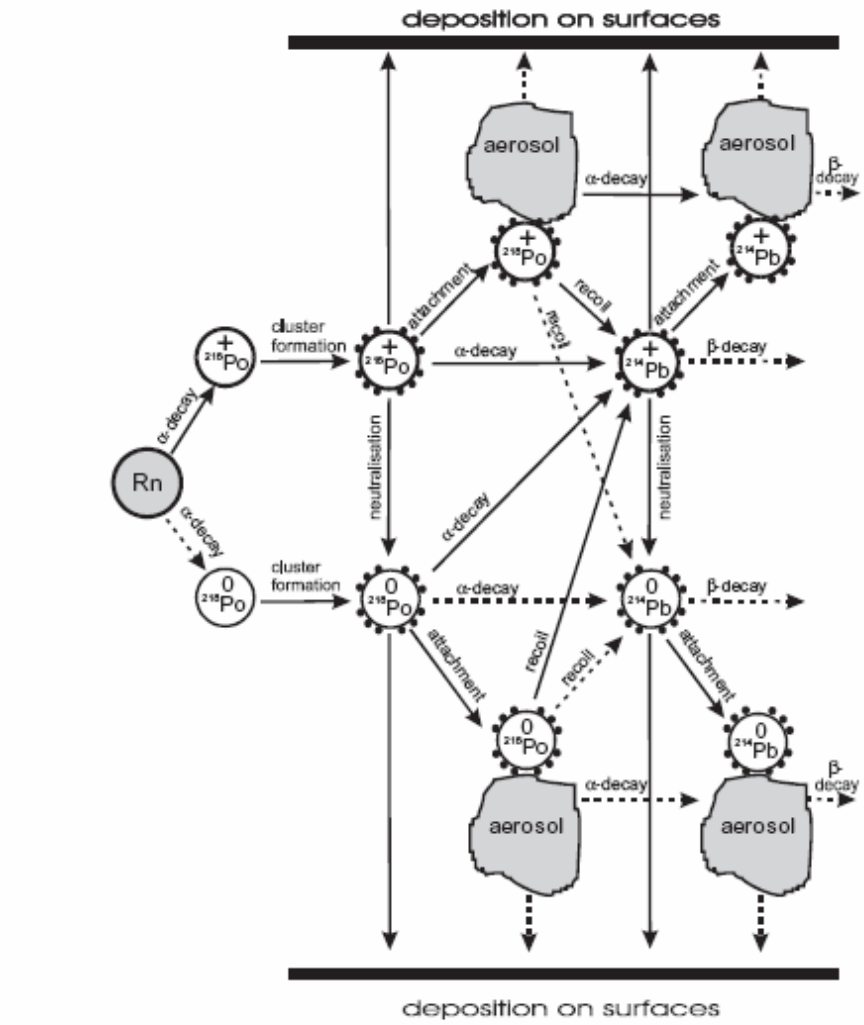

Figure 2.2: Radon progeny behavior in air [26].

2.3.1 Recombination by small airbone negative ions

The radon and its decay products emit ionizing radiations producing positive and negative ions in air, including electrons, which can recombine itself or

neutralize the $^{218}Po^{+}$ clusters. The following equation describes the negative ions production rate[28]:

$$\frac{\delta n_{-}}{\delta t} = \xi \cdot n_0 - \alpha \cdot n_{+} \cdot n_{-} \tag{2.1}$$

where n_{+} and n_{-} are respectively the positive and negative ions concentration in air, ξ is the ion pair production rate after ^{222}Rn decay, n_0 is the radon concentration in units of cm^3 and α is the ion pair recombination coefficient: $\alpha = 1.4 \cdot 10^6 cm^3 s^1$ [25].
Assuming the same concentration in the air both positive and small negative ions, we consider the stationary case:

$$n_{+} = n_{-} = \sqrt{\frac{\xi n_0}{\alpha}} \tag{2.2}$$

The neutralization rate K depends linearly on the airborne negative ion concentration and so:

$$K = a\sqrt{\frac{\xi n_0}{\alpha}} \tag{2.3}$$

where the constant a is about 10^{-5} and suggests that the neutralization mechanism with airborne small negative ions may be significant only at radon concentration of the order of $kBqm^3$ [25][28][29].

2.3.2 Change transfer with airbone neutral atoms

The neutralization, in terms of the charge transfer mechanism, consists in the electrons being directly removed via colliding neutral molecules. This mechanism appears unlikely because the first ionization potential of polonium ($8.43eV$) is lower than that of various airborne molecules. Nevertheless the unstable $^{218}Po^{+}$ may react chemically with the air oxygen to form polonium dioxide, PoO_2^{+}, whose ionization potential is $(10.44 \pm 0.05)eV$ [28].

PoO_2^{+} has an higher ionization potential and it can be neutralized by removing electrons from water vapour or from trace gases, such as NO or NO_2, with a lower ionization potential. The charge transfer mechanism is highly dependent on the air ionization potential, on the content of gas traces and/or organic vapours and on the concentration of the airborne ^{222}Rn. Another feature is that the neutralization rate through the charge transfer is fast since the electrons can be transferred directly by a single collision with a donor molecule.

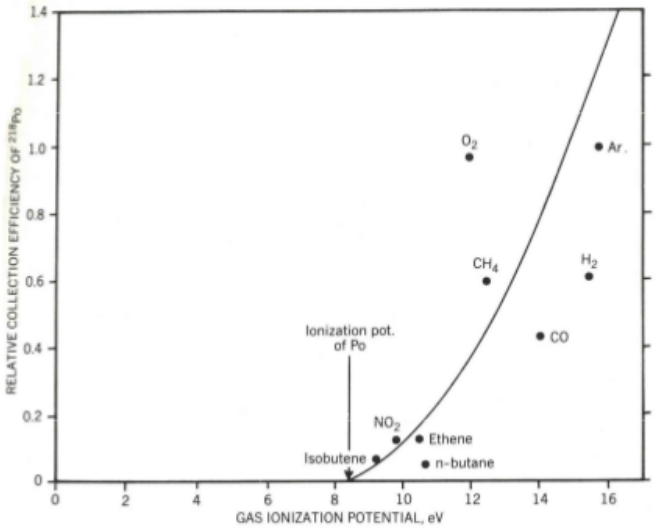

Figure 2.3: Relative collection efficiency of ^{218}Po as a function of gas ionization potential. The charge transfer process can occur only if the polonium reacts with oxygen to form PoO_2 [28].

2.3.3 Electron-scavenging by airbone OH radicals

It has been observed that polonium ions can be neutralized by water vapor or NO_2 in nitrogen, as well as in air [27]. The radiolysis is a dissociation of molecules caused by nuclear radiation; in the water vapour it occurs through the radon progeny radiations and it produces the hydroxyl radicals ($^{\bullet}OH$). The hydroxyl radical, called molecular scavenger, is an excellent electron acceptor for its high electron affinity ($1.83eV$). The electrons scavenging by the OH-radicals is responsible for an increased local concentration of negative small ions that enhances the polonium recombination rate.
The electron scavenging mechanism through the water vapour molecules is explained by the following reactions, tested by adding a radical scavenger (ethanol) [25]:

$$H_2O^{-} \longrightarrow H^{\bullet} +^{\bullet} OH \tag{2.4}$$

$$^{\bullet}OH + e^{-} \longrightarrow^{\bullet} OH^{-} \tag{2.5}$$

$$^{\bullet}OH^{-} +^{2\ 18}Po^{+} \longrightarrow^{\bullet} OH +^{2\ 18}Po \tag{2.6}$$

The hydroxyl radicals concentration can be evaluated from the equation:

$$\frac{\delta\,[^{\bullet}OH]}{\delta t} = Q\,[H_2O] - k_R\,[^{\bullet}H]\,[^{\bullet}OH] \tag{2.7}$$

where Q is the water molecules disintegration constant, k_R is the radicals recombination constant and $[^{\bullet}H]$ and $[^{\bullet}OH]$ are the radicals $H^{\bullet}$ and $^{\bullet}OH$ airborne concentrations. Hypothesizing the steady state as same concentration level for the radicals, $[^{\bullet}H] = [^{\bullet}OH]$, the hydroxyl radicals concentration can be expressed as:

$$[^{\bullet}OH] = \sqrt{\frac{Q\,[^{\bullet}H_2O]}{k_R}} \tag{2.8}$$

Since the hydroxyl radical concentration in air is proportional to the square root of the water vapour concentration, also the neutralization rate has the same proportionality.

2.3.4 ^{218}Po ions neutralization rate

It is very important compare the measured neutralization rate with the average time for the polonium ions electrostatic collection. In normal environmental air condition the neutralization rate, v, previously indicated with $\frac{\delta n_-}{\delta t}$, is given by:

$$v = v_{IR} + v_{CT} + v_{OH} \tag{2.9}$$

where v_{IR} is the ion recombination rate, v_{CT} is the charged transfer mechanism recombination rate and v_{OH} is the neutralization rate due to the electron scavenging by hydroxyl radicals.
The neutralization rate is dependent both on the radon mean concentration, responsible for the ions production in air, both on the humidity. In particular, the humidity dependence can be ascribed only for electron scavenging mechanism. The neutralization rate by charge transfer has always constant value ($v_{CT} = 0.4 \cdot 10^{-3}$), while for the other two phenomena the following expressions are valid:

$$v_{IR} \propto 10^{-3}\sqrt{Rn} \tag{2.10}$$

$$v_{OH} \propto f(RH)\sqrt{C_{Rn}} \tag{2.11}$$

where C_{Rn} is the radon concentration (Bq/m^3) and $f(RH)$ is a relative humidity function. The neutralization rate as a function of these factors is shown in figure 2.4.

Previous studies, conducted by Chu and Hopke, also showed the functional neutralization dependence from humidity, but with different order of magnitude of the neutralization rate value at 50% RH:

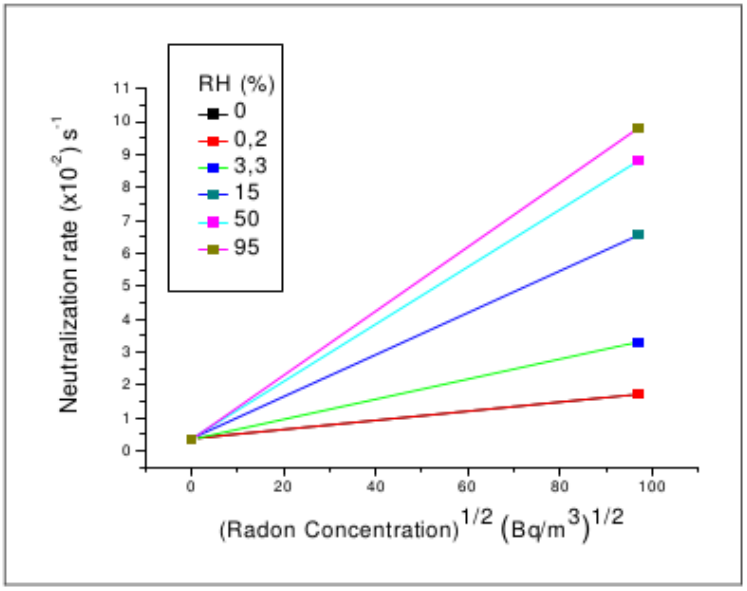

Figure 2.4: Neutralization rate as a function of radon concentration and humidity [24].

$$v \approx 0.05s^{-}1 \qquad (Dankelmann, 2001) \tag{2.12}$$

$$v \approx 50s^{-}1 \qquad (Chu - Hopke, 1988) \tag{2.13}$$

This apparent discrepancy can be explained by the different radon concentration used in two different studies: $\approx 10^4 Bq/m^3$ for Dankelmann and $\approx 10^6 Bq/m^3$ for Hopke, for which the effect of the ions recombination increase the neutralization rates. Moreover these estimations could be affected by the high uncertainty associated to the ^{218}Po ion mobility, which must to be known for the evaluation of the neutralization rate. In conclusion the neutralization rate increases with the increase relative humidity at a given radon concentration in air and in argon gas [31][32].
It is clear that the response of a device based on the electrostatic collection of $^{218}Po^{+}$ is influenced by the effect of the humidity on the polonium neutralization. For these reasons, for the radon concentration measurements with this technique, it is required to evaluate the response dependence on radon concentration and on humidity, for their different influence on the ^{218}Po ion neutralization rates.

2.3.5 $^{218}Po^{+}$ mobility

The spectrum mobility of the decay products of ^{222}Rn and ^{220}Rn, in artificially enriched air with radon isotopes progeny, is shown in figure 2.5. There is no single value for the mobility of the ionized radon daughters, the experimental distribution of mobility is bimodal: the first range of the spectrum, a few percent of ions with mobility in the range $(1.9 \div 2.3) cm^2 s^{-1} V^{-1}$, probably accounts for the unattached ion fraction, and the second, in the range $(0.3 \div 1.2) cm^2 s^{-1} V^{-1}$, for the attached or clustered one.

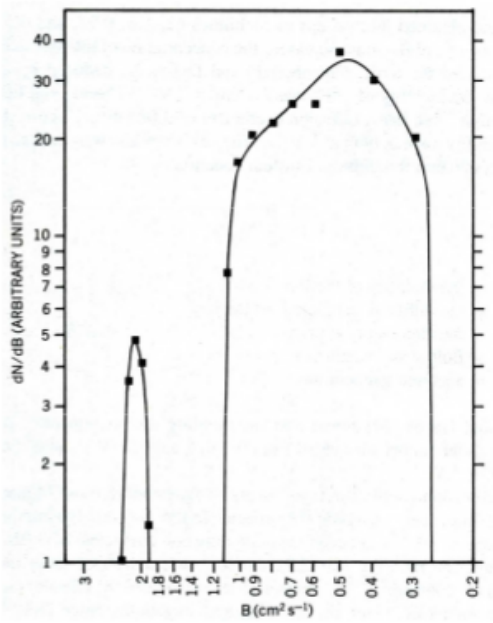

Figure 2.5: The mobility distribution ions derived from radon isotopes in unfiltered air when enriched with ^{222}Rn and ^{220}Rn progeny [8].

Inside the electrostatic chamber, only the unattached fraction is collected, because the typical attachment rates are much lower than the neutralization ones. The ion mobility μ can be calculated with the *Einstein equation*:

$$\mu = \frac{eD}{kT} \tag{2.14}$$

where e is the elementary charge, D is the ion diffusion coefficient, k is the Boltzmann constant and T is the absolute temperature.

The mobility estimated values, for unattached $^{218}Po^{+}$ or for $^{218}PoO_2^{+}$ ($\mu \approx 1.9 cm^2 s^{-1} V^{-1}$), can be used for the evaluation of neutralization rates, but the gas temperature changes during the measurement must be observed because the ions mobility spectrum is dependent from it [33].

2.4 RAMONA System

As previously mentioned, one part of this research work is focused on the RAMONA device upgrade aiming to allow its operation in environments characterized by non-standard weather and environmental conditions.
RAMONA was developed in the framework of a collaboration between the sections of Naples INFN (National Institute of Nuclear Physics) the Physics Department of the Naples University "*Federico II*". The system allows the continuous monitoring of radon concentration in air and in the soil gas and of the weather parameters, which are needed to normalize the concentration to standard environmental conditions. It is equipped with an ethernet interface that makes possible to drive remotely many stations, each identified through its own IP address.
It is composed by two parts: detection and acquisition/control units.
The detection unit of the system consists of the electrostatic collection chamber shown in figure 2.6. It corresponds to a one liter volume and it consists of a aluminum cylinder of $10cm$ diameter and height.

Inside the collection chamber, in the upper part of it, is mounted an electronic board that includes a solid state silicon detector, an integrated preamplifier, the environmental sensors for temperature, humidity and pressure and their conditioning circuits. The knowledge of climatic parameters is crucial because the instrument response depend on them [22]. The chamber is hermetically closed and its walls have two taps for the inlet and outlet of radon with its carrier gas; they are made in teflon so that the radon do not diffuse in. Inside the chamber, at the entrance point of the radon in the active sampling volume, a Tyvek filter is placed, whose function is to block the entry of the radon decay products in the collection volume, allowing the entrance of the radon gas only. In this way in the active volume only the decay products coming from radon in the sampling volume are detected.
In this chamber the spectroscopy of alpha particles is performed. The radon activity measurement comes from the measure of its decay products (^{218}Po, ^{214}Po, for radon and ^{216}Po, ^{212}Po for thoron). In fact, it is not possible to observe the alpha particles emitted from the radon nucleus because, as inert gas, it expands throughout the available volume, so that the few alpha particles that reach the detector appear degraded in energy and unrecognizable.

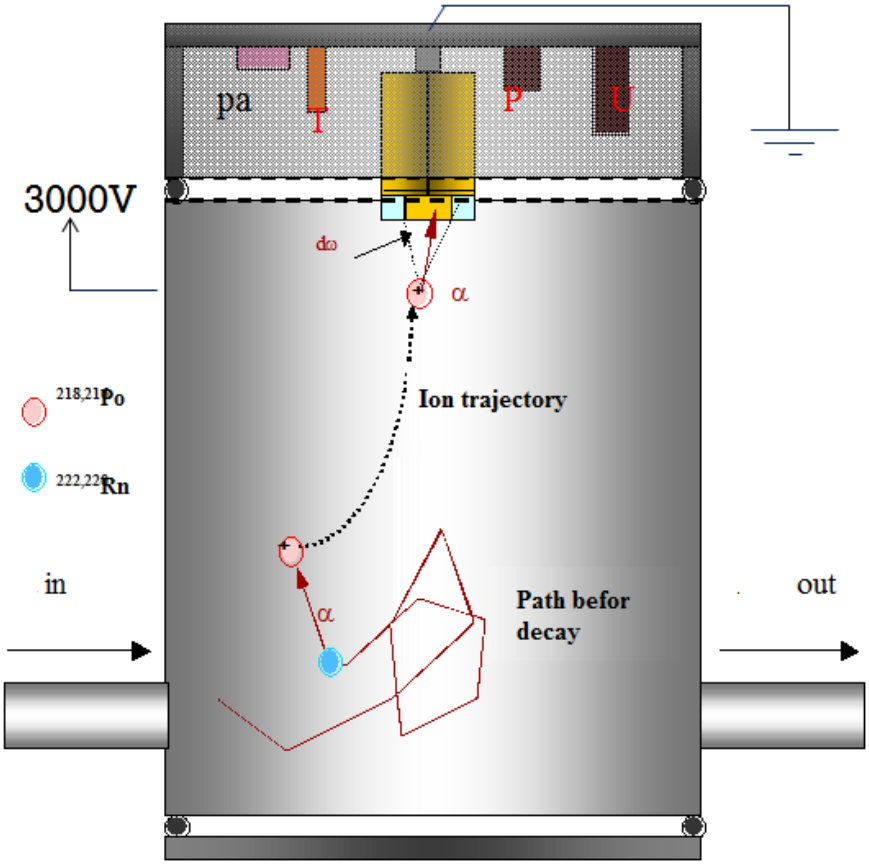

Figure 2.6: Scheme of the RAMONA electrostatic chamber.

The radon daughters are ionized and thus transported by an electrostatic field towards a silicon detector surface, where alpha particles are emitted. In this way there is not an air layer that reduces alpha energy, hence the resolution is such that the good separation of alpha particles of both isotopes is possible.
A typical spectrum produced with a mixed radon and thoron source is shown in figure 2.7.

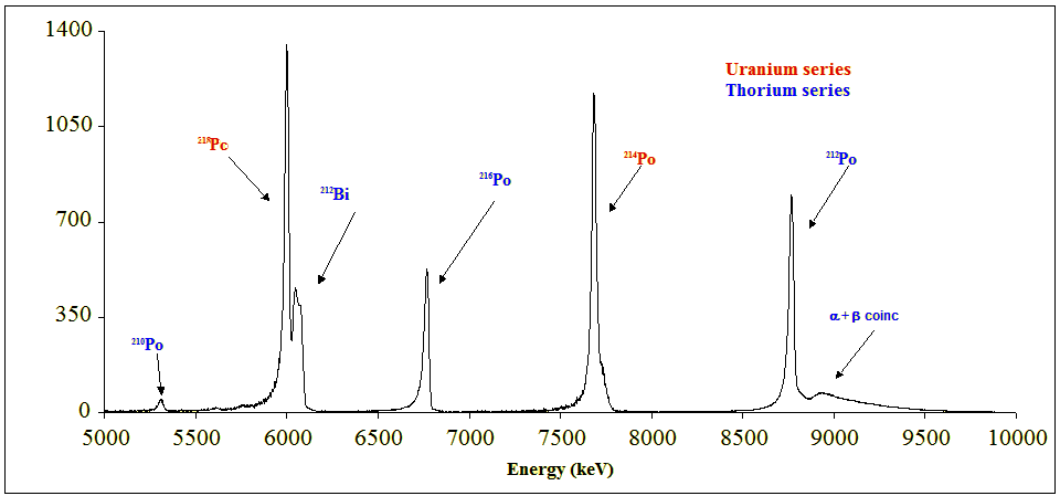

Figure 2.7: Alpha spectrum of the radon and thoron daughters.

During the operation, the chamber wall is put at $3000V$. For safety reasons, the whole chamber is inserted in a insulating holder which avoids accidental contacts of people with the chamber when high voltage in on.
It is important to stress that RAMONA peculiarities are worthwhile in soil radon concentration measurements when both radon isotopes are present.
The other RAMONA characterizing part is the acquisition/control unit. This unit contains the electronics for the signals formation, multiplexing and A/D conversion. It also includes:

- a power supply for the chamber polarization up to $4kV$ and for the silicon detector and a preamplifier,$(\pm 26 \div 60V)$;
- a microprocessor *Rabbit core* 2200 that controls the external communication through an Ethernet interface using the TPC/IP protocol.
- a memory $(64kByte)$ for the software able to drive the system and save data.

All the electronics is integrated in only one module with size $(9x16x30)cm^3$. In this way it is possible to transport it from a measure site to the next one. In particular, it has to be highlighted that this control unit can be used as part of a electronic chain for spectroscopy using the connection of an output from a second detector, for example a $NaI(Tl)$ or a $HPGe$ detectors.

Figure 2.8: RAMONA System: electrostatic chamber and acquisition unit.

A dedicated software controls the spectrum acquisition and the mode of sending data from its internal buffer. Through the software it is possible to start and stop the acquisition, set the HV voltage applied to the collection chamber, set the region of interest, initialize and program acquisition cycles, visualize variation of environmental parameters versus time, calibrate energy spectrum and save the acquired data in text format for off-line analysis. In the figure 2.9 it is shown the typical screenshot of RAMONA.

In the table 2.2, some parameters characterizing of Ramona are presented.

2.4.1 Detection efficiency

The detection efficiency of RAMONA collection chamber, is defined as the ratio between the count rate in the interesting peak and the activity concentration in the chamber. This ratio depends on the ions collection, influenced by the environmental parameters, and by the chamber geometry. The

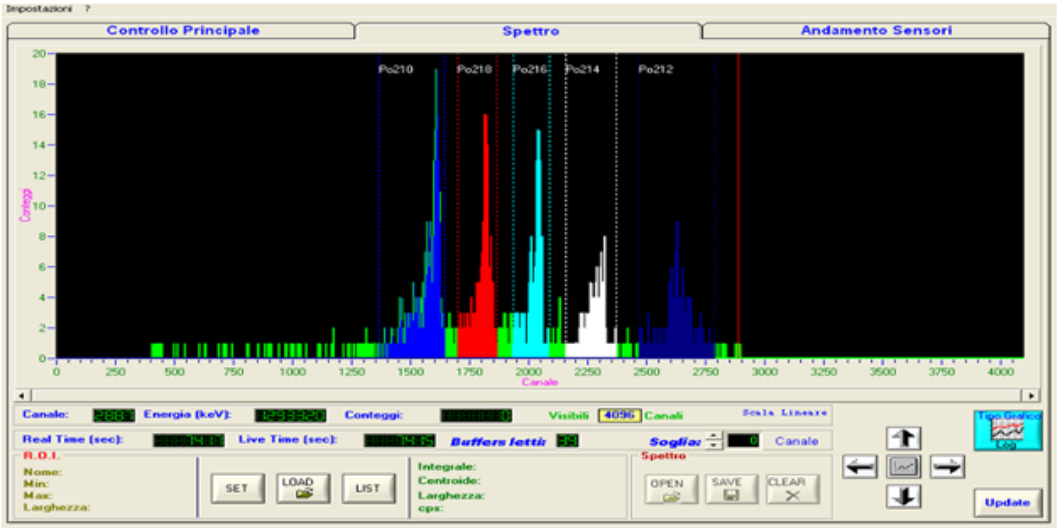

Figure 2.9: Energy spectrum of radon and thoron decay products by RAMONA software.

Main features of RAMONA control unit	
Input for other detector (preamplifier output)	
Discrimination on the input signal	
Pole zero correction	
Gross gain amplifier	1x, 10x, 100x
Fine gain amplifier	with trimmer
Signal formation constant	$3\mu s$
Total conversion time	$20\mu s$
Input signal polarity	$\pm$
HV voltage	$(0 \div 4)kV$ (remotely controlled)
Ethernet interface	$10Mbps$
Alimentation	12 V, 6Ah (rechargeable battery)

Table 2.2: Specifications of the RAMONA control unit.

analysis of these factors is needed to characterize and optimize the chamber performances.
Concerning the first factor, its dependency from the applied high voltage to the chamber walls has been studied. The collection efficiency increases with the high voltage up to a saturation around $\approx 3.0kV$ [34]. Applying a voltage of $3000V$ to the chamber walls, the obtained electrostatic field is such that the polonium ions are collected in a time of the order of milliseconds. In this case the mean speed of polonium ions through the entire chamber ($10cm$) is of the order of $10^4 cms^{-1}$. The mean time of the chamber crossing has an upper limit of about $T_m = 7 \cdot 10^{-3}s$, negligible compared to the ^{218}Po half-life that is $180s$. For this reason, the majority of the ions decays on the silicon subsequently at arrival time.
As explained in the previous section, the transport and the collection of the polonium ions are influenced by weather parameters, which affect their recombination and mobility. An increase of pressure and temperature in the collection chamber produces an increase of the ions recombination probability. As for the pressure, this is due to an increasing density that facilitates the collisions, as the temperature increases thermal agitation is produced as well as ions mobility is reduced. The dependence of the efficiency on the above parameters was studied at ENEA-INMRI and the results are shown in the figures 2.10, 2.11, 2.12 [35].

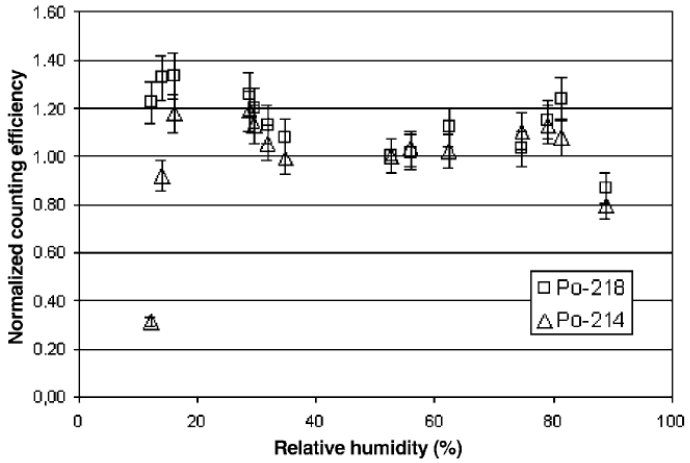

Figure 2.10: Dependence of the collection efficiency on the relative humidity for both polonium isotopes. Values are normalized to the corresponding values at 50% relative humidity. Measurements were made at a fixed radon activity concentration ($\approx 30kBqm^{-3}$) and at constant temperature ($\approx 25^oC$) and pressure ($0.09670.100MPa$) [35].

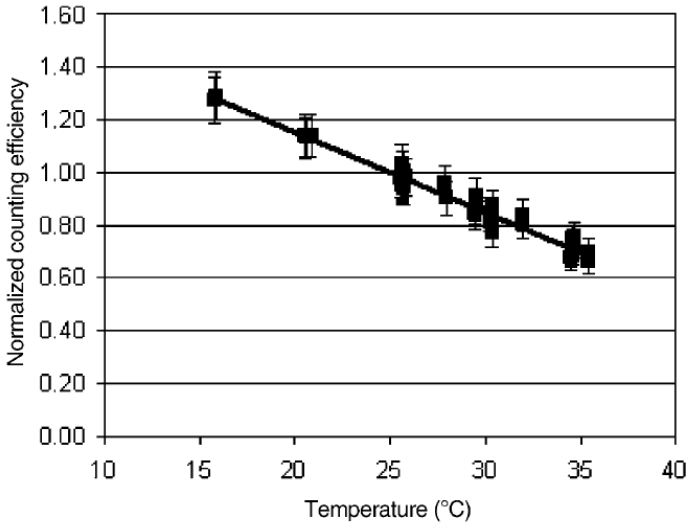

Figure 2.11: Dependence of the ^{218}Po counting efficiency on air temperature well fitted by a straight line. Values are normalized to the counting efficiency at 25^oC [35].

Another important factor is the geometric efficiency. In our case it is influenced by the silicon detector shape. The used detector is "Ion-Implanted-Silicon Charged-Particle Detectors ULTRA" (Ortec), shown in figure 2.13. It is clear that only a part of the detector surface is active, while the ions that collected on it through the electrostatic field are distributed on the total area.

If we analyze in more details, the ions decay can happen in three different areas:

- the active area, that is a circular surface transverse to detector axis ($S_a \approx 50mm^2$);
- the internal cylindrical wall whose generatrix is parallel to detector axis ($S_l \approx 5mm^2$);
- superior circular ring of the detector frame exposed to the incident flux ($S_c \approx 169mm^2$).

Estimating that the intrinsic efficiency detector is 100%, it is needed to evaluate the ion fraction distributions over the above different areas in order to obtain the geometric efficiency. In addiction it is known that only the 80% of the ^{218}Po is ionized. From these considerations and from experimental data, the calibration factor of the device is about $\approx 0.05cps/(Bq \cdot l^{-1})$.

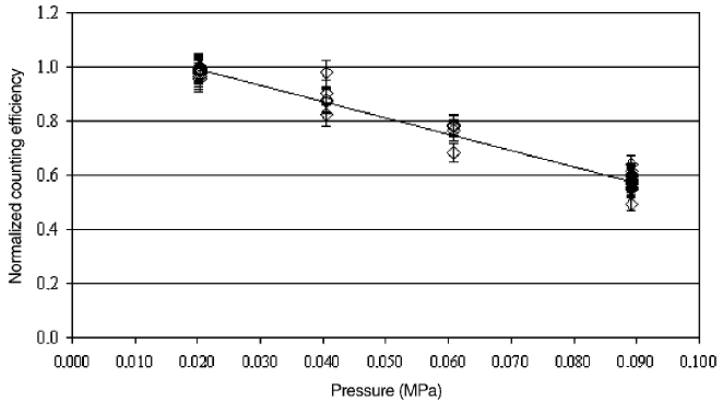

Figure 2.12: Dependence of the ^{218}Po counting efficiency on air pressure well fitted by a straight line. Values are normalized to the counting efficiency at $0.0203MPa$ [35].

Figure 2.13: The silicon detector used inside the RAMONA collection chamber is an a silicon ultra detector of Ortec company.

2.4.2 Alpha line shape

The alpha lines shape observed with RAMONA are not correctly described by a Gaussian functions, as results from figure 2.7. The left-hand tail on the peaks is explained by different factors. The first one is the surface dead layer of the silicon detector, 500 Angstrom thickness. In fact, the polonium atoms, which are deposited on the detector surface after the electrostatic collection, emit half of their alpha particles toward the sensitive layer over a wide range of angles. Thus, the alpha particles, before entering into the active zone, loss an amount of energy ranging on an interval depending on the angular spread. Moreover, the ^{218}Po is deposited also on the upper part of the detector conductive frame. For this reason the alpha particles, before entering in the active volume, can lose part of their energy in air, as shown schematically in figure 2.14.

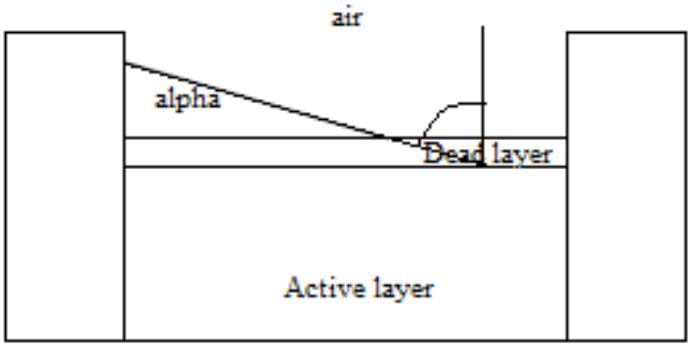

Figure 2.14: Scheme of the emission from the conductive detector edges and from the detector surface.

A simple calculation with a Monte Carlo code confirmed the above hypotheses (see figure 2.15). In particular, the contribute due to the alpha emitted from the edge is much lower ($\approx$ 5%) than one from the detector surface emission [36]. In order to evaluate the correct value of the polonium, this study suggests to define a Region of Interest (ROI) including also the tail; it was estimated that the 98% of the total ^{218}Po alpha counts is in a $0.5MeV$ range below the peak.

In the figure 2.16 the radon spectrum is shown. The high energy peak shape is different between the two polonium isotopes, ^{218}Po and ^{214}Po. The

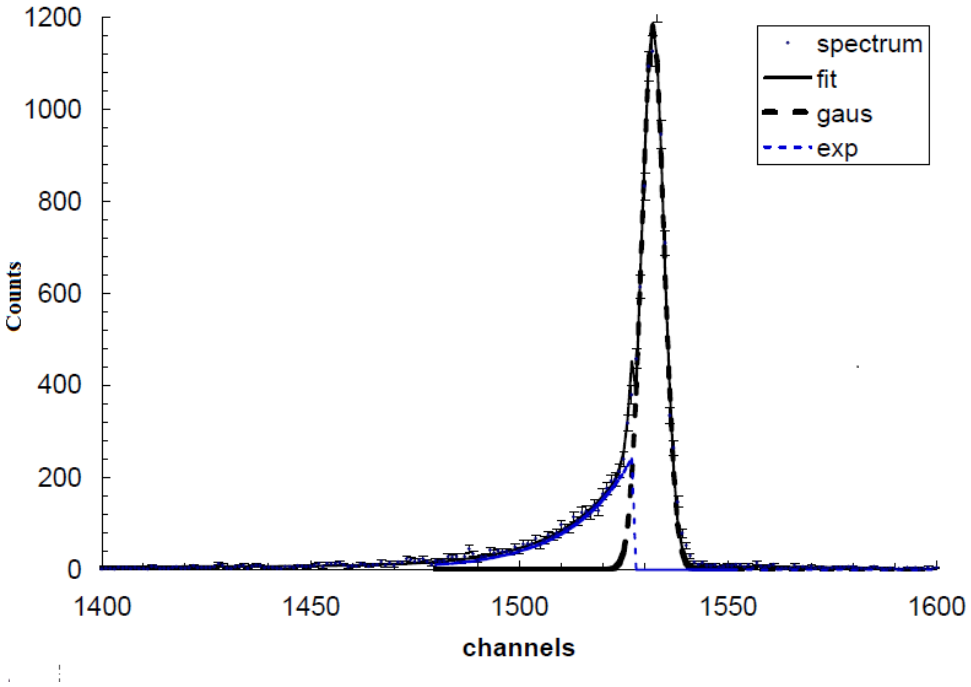

Figure 2.15: Comparison between experimental and calculated ^{218}Po alpha peak [36].

^{214}Po shape a tail on the left-hand side of the peak, whose origin is the same as the tail showed in figure 2.7. Moreover, there is a little second tail on the right-hand side of the peak, which is due to the contribute of the beta particles emitted by ^{214}Bi, the direct ^{214}Po father nuclide, in coincidence with alpha particle of $7.69MeV$.

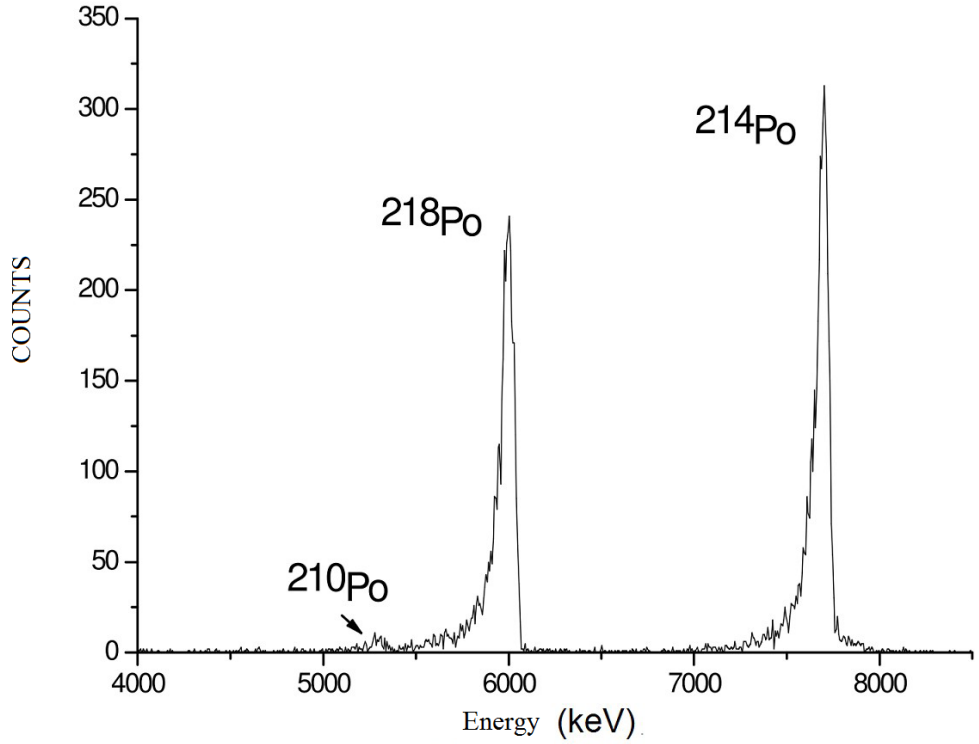

Figure 2.16: ^{222}Rn daughters spectrum. It 'also showed the peak of the background of ^{210}Po.

Chapter 3

Calibration facility for radon and thoron detectors

The growing attention to the radon concentrations measurements, due to several reasons already explained in the first chapter, makes it necessary to develop calibration methods that reproduce the specific activities of ^{222}Rn and ^{220}Rn in real life situations, where both isotopes are present. The device characterization is strongly linked to the environmental parameters, so it is needed to monitor temperature, pressure and humidity, during the calibration process. This allows to verify and correct the techniques used to measure the radon isotopes concentrations in different environmental conditions, taking into account the relative concentration of radon and thoron. It is important to stress the need to report all calibrations to primary standards environmental conditions.
In general, there are two different calibration methods for radon depending on the characteristics of the instrument to be calibrated, namely if it is active or passive. The first one provides a gas transfer directly into the detector chamber, the second one involves the detectors positioning inside the exposure chamber, due to their typical little sizes.
In our laboratory, a calibration facility for radon detectors, passive and active, was developed keeping in mind the procedures of the National Metrological Institute (ENEA-INMRI) [38]. This facility is also able to monitor and control the weather parameters, so it has been used also to study the RAMONA efficiency dependence on temperature, pressure and humidity.
In this chapter, this calibration facility, its upgrade to calibrate both radon and thoron detectors and the developed method for the thoron sources characterization are described.

3.1 Radon isotopes sources

For calibration purpose some reference sources, for both the radon isotopes, with different activity concentrations are necessary.
In our laboratory, two traceability chains for the realization of independent internal atmospheres of known specific activity, one for the ^{222}Rn and the second one for the ^{220}Rn, have been developed. These atmospheres are used for the measuring devices calibration in an exposure chamber specially made, described in the next section. The relative long half-life facilitates the production of a reference sample for the radon activity, while the short half-life makes difficult the production of a reference sample for the thoron activity, as can be inferred from the graphs in figure 3.1.

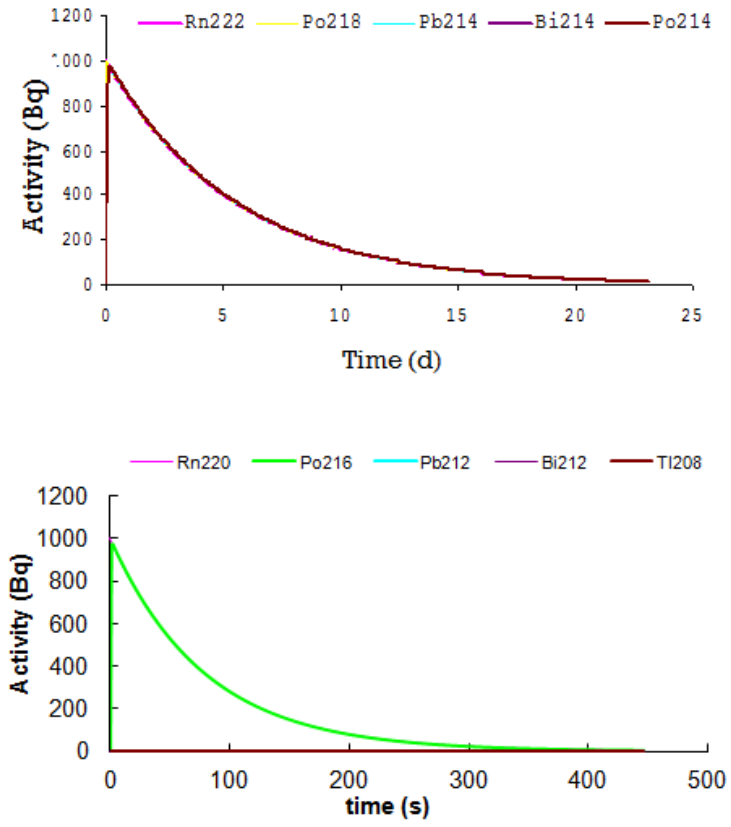

Figure 3.1: In the upper side of the figure, the activity of radon and its products decay versus time is shown. In the lower side, the activity of thoron and it daughters. It is important to stress the different order of magnitude of the time scales, days for radon and second for thoron.

Let analyze the two methodologies to obtain radon isotope source in detail, the first one, already developed, for radon sample atmosphere and the second one for thoron sample atmosphere.

3.1.1 ^{222}Rn source

The radon sample atmosphere is provided by a radium source (Pylon.RNC-RN-1025) with a nominal activity $\approx 106.3 kBq$. The dry powder of ^{226}Ra constitutes the source. It is contained in an aluminum cylinder hermetically closed so that the ^{226}Ra can be in equilibrium with ^{222}Rn [37].
The radon produced by the source is collected by diffusion in a glass ampoule connected to the source; its volume is equal to $33 cm^3$. After that it is hermetically closed and removed from the source. The radium source and the ampoule are shown in figure 3.2.

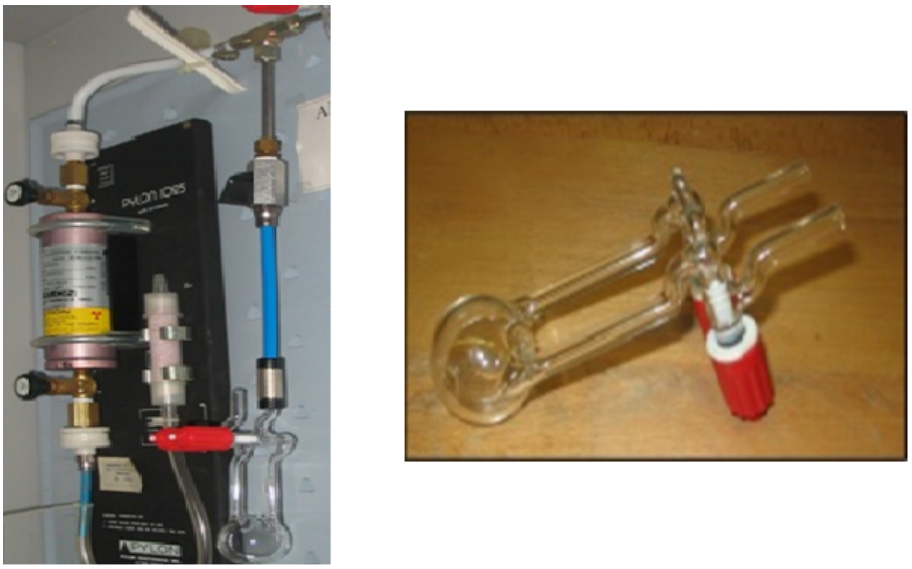

Figure 3.2: On the left side, the radium source (Pylon.RNC-RN-1025) with the ampoule connected is shown, while in the right side the used glass ampoule as reference radon source is shown.

It is needed to wait about 3 hours to ensure that the radon decay products, that are present at the moment of the ampoule closure, reach the equilibrium with it, as we can see in figure 3.3. While about 10 hours to give time to decay products, already present, to decay completely are necessary.

The radon activity is measured via γ spectroscopy with a HPGe-detector, ORTEC GMX 45P4-ST. Among the gamma emitted by radon progeny, the

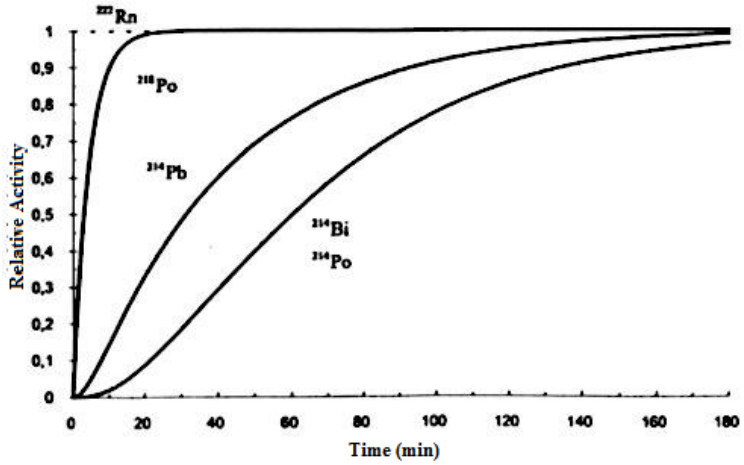

Figure 3.3: Relative activities of radon products decay versus time up to reach the equilibrium with the radon one.

gamma most intense are used, namely the ones produced by ^{214}Pb and by ^{214}Bi decay, whose energies are respectively (295 and 352)keV and 609keV [39]. In figure 3.4, it shown a typical gamma spectrum of radon progeny.

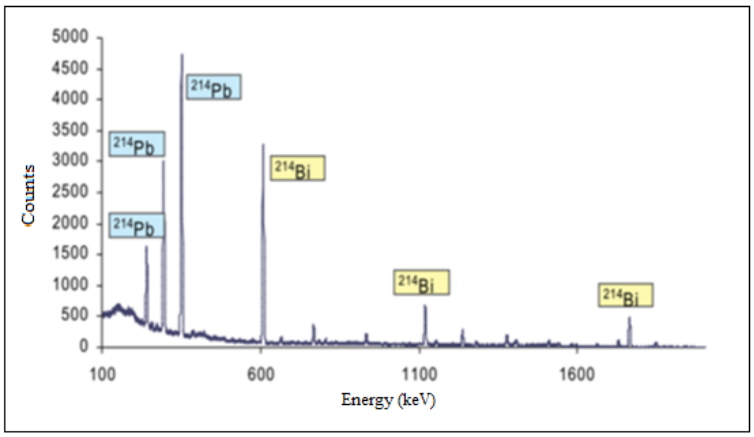

Figure 3.4: Typical gamma spectrum of ^{222}Rn.

The detector is calibrated beforehand with certified radon sources provided by the ENEA-INMRI. The main characteristics of the HPGe-detector (ORTEC GMX 45P4ST) are the resolution (FWHM) of 2.16keV at 1332keV (^{60}Co) and the measured relative efficiency of about 48%. The electronic chain consists of a preamplier (ORTEC A257N) and a signal digital pro-

cessor (ORTEC DISPEC LF) connected to a PC, which makes possible to visualize the spectrum and to perform the peak analysis [37].
The radon activity is obtained by the count rates of gamma emitted by the radon daughters, that are defined as the ratio between the full energy peaks area (N_γ) and the acquisition live time (t_l), $cps = N_\gamma/t_l$. In this way, it is possible to define the activity of each gamma transition, hence the radon activity, as:

$$A_i = \frac{cps_i}{\epsilon_i BR_i} \tag{3.1}$$

where cps_i are the count rates related to the i-th peak, ϵ_i is the detector efficiency for the energy E_{γ_i} taking into account the geometry and BR_i is the relative branching ratio. The count rates measured are corrected by the decay during the measurements and by a decay factor depending on a chosen reference time (t_0), by the relationship:

$$cps(t_0) = cps(t) \cdot e^{\lambda(t-to)} \cdot \frac{\lambda t_{mis}}{1 - \exp(-\lambda t_{mis})} \tag{3.2}$$

where $cps(t_0)$ are the counts reported at the reference time t_0, $cps(t)$ the counts at the end of the measurement, at time t, $e^{\lambda(t-to)}$ corrects for the decay during the past time and $\lambda t_{mis}/\left[1 - \exp(-\lambda t_{mis})\right]$ corrects for the happened decay in a single measurement with duration t_{mis}.
With such radon activity the radon monitor can be calibrated.

3.1.2 ^{220}Rn source

As already exposed in the previous section, there are established methodologies for creating ^{222}Rn known activity atmospheres, while for thoron sample atmospheres these methodologies are still under study. The realization and the management of thoron standard atmosphere is hampered by its short half-life, which does not allow to employ the techniques usually adopted for radon.
For this radon isotope there is no still national standard, so a standard for internal working has been developed in our laboratory. Also this procedure starts with a measurement of thoron performed with the HPGe detector, whose efficiency was obtained [41] [42].
In order to develop a thoron sample atmosphere, it is necessary characterize the source in terms of emanation and then develop a methods to measure its exhalation rate.
Two types of sources, discriminated by their activity, have been used. The

first ones have a low mean activity and they consist of lantern mantles[1] containing thorium nitrate, shown in figure 3.5 [43]. The second ones have a high activity and they are obtained from about 20g of material containing thorium oxide.

Figure 3.5: Lantern mantles used ad ^{220}Rn sources.

There were 16 available mantles and they were divided into groups to obtain sources with different activities. The same thing was made with the other material, in other words some sources with high activity are obtained separating the salts. Each thoron source is put in a cylindrical PTFE box, specially designed as shown in the scheme in figure 3.6. Inside this box there is a metallic grid united with a Tyvek layer, that contribute to fix the source geometry and to release from the box only thoron when it is open.

The thoron exhaled from these thorium sources is our ^{220}Rn source. Each sample containing ^{224}Ra has a certain emanation coefficient. By closing one of these sources within a reference volume, you get a thoron constant known activity concentration, making possible measurements on a long time

[1]The mantles containing thorium were invented by the Austrian chemist Carl Auer von Welsbach in 1884. The used butane gas in camping lamps (gas) burning emits, a light blue almost invisible during the day and slightly visible in the dark, to convert the heat into visible light it is necessary burn another substance. When it is burned in air, it emits a strong white light. To do this, he wove the wire gauze with a fabric resistant to high temperature enriched by small quantity of thorium, as hydroxide and thorium nitrate; the thorium, burning in the air, it emits an intense white light. Today, for reasons of safety, yttrium is used. It is less bright, but at least not radioactive. Radioactive mantles are still on the market in countries where they are permitted or are remnants of the old productions.

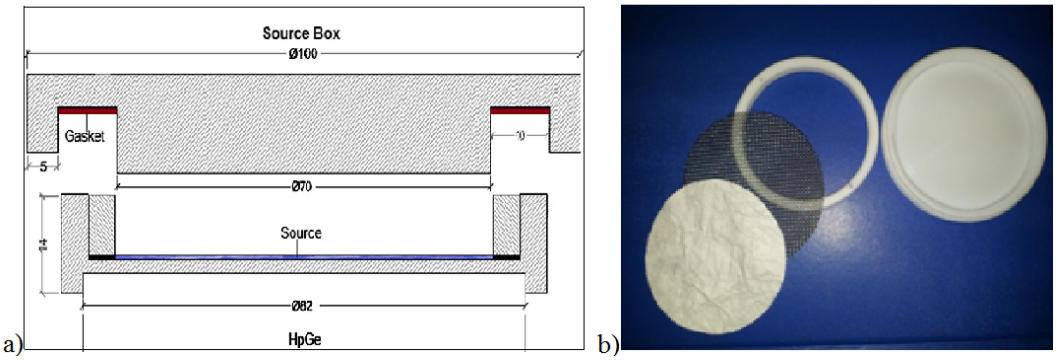

Figure 3.6: Dedicated cylindrical PTFE box containing thoron source. a) The box scheme for the measurement with HPGe detector; b) the disassembled box.

and overcoming the problem of thoron short life.
The method to obtain a reference thoron atmosphere consists of three steps:

- thoron measurements in equilibrium with its precursors;
- not exhaled fraction measurement from the sample;
- exhaled activity measurement by the difference of the previous measurements.

The thoron activity is always measured via the ^{212}Pb activity. More precisely, the methodology used for the development of a reference sample for thoron activity concentration can be divided in two step. The first step is the measurement of the activity concentration of the sealed source after 4 day, with germanium detector. This measurement is used to estimate the thoron activity concentration in equilibrium. In the second step, the box with salts is open. The measurement is made using also a high efficiency extraction system in order to remove quickly the exhaled thoron, as shown schematically in figure 3.8.

This extraction system is very important in this phase, because in this way the air flux carries far from the detector the exhaled thoron and its progeny and ensures that only the decay products of thoron not exhaled fraction have been measured. The extraction system has been monitored by background measurements before and after the unsealed source measurement [40]. This second measurement is used to estimate the activity of ^{212}Pb in equilibrium with thoron not emanated by the source. From the difference between these two measurements, the activity concentration of exhaled thoron

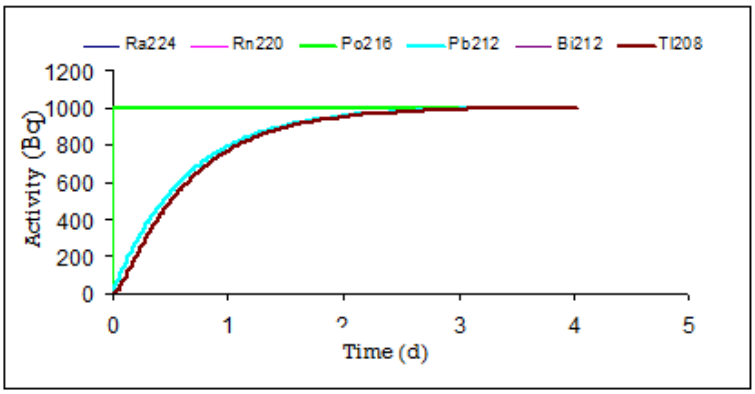

Figure 3.7: Activity trend of emanated ^{220}Rn by the source and its decay products in time. The figure refers to the activity in an airtight container.

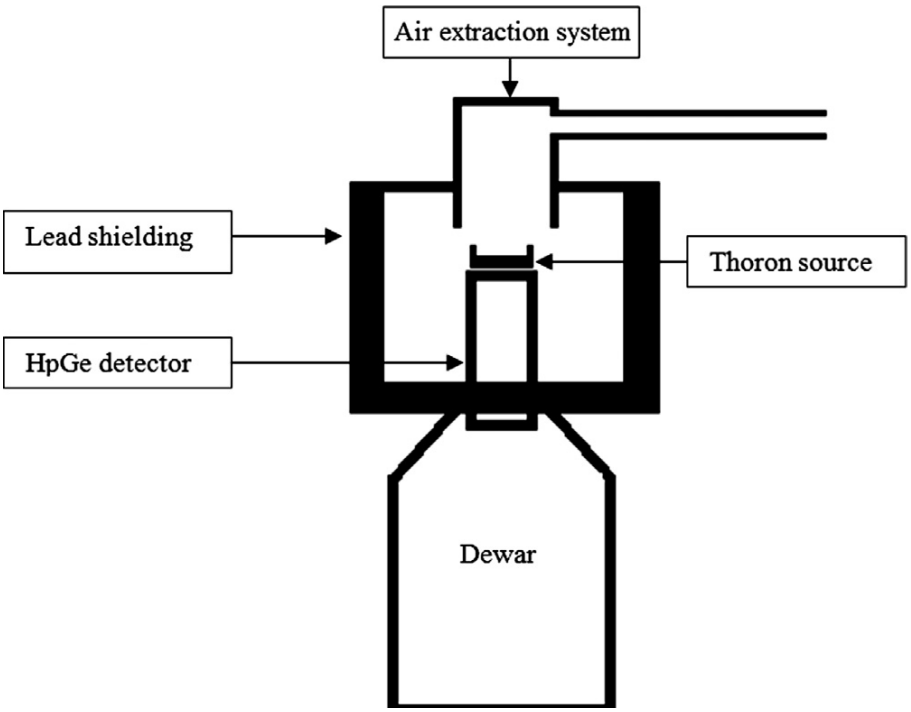

Figure 3.8: Scheme of the source-detector configuration with air extraction system [40].

is evaluated.
The thoron activity has been determined from the $300keV$ gamma line of ^{212}Pb; this line is not very intense, but it is not affected by interference phenomena. In mathematical terms, the exhaled thoron activity of the sample atmosphere, A_{220Rn}, is calculated as:

$$A_{220Rn} = \frac{[C_s(^{212}Pb) - C_u(^{212}Pb)]}{\epsilon_{HPGe}(300KeV) \cdot Br} \tag{3.3}$$

where $\epsilon_{HPGe}(300keV)$ is the germanium detector efficiency at $300keV$, and $C_s(^{212}Pb)$ and $C_u(^{212}Pb)$ are the count rates of $\gamma(300keV)$ of ^{212}Pb in the sealed and unsealed source configuration respectively. The detector calibration has been carried out using a standard γ source having the same geometry and the same density of thorium sources. From the efficiency curve, the efficiency value at 300 keV has been calculated [40].
The different thorium sources are reported in table 3.1.

Source code	A_{Rn220} Ehxaled Activity	Expanded uncertainty (k=2)
STh1	$(1.89 \cdot 10^3)Bq$	$(0.22 \cdot 10^3)Bq$
STh2	$(5.10 \cdot 10^3)Bq$	$(0.51 \cdot 10^3)Bq$
STh3	$(6.00 \cdot 10^3)Bq$	$(0.65 \cdot 10^3)Bq$
1MThA	$(1.3 \cdot 10^2)Bq$	$(0.6 \cdot 10^2)Bq$
1MThB	$(1.7 \cdot 10^2)Bq$	$(0.7 \cdot 10^2)Bq$
1MThC	$(1.6 \cdot 10^2)Bq$	$(0.7 \cdot 10^2)Bq$

Table 3.1: ^{220}Rn activity exhaled from the sources, A_{220Rn}, with budget uncertainty using a coverage factor $k = 2$. With "$STH\ldots$" the salts source are identified, while with "$MTh\ldots$", the mantles.

There is a second method for measuring the exhaled thoron activity. It is based on the direct observation of the disequilibrium between the first part of the thorium series and the second one, but it can be applied only if the secular equilibrium between thorium and its decay products in the source material is reached. This condition is only verified for the sample of thorium salts but not in the lantern mantles; for this reason, we preferred to use the previous method.
Putting this ^{220}Rn source in a know closed volume, a thoron sample atmosphere is realized. This source is used to calibrate internal monitor of the facility or other thoron detectors.

3.2 Calibration system

The objective of the sources production is the realization of known activity concentration atmospheres, in which one or both radon isotopes are present. These atmospheres samples, with a calibration facility, allow to characterize active and passive detectors.
As already explained in our laboratory two independent chain of traceability, one already existing for radon and the new one for thoron, are present. Using these two methodologies, stable and controlled atmospheres containing ^{222}Rn and ^{220}Rn can be developed. There are some important steps in the radon isotopes calibration chain. It is possible to divide these into four phases:

- production of a radon/thoron gas sample;
- sample measurement with a refered to national standard detector;
- gas transfer in the exposure chamber;
- measurement procedure.

Each step is an basic part of the measurement and it is necessary for traceability. All the different phases must be kept under control and be repeatable to allow to report the measurement to the initial standard.
Let's start analyzing the calibration facility in more detail.
In the facility shown in figure 3.9, all components of the apparatus are disposed along a circuit through which gas flows [22]. It is divided into two fundamental sections. The first one is linked to the weather parameters management, the second one is the exposure chamber, that is the reference monitor of the whole system.

The facility elements are connected with PTFE tubes, with inner and external diameter respectively of $6mm$ and $8mm$. Each facility part is tightly sealed with respect to external air. The total system is composed by:

- a membrane pump *KNF model N 726 FTE*, to carry the air or radon gas with a maximum flow rate of $15 l min^{-1}$;
- a system to connect radon source, namely glass ampoules containing radon source;
- a humidier and dryer sytem that allows changing the humidity into the air circuit in a controlled way;

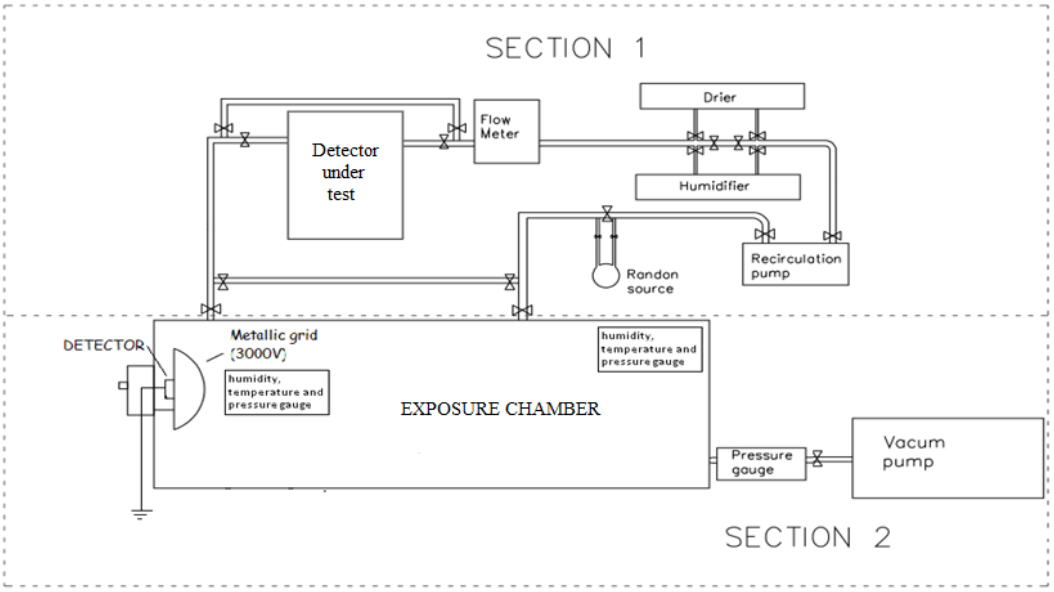

Figure 3.9: Calibration facility scheme. The section one is linked to the weather parameters management, the second one is the exposure chamber.

- an electronic flux-meter with relative controller *MKS Mass Flow Controller 1179A*, able to vary the air flux up to $1 l min^{-1}$ with uncertainty smaller than 0.5%.
- a pressure gauge *MKS Baratron 626A*, to measure the pressure in the circuit with good precision; its uncertainty is about 0.1% in the range $[1 - 100]\, kPa$;
- a vacuum pump, used to clean the circuit and to reach a fixed pressure value into the system.

Before the radon source inlet in the system, and before each measurement, it is necessary to clean the circuit. It is done via dry and aged air, that is radon and humidity free. The cleaning is made by pumping the air until a $10 mbar$ vacuum is reached. After that the volume is filled with aged air taken from a gas bottle previously connected with the circuit.

3.2.1 Weather parameters management

A calibration facility section controls and stabilizes the environmental parameters values. In particular, it controls the pressure and the humidity, while

the temperature of the apparatus corresponds to that of the room, which is controlled. A continuous monitoring for all these parameters is provided. In this way it is also possible to characterize, as a function of these parameters, radon detectors inserted in the circuit, or in the exposure chamber.
With respect to the pressure, using the pump you can change it into the circuit and reach the chosen value measuring the pressure gauge. Due to a good seal of the system, the value remains almost constant; in any case the variations are monitored also via the sensor inside the exposure chamber.
The Perma Pure flexible pipes allow to regulate the atmosphere damp level in exposure chamber. This system is shown in figure 3.10, that represents a small part of the total circuit.

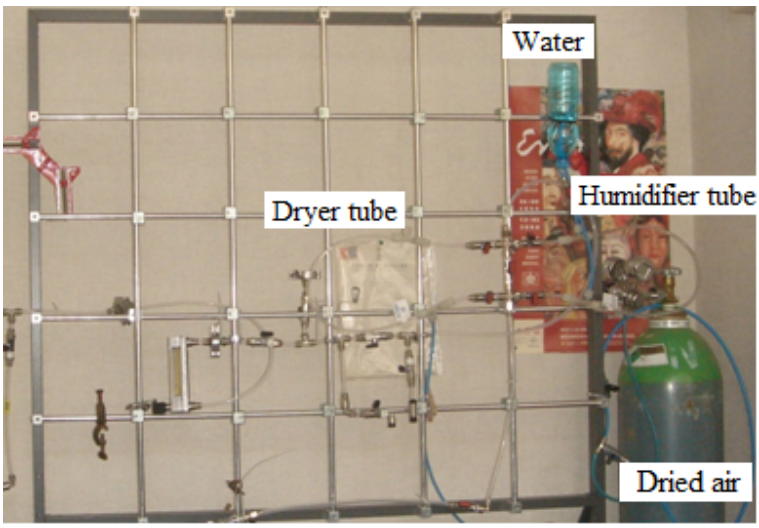

Figure 3.10: Drying and humidifying system composed by Perma Pure flexible pipes.

With both dryer and humidifier, it is possible to regulate humidity variations from 20% to 80%. Both of them are composed by two concentric tubes, the inner one made by nafion membrane. The humidifier mode is based on permeation principle, namely the nafion membrane ability to allow water to permeate. The sulfonic acid present in the nafion, indeed, has an high hydration degree. The water comes from an external beacker and joins to gas in the form of steam. The processes are allowed due to the pressure difference inside the concentric tubes. The water molecules are absorbed from the wall of the internal tube and then are released in the gas flux. The gas dryer uses exclusive Nafion permeable membrane tubing to continuously dry gas streams, removing only water vapor. Water molecules permeate through the Nafion tube wall, evaporating into the purge gas stream. Also in this

case, the different water concentration between the two gas streams drives the reaction, quickly drying the air or gas. The purge gas is the dry air.

3.2.2 Exposure chamber

The exposure chamber is where the known activity concentration atmosphere is produced. It is constituted by a steel cylinder by volume $(32.7 \pm 0.7)l$, shown in figure 3.11.

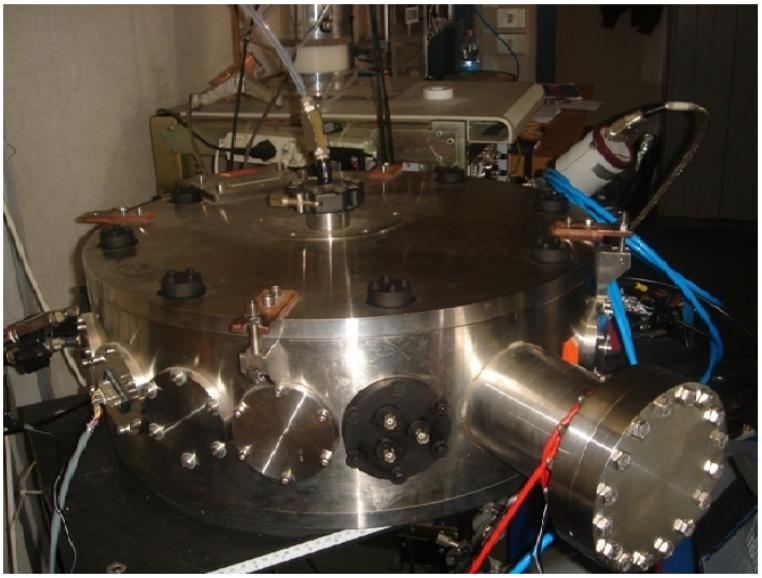

Figure 3.11: Exposure chamber.

Inside one detector, some sensors for the monitor of temperature, humidity and pressure and several valves for the entrance and the exit of gas from the chamber are present. In particular there are fan systems for the gas recirculation. The fans create the air flow in circuit to redistribute the air, in order to have a gas uniform distribution inside.
After the sources measurement via the gamma spectroscopy, there is a different process to transfer them into the chamber. For the radon, the gas ampoule is connected to the circuit fitting. After that, the ampoule tap can be opened to allow, through the membrane pump, the radon entrance in the facility. Differently, the thoron sources are directly put in the chamber due to their extremely short mean life.
The fan system developed allows to move the exhalated thoron from the source surface to the total chamber volume and then the uniform gas distribution. In this case, the external circuit for the gas transport is not used, so

you can not adjust the humidity within the chamber. Otherwise the detectors exposed, in the transient phase, would see variables humidity values. In mixed atmospheres case, when both radon isotopes are present, the limitations due to the typical exposure to thoron remain.
From previous study, the chamber homogeneity was checked using an active system based on the installation of electrodes inside the chamber to measure the ionization current produced by the radiation of the entire volume, as well as via the passive detectors, E.Perm[2] and LR-115[3], inside the chamber. The results are better than 10% for the radon and 15% for the thoron [37]. After the mixed atmospheres creations using both the different methodologies for radon and thoron sources, other homogeneity tests has been performed using sixteen LR-115 detectors uniformly placed on the bottom of the chamber and exposed for three days. After the exposure, the measurement of tracks density gives us the activity value, due to their proportionality. The standard deviation of results, for the thoron, is 12% that represent an upper limit in the estimation of homogeneity [40]. In the figure 3.12 the result obtained by this last passive measurement is reported.

The most important part of the calibration facility is the internal monitor of the exposure chamber. It is a detector, an Ortec ULTRA ion-implanted solid state, based on the electrostatic collection on silicon detector, as we can seen in figure 3.13.

It is composed by a spherical cap, constituted by a metal mesh, at high voltage ($1500V$) closed around a silicon detector electrically isolated from it [4]. The detector, at $50V$, is grounded together with the chamber radon walls. The active surface and the active thickness of the detector are respectively $100mm^2$ and $100\mu m$. The force lines of the field within the volume are directed by the grid towards the detector, outside ranging from hemisphere

[2]An electret detector consist in a charged Teflon disk carrying a stable electric charge mounted at the bottom of a sampling chamber whose air inlet is filtered at the entry. The filters allow the entry of radon or thoron, excluding their progeny and dust particles. Radiations coming out from radon and its progeny borns inside the chamber generate ions that can be collected by the electret [46]. In this case the charged disk is not only a sources of the electrostatic field, but also as a radiation sensor.

[3]The LR-115 detectors are alpha track detectors, they are based on film Kodak LR-115 SSNT (Solid State Nuclear Track). The LR-115 film has a special nitrocellulose coating ($12\mu m$) on a polyester base ($100\mu m$). The film sensitive part is covered by a aluminate mylar layer of $6\mu m$, necessary to increase the detection efficiency of alpha particles with energy between 6MeV and 9 MeV.

[4]From previous studies, in order to choose the optimal collection voltage, the measurements were performed with constant activity concentration by varying the collection voltage. To control the collection as a function of voltage, the ^{216}Po is used because it reaches immediately the equilibrium with the thoron and having half-life very short $0.15s$, it gives no accumulation problems on the detector.

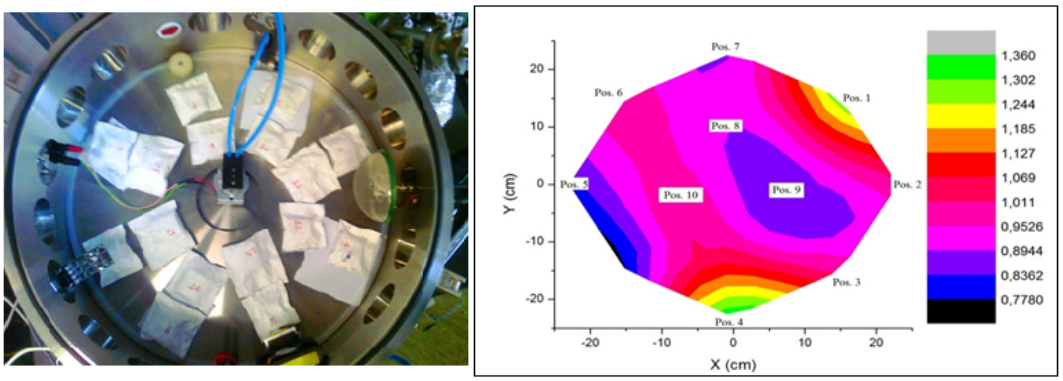

Figure 3.12: On the left side, there are the LR-115 detectors into the exposure chamber in order to analyze its homogeneity; on the right side, the thoron activity concentration map, as measurement result.

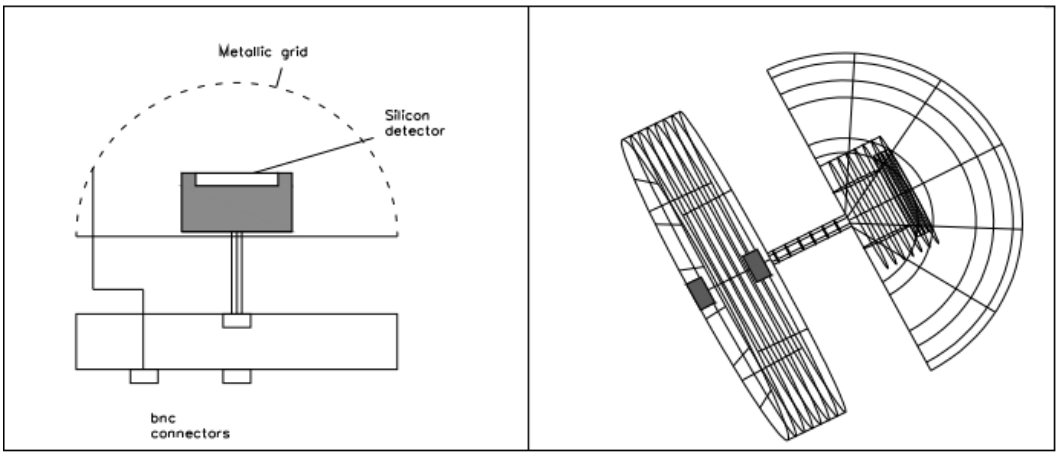

Figure 3.13: Internal monitor of the exposure chamber [37].(in realt TESI non articolo)

towards the chamber walls. This allows the electrostatic collection of radon decay products, formed within the volume of the detector, but also the shield of the decay products that decay outside of it. In any case, a Tyvek layer around the active volume can stop the radon daughters, as shown in the following section. This material, in fact, allows the entry of thoron or radon, while filters their decay products. It is a material composed by polyethylene fibers of high density, very resistant but easily to be cut. Moreover, this material is highly breathable, while it is waterproof. For these characteristics the Tyvek is used in a variety of industrial applications: envelopes, air filters and barriers to delete water intrusion, labels, roofing for buildings, etc [44][45].

3.2.3 Measurements and results

After some time from the radioactive gas transfer into the exposure chamber, the equilibrium between sources radon isotopes and their decay products is reached. This time interval has to be calculated measuring the radon/thoron content inside exposure chamber and verifying that the concentration, corrected for decay, remains constant. Using the internal monitor, it is possible to follow the radon daughters trends as a function of the time. In the thoron case, as we can see in figure 3.14, the source is directly put inside the chamber, so there is not a data correction for decay.

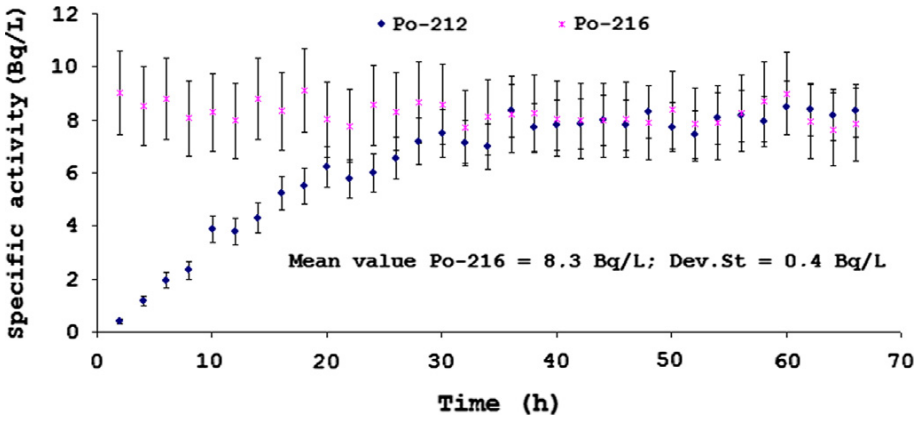

Figure 3.14: Specific activity as a function of time for ^{216}Po and ^{212}Po, after the thoron source positioning in the exposure chamber[40].

A typical thoron alpha spectrum is reported in figure 3.15. The counts distribution on the right of ^{212}Po line is due to random coincidences between

its alpha particles from this polonium isotope and beta particles emitted by the ^{208}Tl.

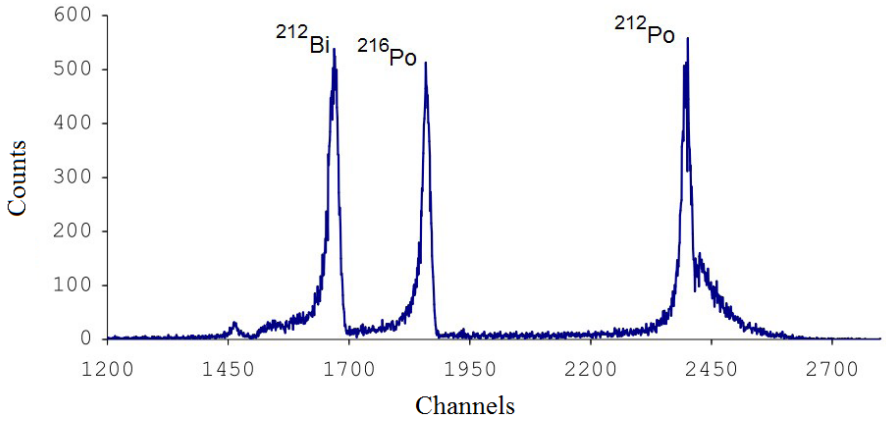

Figure 3.15: Typical spectrum of Rn220 . The counts distribution to the right of line of Po212 is due to random coincidences between its alpha particles and beta particles emitted by the ^{208}Tl.

The typical alpha spectrum of the exposure chamber monitor has the same characteristic of the one of the Ramona device, being both of them electrostatic collection detectors, but it has a smaller efficiency due to its reduced sampling volume. The use of known activity concentrations allows to calibrate our system, by the calibration factor evaluation for each radon decay product.
The spectra are acquired by the system by cyclical measurements with a fixed acquisition time. For each spectrum, the count rates of alpha emitted by the radon/thoron daughters (cps_{21i}), defined as the ratio between the peak area and the acquisition live time, are corrected for decay and reported to a fixed time, as in the gamma measurements. The calibration factors ϵ_{21i} are then calculated using the following relation:

$$\epsilon_{21i} = \frac{cps_{21i} \cdot V}{A} \tag{3.4}$$

where V is the active volume, A is the radon (or thoron) activity concentration (in Bq), previously measured by gamma spectroscopy. The subscript "$21i$" indicates the specific decay product, for example cps_{218} means the ^{218}Po counts. The calibration factor dimension is then $[(cps \cdot l)/Bq]$.
In the calibration factor evaluation, it is important take into account that the radioactive equilibrium with radon is reached after about 20 minutes if we use the ^{218}Po peak integral area because this nuclide has a short half-life

($3.05min$); while approximately 5 minutes are needed to reach the equilibrium with thoron, for the very short ^{216}Po half-life ($0.15s$).
The calibration and characterization of the reference monitor is the most important step for the traceability of the made atmosphere at metrological standards. To achieve these goal, many exposures of passive detectors have been carried out individually for each gas, as well for mixtures. An example of alpha spectra of radon and thoron daughters, both present in the exposure chamber with two different initial ratios, is shown in figure 3.16.

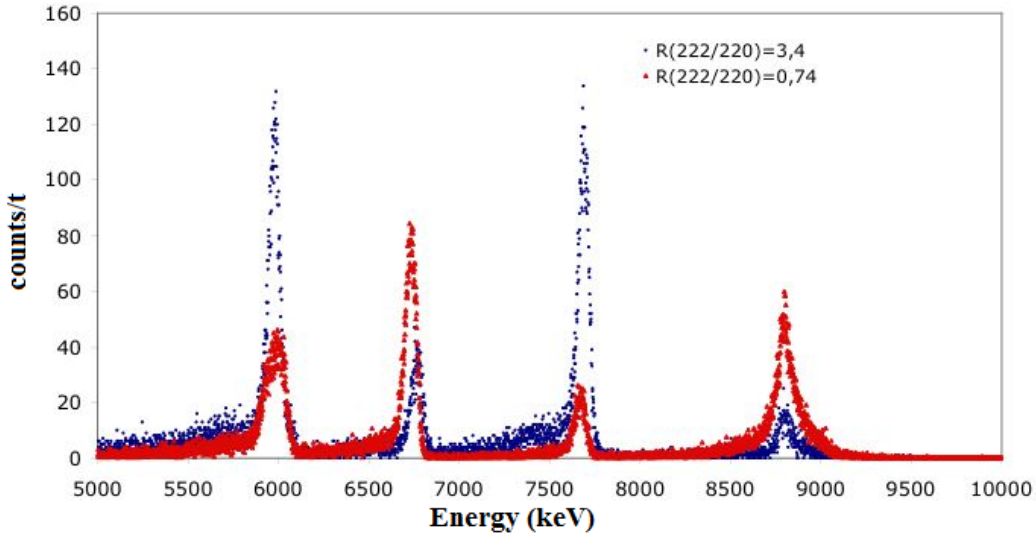

Figure 3.16: Two alpha spectra of radon and thoron daughters both present in the exposure chamber with different ratios. the acquisition time is 30 minutes.

The use of an internal monitor for exposure control becomes indispensable in the case of mixed atmospheres, where each isotope can be considered an element of noise for the other. The case of the ^{218}Po line to $6MeV$, very close to that of ^{212}Bi at $6.1MeV$, is particularly interesting as example of this phenomenon. This effect can be offset only by the high resolution spectroscopic separation combined with the patterns knowledge of concerned nuclides decay or by analytical procedures.
In a spectrum produced in a mixed atmosphere, the low energy tails of each line creep beneath the other ones. In case of presence of a single radon isotope, these tails (backgrounds) are quantifiable and eliminated from the counts. They have indeed a dependent weight on the decay chain to which

the radionuclides observed belong and therefore they are determinable and constant. In case of mixed atmospheres, this last assumption is not confirmed. The corruption degree, although defined at every instant, varies over time due to the presence of the two isotopes decay progeny with very different half-lives. This situation is very clear in figure 3.17: the rate decreasing trend of the ^{216}Po, which must be constant because it is produced continuously inside the chamber, is not due to a loss of the chamber itself, but it is caused by the decreasing tail contribution of the^{214}Po alpha line, which comes from the radon and then decreases with its half life .

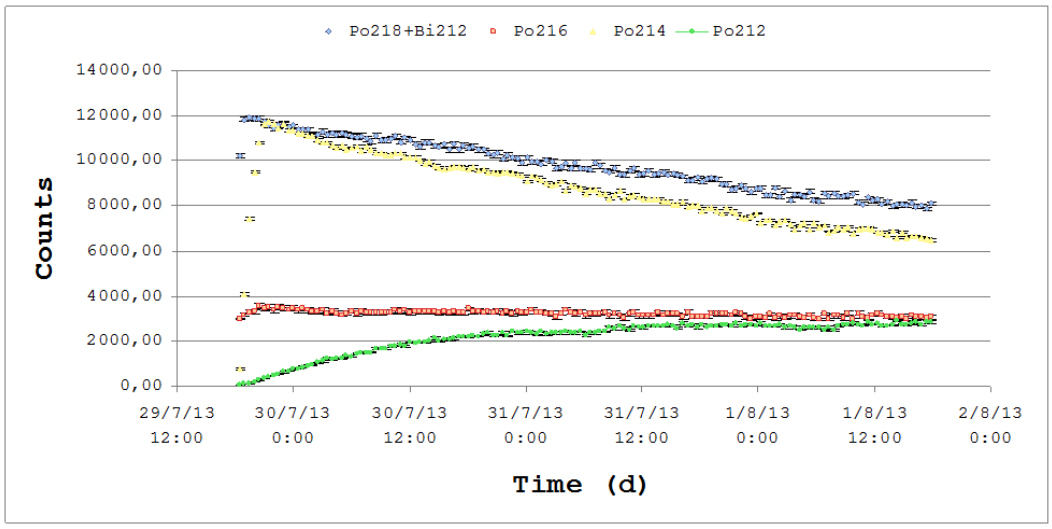

Figure 3.17: Counts of radon and thoron daughters as a function of time for a mixed atmosphere in the exposure chamber.

The figure 3.18 shows the same measurement reported in the figure 3.17, but displays the trend of the count rate, *cps*, after decay correction. The ^{218}Po count rate, cps_{218}, is obtained by subtraction the ^{212}Bi count rate. The rate of ^{212}Bi is calculated as fraction (one-half) of ^{212}Po rate on the branching ratio basis.

In general, the presence of both radon isotopes and their different ratio influences the background tails, that are significantly different in the two cases shown in previous figure 3.16. This diversity naturally changes over time and with it the spurious contributions on the measured lines intensities. This means that the contributions can not be reduced to a fixed percentage, but they should be recalculated in the time, for each spectrum, and in any case would be affected by an additional uncertainty, arising from the detector resolution and from the acquisition system dynamics. The data analysis

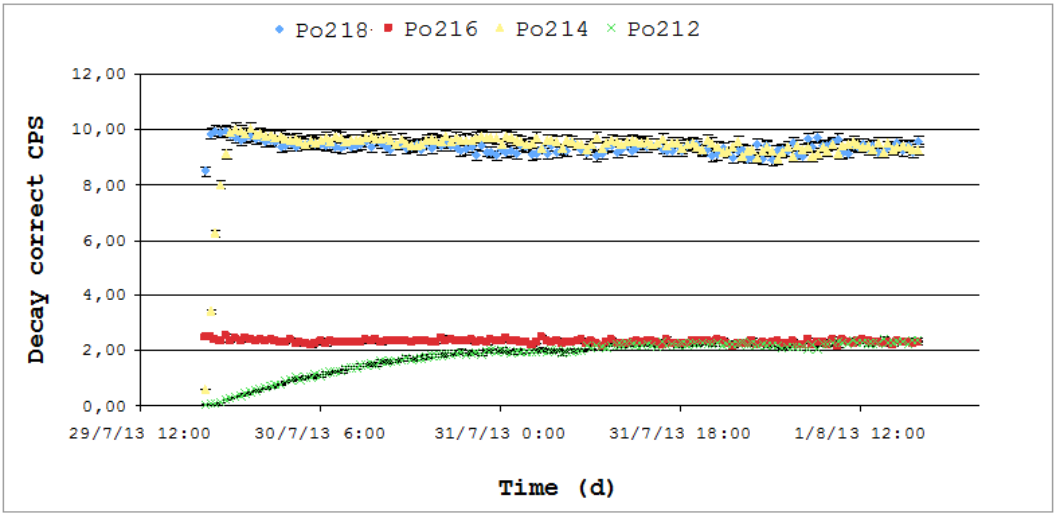

Figure 3.18: Counts trends of radon and thoron daughters for a mixed atmosphere in the exposure chamber, after the decay corrections.

takes into account the particularities of each measurement through the spectrum fit with a series of Gaussian functions and the growing exponential. In this way it is possible to calculate the peaks areas and the net background contributions.
A Tyvek layer stabilizes the efficiency of internal monitor. The figure 3.19 shows the different calibration factors values obtained without and with the use of this filter. The values obtained without the Tyvek filter are not constant and seem to be dependent on the specific activity of the radon. This can be due to the entry of the decay products not in equilibrium with radon in the active volume of the monitor. In the measurements, the better stability and also the independence of its response of the specific activity in the interval considered is evident. This result confirms the Tyvek filter effectiveness.

This approach on the mixed atmosphere measurements leads to the calibration factors for our facility, obtained by the study of three polonium isotopes at different specific activities in the range $(14 \div 665) Bq/l$ and shown in the table 3.2.

As explained before, previous characterization studies have made possible to estimate the dependence of the efficiency as a function of environmental parameters and, therefore, measure and compensate their influence [22]. For all the results shown in this paragraph, the system is used in fixed climatic parameters conditions. In particular $(25.5 \pm 0.5)^oC$ for the temperature, $(100.3 \pm 0.2) kPa$ for the pressure and $(48 \pm 4)\% HR$ for the humidity. The

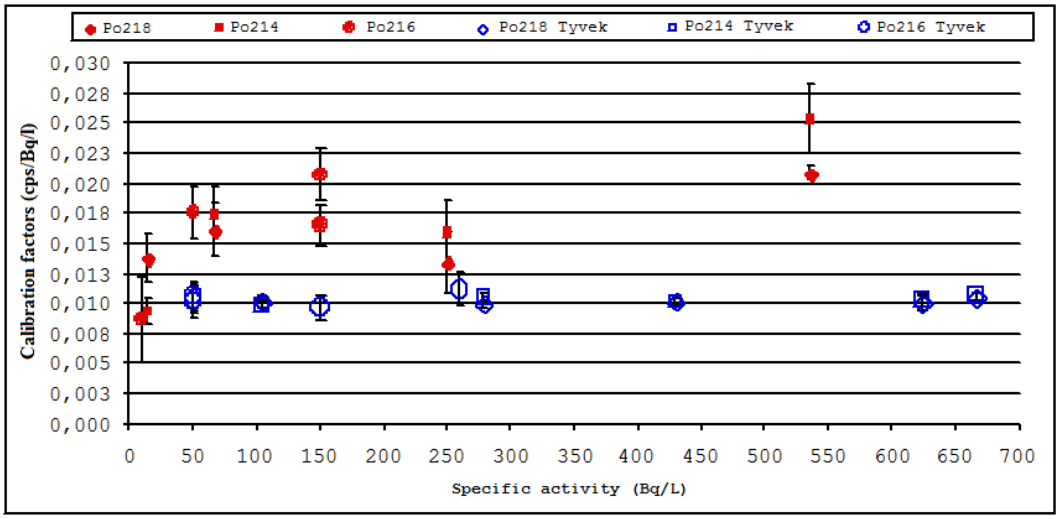

Figure 3.19: Calibration factors values, for the exposure chamber, obtained without and with the use of Tyvek filter.

Polonium ion	Calibration factor $[(cps \cdot l)/Bq]$	Standard deviation $[(cps \cdot l)/Bq]$	% Error
^{218}Po	0.0100	0.0002	2
^{214}Po	0.0102	0.0004	4
^{216}Po	0.011	0.001	8

Table 3.2: Calibration factor values of the three polonium isotopes.

study of the their influence will be investigated in the next future.
Presently the chamber is equipped with a system that permits the control and the regulation of environmental parameters, but soon it will be equipped also with a monitor of the aerosol characteristics and with an active instruments for the homogeneity measurement.

3.2.4 First application of calibration facility

Some measurements have been performed in order to calibrate the upgraded RAMONA device, but they will be shown in the next chapters. Another commercial detector has been tested with our facility. The reason of this test is the upgrade for the thoron measurement. This active detector does not perform the spectroscopic analysis, but it obtains activity measurements of both radon isotopes through particular algorithms. To verify the new procedure for the thoron measurement, the manufacturing company sent us a detector. The results of these tests are shown in the plot in figure 3.20. It is possible to note a good agreement for radon measurement between the detector under test and the reference monitor; when only the thoron is present, the activity concentration is underestimated, probably due to a not correct background subtraction.

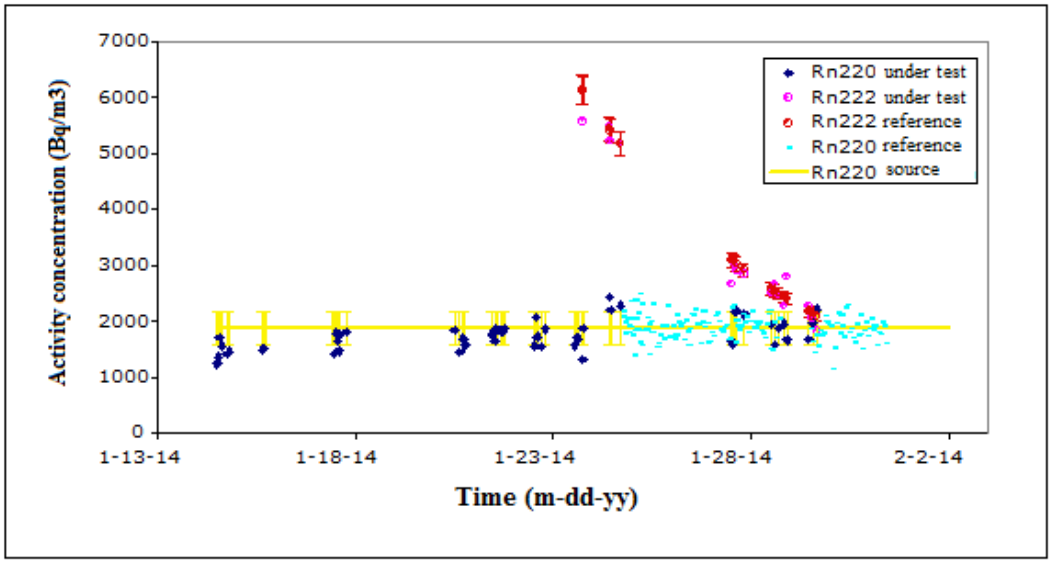

Figure 3.20: Radon isotopes activity concentration versus time both for the facility internal monitor, both for detector under test. In the first part of the measurement there is only the thoron gas, the blue points are the measured value form detector under test, while the yellow points indicate the source value. In the secon part, the radon gas is introduced into the chamber; the red points are related to the radon reference measure, while the pink ones represent the measurements with the tested detector.

Chapter 4

RAMONA upgradings

Part of this work is focused on RAMONA upgrade aimed to allow the device operation in environments characterized by non-standard weather and environmental conditions.
The presence of sensors inside the RAMONA chamber gives the possibility to study and monitor climatic parameters, such as temperature, pressure and air humidity, which influence radon daughters collection in a significant way, as already explained in the previous chapters.
However, there are particular situations in the radon measurements outside the laboratory, in which it is very important to change the gas condition to be detected. These are the cases in which parameters like gas humidity and temperature not only condition the ions collection on the detector, but also the device operation itself. Sometimes during the monitoring of the soil gas, the device is forced to work for long time under conditions that damage the device itself.
In this cases, like the volcanic areas, the sites are indeed characterized by extreme environmental conditions for the presence of corrosive gases and water vapor, so the radon monitoring with the actual technology becomes very hard. This is exactly the case of the Phlegraean Fields: a particular seismo-volcanic area, frequently subjected to bradysismic events, in which we want to realize an active monitoring network. In this chapter some improvements relative to RAMONA device are presented.

4.1 Monitoring in "hostile" environments

To monitor the radon in "hostile" areas it is necessary to develop some prevention systems. Such systems could prevent the gas to reach an extreme measure condition into the detection chamber, via methods for the reduction

(killing) of gases that damage the electronic of the detector and through the creation of a protected environment for the electronic components. In the following section the operations linked to the hostile environmental parameters are analyzed.

4.1.1 Temperature

It is well known that the high temperature complicates the device operation by producing noise in the silicon detector and in the electronic components and by damaging the materials composing the chamber and related to the system seal.
When the radon measurement is carried out in presence of corrosive and hot gases, some procedures are need to prevent the device damage. In our case, the chamber is modified in order to create an hermetic separation between the collection volume and the electronic components.

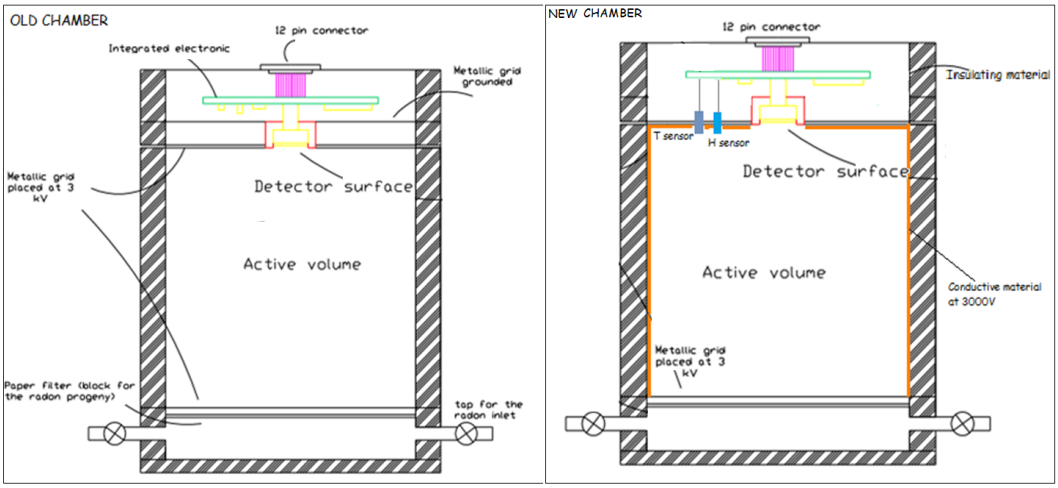

Figure 4.1: In the left side of the figure, there is the old project for the collection chamber structure; on the right side, an hermetic separation between the collection chamber and the electronic components is shown in the new chamber project.

As shown in figure 4.1, the materials related to the chamber structure are insulating and light and inside the collection volume only detector and environmental parameters sensors are positioned.

4.1.2 Pressure

The pressure is not a parameter significantly variable during a radon activity measurement. In fact it is linked to the place altitude in which the measure-

ment is performed. It is important to test the device performances during a continuous monitoring at not standard pressure to understand if a system upgrade on this point is needed as well.
Thanks to a collaboration with the Argo experiment, five RAMONA devices have been installed in Tibet, where the pressure is about $600mbar$. The reason of this application is the evaluation of the background variations induced on the RPC detectors of the ARGO experiment by radon and thoron daughters [47].
Before starting the measurements in the Tibetan soil, some tests on the collection voltage were made in our laboratory. One of the test results is reported in figure 4.2.

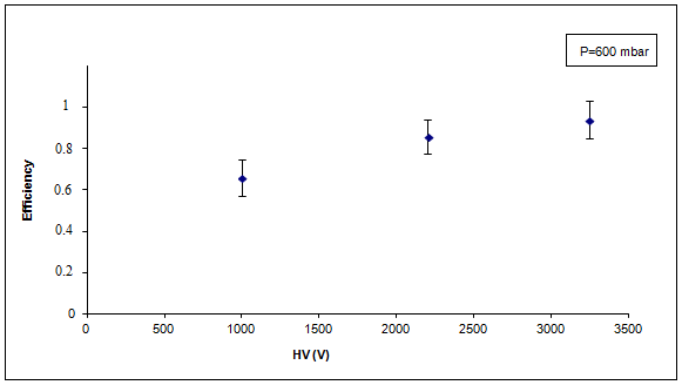

Figure 4.2: Efficiency as a function of the collection voltage for a fixed pressure value, $P = 600mbar$.

These tests were performed for all the chambers involved in this experiment and were aimed at fixing the optimal high voltage value for the electrostatic collection so that the efficiency is approximately equal to that at standard pressure and discharges do not occur. The chosen working point is at $1500V$.
The RAMONA devices are shown in figure 4.3.

In the plot in figure 4.4, the radon daughter concentrations as a function of time are reported for one of the five measure point. These variations are small in comparison to the typical ones in the seismo-volcanic sites.

These measurements prove that our monitoring system works without problems at very low pressure and in general in the pressure range between $(550 \div 1100)mbar$. Therefore there is no need to improve on this parameter.

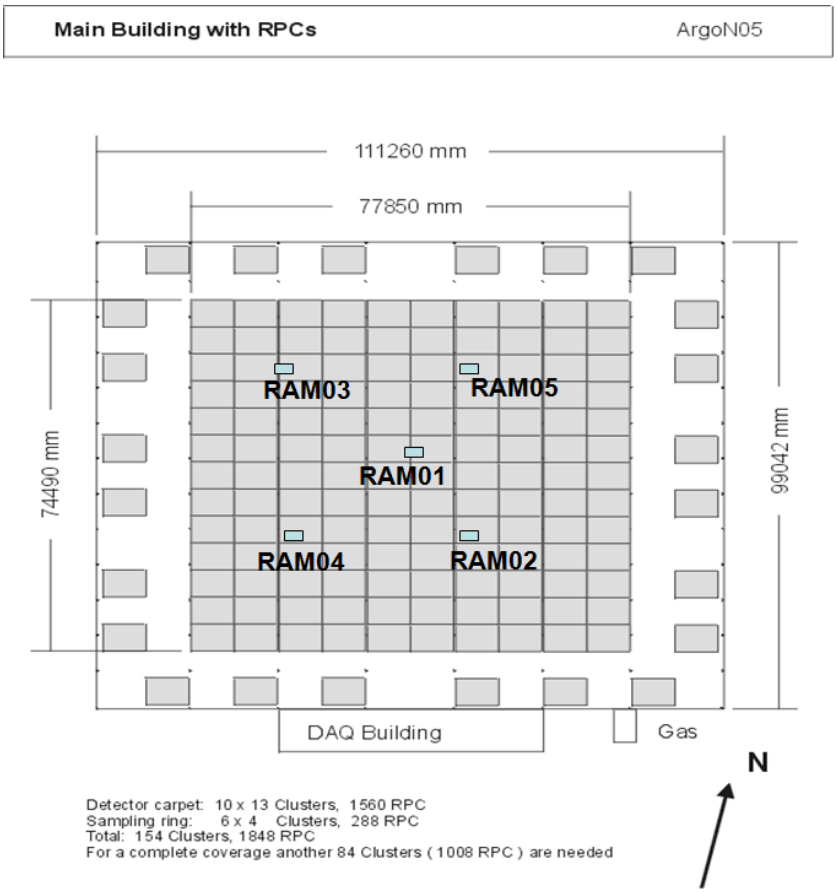

Figure 4.3: Scheme of the main building with RPC and the RAMONA positions for radon monitoring.

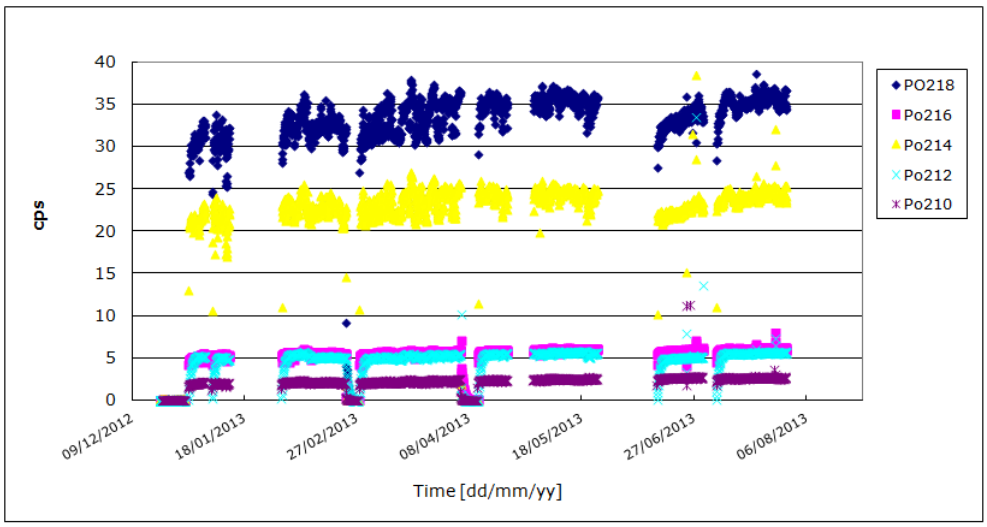

Figure 4.4: Radon monitoring in Tibet. Count rates of the radon daughters as a function of the time.

4.1.3 Humidity and corrosive gases

The development of methods for the reduction of "hostile" gases and humidity is performed to achieve good gas conditions into the radon chamber, in order to prevent damages to the electronics and to the detector. To reach this aim, the usage of many tools is needed. An ideal system should be composed by a cold trap and two and gas drying units, that are based on physical and chemical operation principles, as shown in figure 4.5. Only one part of this apparatus is not completely efficient to make measurement in "hostile" environment, as volcanic site.

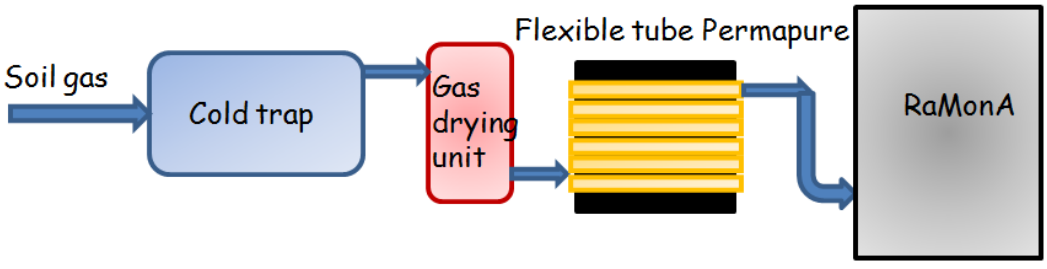

Figure 4.5: System to reduce the hostile gases and humidity into RAMONA chamber.

A cold trap is a device that condenses all vapors. It will be realized by a

container whose walls will be cooled by pipes with liquid at low temperature. When the gas will cross it, it will condense and it will be free by big part of the water.
A DRIERITE tube is a good tool as gas drying unit. DRIERITE desiccants are made from the naturally occurring mineral, gypsum (Calcium Sulfate) and are available in several varieties designed to solve drying problems. Indicating DRIERITE gives constant visual assurance of active desiccant. When active, indicating DRIERITE is a distinct blue color. When exhausted, it turns pink.
Particular attention has been given to the third stage of the dehumidifying system. Many tests have been performed on the *Perma Pure* MD^{TM} – *Series* gas dryer, already explained in the previous chapters. The gas dryer uses exclusive Nafion selectively permeable membrane tubing to continuously dry gas streams, removing only water vapor. Water molecules permeate through the Nafion tube wall, evaporating into the purge gas stream. The different water concentration between the two gas streams drives the reaction, quickly drying the air or gas. Purge gas should be dry air or other gas. The general features of this system are summarized in the following points:

- only water vapor is removed;
- low dew points are achieved;
- no electricity is required;
- No moving parts;
- Excellent resistance to corrosion;
- Low pressure drop.

The performed tests affect the seal of a Perma Pure dryer tube one meter long. Its radon losses have been evaluated through two different methods: gamma and alpha spectroscopy. In the figure 4.6, the configurations for both the measurements are shown, on the left side for the gamma spectroscopy, while on the right side for the alpha measurement. As the tube is composed by two concentric tubes in turn, the inner one made by nafion membrane, the tests must investigate on both the components.

The first test was about the total seal of the tube. For both methods, the pipe was filled with a known radon activity and the results were good and in agreement with each other. Taking into account the decay law and bringing back the date to the same time, the gamma spectroscopy results showed a constant activity inside the tube, as appears in the figure 4.7.

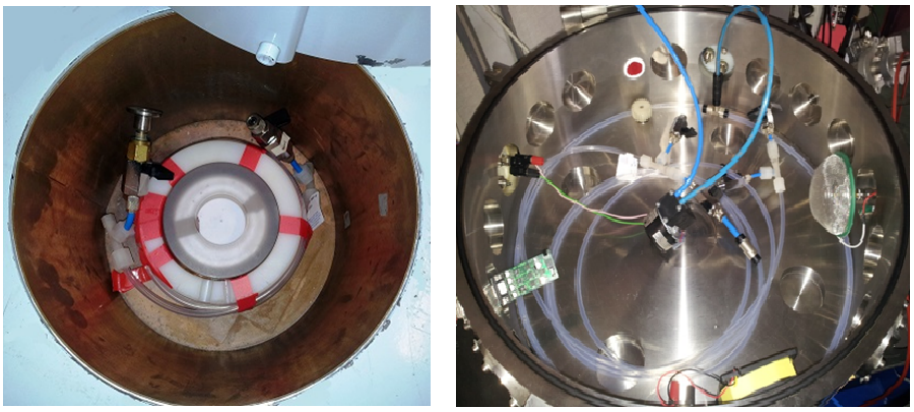

Figure 4.6: The Perma Pure dryer in the configuration for the gamma spectroscopy on the left side, for the alpha spectroscopy on the right side.

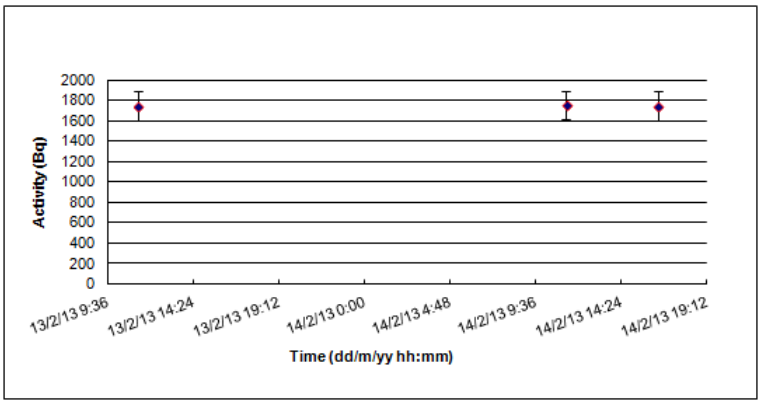

Figure 4.7: Constant activity inside the tube as result of the gamma spectroscopy.

The total seal of the tube was investigated also through the alpha spectroscopy, putting the pipe into the exposure chamber; this method showed that the measurement of radon daughters is comparable with the chamber background.
The Nafion membrane seal has been tested only using alpha spectroscopy. After the insertion of the tube filled with radon inside the exposure chamber, it has been evaluated how much radon comes out from the pipe, when it dries the gas. In this case, the detector shows the radon daughters that crossed the Nafion membrane and entered the chamber for diffusion. The result, shown in figure 4.8, reveals that the lost activity is $\approx 0.005 Bq/h$, which is negligible compared to the usual radon activities.

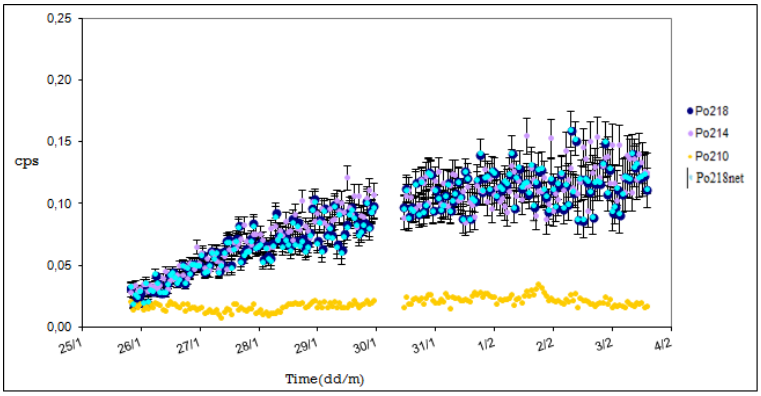

Figure 4.8: Lost activity by nafion membrane, evaluated by alpha spectroscopy.

4.2 New chamber development: exhalator

To work in environments where the soil gas is too rich of corrosive gases and water vapor, a different collection chamber might be convenient. For this reason, a new chamber without bottom was realized, so the gas enters the chamber by direct exhalation from soil surface. In this way the gas flux in chamber is reduced in comparison with the case in which the gas entry is forced by pump. As it is also possible see in figure 4.9, this chamber is made by a plastic material, with a metallic grid inside at high voltage such to permit the ions collection, while the electronic board and the silicon detector are the same of RAMONA.

Before studying the chamber performances in the field, has been necessary to develop a method to calibrate it.

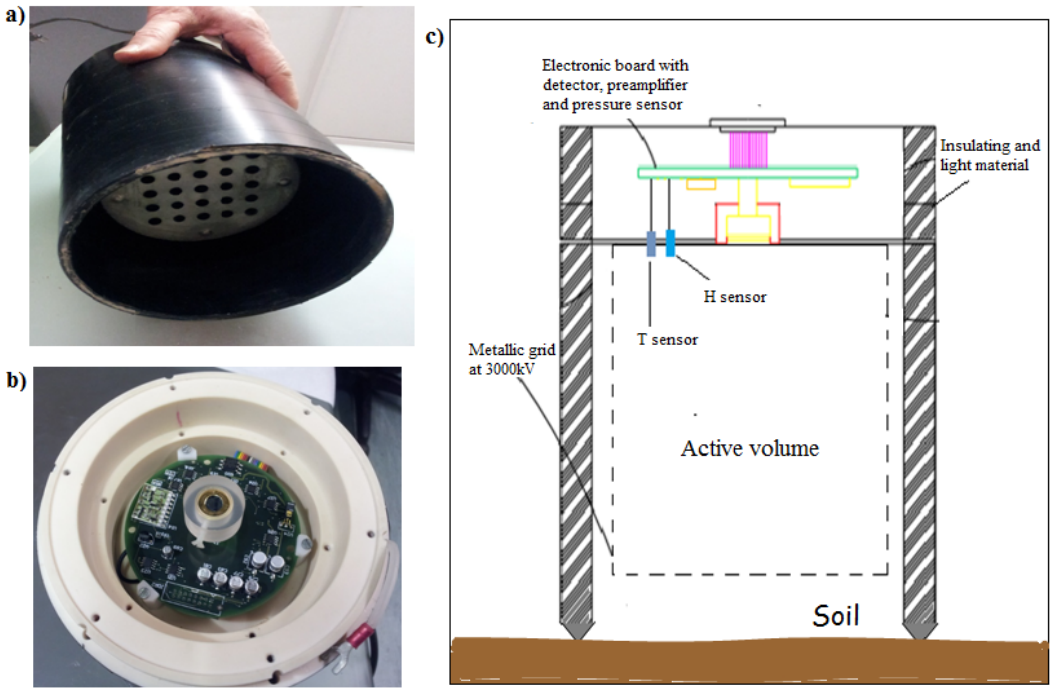

Figure 4.9: **a)** Exhalator chamber; **b)** electronic board with silicon detector on the chamber top part; **c)**scheme of the new chamber.

4.2.1 Calibration method

For the calibration, a soil sample from Mt.Olibano, in the Phlegraean area, was used.

After removing the soil sample from the ground, it was only reduced to a grain of $2mm$, without oven passage typically employed during emanation and exhalation measurements. The sample was partly used to evaluated the concentration of radon isotopes activity in equilibrium with their fathers (radium and thorium); the remaining part of the sample was used to calibrate the new chamber.
To analyze the soil sample a dedicated chamber, based on the same operation principles of Ramona, was used. It consists of two metal cylinders, both of them with internal volume equal to $0.83l$. In the configuration for the emanation measurements, a metal grid is inserted between the two cylinders to separate the volume containing the sample, positioned in the the lower part, from the collection volume, as shown in figure 4.10.

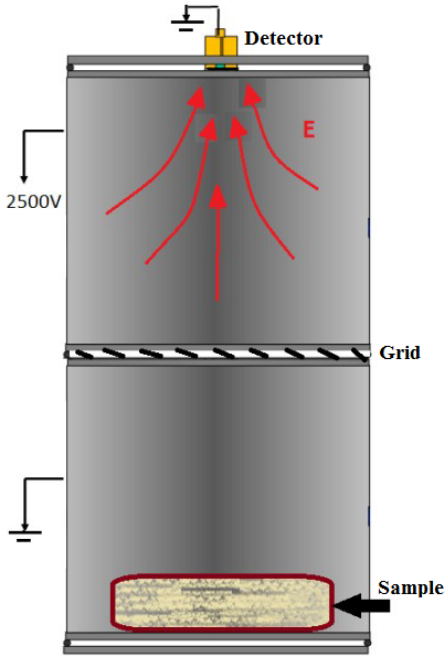

Figure 4.10: Collection chamber diagram for the emanation measurement [48].

The calibration factors of this chamber for the detection of radon isotopes decay products are reported in table 4.1.

If a soil sample to be analyzed, has dimensions smaller than the radon dif-

ϵ^{218Po}	$(0.25 \pm 0.02) cps/Bq \cdot l^{-}1$
ϵ^{214Po}	$(0.26 \pm 0.02) cps/Bq \cdot l^{-}1$
ϵ^{216Po}	$(0.0054 \pm 0.0005) cps/Bq \cdot l^{-}1$

Table 4.1: Calibration factors for the emanation chamber [48].

fusion distance[1] L in a medium, so that all the issued radon in the interstitial spaces of the sample will be exhaled [49], is put into a electrostatic collection chamber hermetically closed, the radon growth in time, until equilibrium is reached in the chamber itself, is expressed by the following equation:

$$\frac{dC(t)}{dt} = \frac{E_{Rn}}{V} - \lambda C(t) \tag{4.1}$$

where, assuming that the initial concentration is zero because the soil sample is not yet in the chamber, E_{Rn} is the exhalation velocity of the radon (Bqs^{-1}), $V = V_{tot} - V_s$ is the chamber volume minus the sample volume and λ is the radon decay constant.
The solution of this equation is:

$$C(t) = \frac{E_{Rn}}{\lambda V}(1 - e^{-\lambda t}) \tag{4.2}$$

where $E_{Rn}/(\lambda \cdot V)$, expressed in Bq/m^3, is the highest exhaled concentration from the sample, that is the value to compare with the results coming from the new chamber, namely the exhalator. For the ^{222}Rn with $\lambda = 2.10 \cdot 10^{-6} s^{-1}$, the saturation value is reached in about 20 days, while only few hours are needed for the ^{220}Rn, due to the value of $\lambda = 0.13 s^{-1}$.
In this solution, it is important take into account two factors. The first one is linked to the chamber losses and the possible radon exchanges with outside; the second one, known also as back-diffusion phenomenon, takes into account that a percentage of the radon is issued, because of the finite volume of exhalation, and can be reabsorbed by sample. This phenomenon is obviously negligible in the early exhalation stages when the available volume of the gas expansion is maximum; this probability is estimated to be inversely proportional to the chamber volume [51]. So, keeping into account what stated above, the radon concentration in the chamber can be described by the following equation:

$$C(t) = \frac{E_{Rn}}{\lambda V}(1 - e^{-\lambda_{eff} t}) \tag{4.3}$$

[1] In general in a dry soil, the value of the diffusion distance is about 1 meter for ^{222}Rn and about 1 centimeter for ^{220}Rn [8].

where $\lambda_{eff} = \lambda + \lambda^*$ is given by the sum of the decay probability and the losses linked to the two factors explained before. With a best fit of experimental data is possible to verify if the decay constant is affected by back-diffusion. From this curve, the exhalation rate is evaluated. An alternative and faster method consists in developing the exponential in Taylor series for $\lambda_{eff}t << 1$, the following linear concentration relation over time is obtained [52]:

$$C(t) = \frac{E_{Rn}}{\lambda V}t \tag{4.4}$$

This expression give us a double advantage: the first one is the reduction of the measurement time, from 20 days to 12 hours, the second one is the dependence elimination from λ and λ^*.
During the measurement of the exhaled concentration from the sample in the saturation condition, the acquired spectra with our system produce a count rate measure, *cps*, therefore the previous relation becomes:

$$C(t) = \frac{E_{Rn}}{\lambda V}t = \frac{cps(t)}{\epsilon V_s} \tag{4.5}$$

With this method, the values of the exhaled concentration, for all decay products, in the saturation condition for the sample used as a reference have been obtained. These results, shown in figure 4.11, and summarized in the table 4.3, have been subsequently compared with the exhalator results.

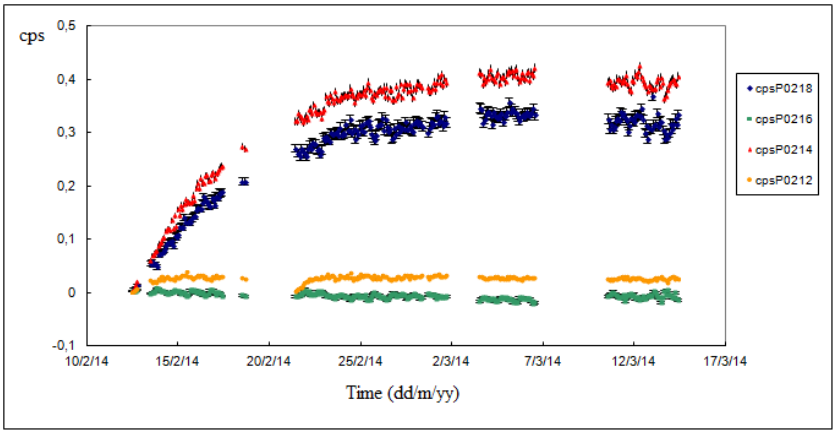

Figure 4.11: Count rates of radon and thoron daughters in the soil sample used as a reference.

In the same measurement conditions, the remaining part of the soil sample from M.Olibano has been put in a box and the measurement with the new

Decay product	C (Bq/l)
^{218}Po	1.31 ± 0.16
^{214}Po	1.54 ± 0.16
^{216}Po	1.63 ± 1.09

Table 4.2: Exhaled concentration, for all decay products, from the sample used as a reference in equilibrium conditions with the respective progenitor.

chamber was started, placing it on the soil surface. The values set for the high voltage and the detector supply are the same that ones used in RAMONA, the only change is the chamber structure and then the measurement type. Also in this case, the count rate of each decay product, for both radon and thoron, is obtained as a function of the time, as shown in figure 4.12.

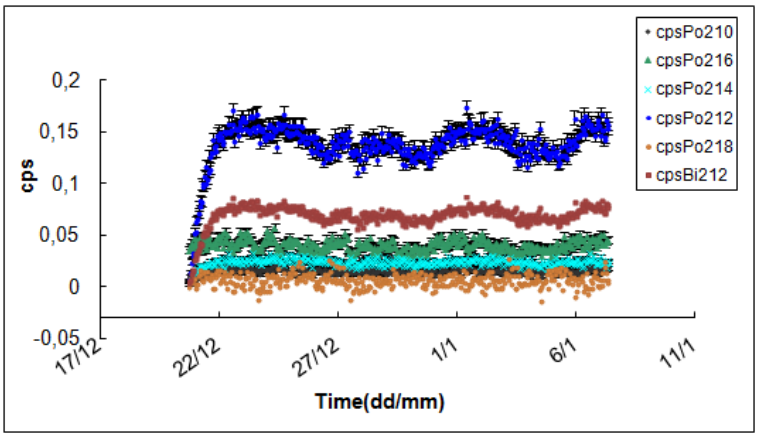

Figure 4.12: Count rates of radon and thoron daughters in the soil sample with exhalator.

The comparison between the known and measured radon activity concentration gives the efficiency of the chamber for both radon dahugters. The relation used in order to evaluate the efficiency value is the following:

$$\epsilon_i = \frac{cps_i}{C_i \cdot V} \tag{4.6}$$

where ϵ_i is the efficiency linked to the $i-th$ decay product, cps_i is its count rate measured with the exhalator, C_i its known activity concentration and V is the exhalator chamber volume. The efficiency values for each radon and thoron daughter for this new chamber is reported in the following table 4.3:

Decay product	efficiency
^{218}Po	0.003 ± 0.003
^{214}Po	0.011 ± 0.002
^{216}Po	0.017 ± 0.013

Table 4.3: Exhaled concentration, for all decay products, from the sample used as a reference in equilibrium conditions with the respective progenitor.

The table shows that the detection efficiency of the ^{214}Po is bigger than the ^{218}Po one. In the radioactive equilibrium the count rate of these two polonium isotopes should be the same, since ^{214}Po is a following product in the decay chain of ^{218}Po. However, this is normally not the case for radon detectors that use electrostatic collection [53]. Part of the not initially ionized ^{218}Po decays and produces, with some probability, positive ^{214}Po ions which can partly be collected on the detector. Consequently, the count rate of ^{214}Po is higher than for ^{218}Po.
In order to reduce the humidity inside the chamber and to stabilize the efficiency value, a thin Tyvek layer was used to cover the metallic grid, as shown in figure 4.13. As already explained in the previous chapter, it is a synthetic material similar to paper, difficult to tear, also resistant to many acids and bases, so its use is very important in the hostile fields in which this chamber has to be employed.

This measurements results are reported in the same plot with the previous ones, fig. 4.14. The efficiency value for each polonium isotopes are comparable within the errors and the result of the Tyvek use is a more stable efficiency.

4.3 Alternative detectors: PiN photodiodes

Another improvement to RAMONA is related to the costs reduction. In this context, other detector types were studied: the PiN photodiodes.
Usually the Silicon photodiodes are employed to photon detection because of their sensitive in the wavelength range from $150nm$ to $1100nm$, thus covering well the emission wavelength of almost all organic and inorganic scintillators and of Cherenkov radiators. There are several studies that link them to the radon activity concentration measurement, so to the alpha detection [54][55][56].
Up to now the used detector is the Ion-Implanted-Silicon Charged-Particle Detectors ULTRA (Ortec). Among its features there are:

Figure 4.13: Disassembled exhalator with two metallic grid configuration, one covered by Tyvek and one without it.

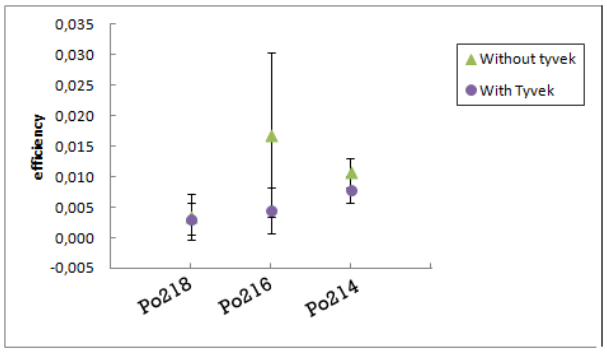

Figure 4.14: Detection efficiency for each polonium isotopes with and without the Tyvek employment.

- ultra thin entrance for optimum resolution;
- high geometric efficiency due to the detector being close to the can spacing;
- rugged and reliable;
- gold plated cans for contacts that last a lifetime;
- advanced surface passivation for total device stability;
- background $\approx 6count/24h$ for $450mm^2$ active area.

In terms of the above parameter, it is a good device, but its negative factor is the high cost, especially if the chamber is employed for measurements in hostile environments, in which the detector has to be more often substituted. The PIN photodiode is one of the simplest types of photodiodes. It consists in an intrinsic piece of high ohmic semiconductor sandwiched between two heavily doped n+ and p+ regions, as shown in figure 4.15.

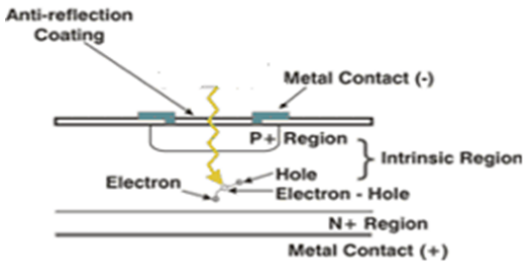

Figure 4.15: Structure of a PIN photodiode [57].

This configuration produces a field such that it tends to separate charges produced in the depleted region, even without an external field. The thick layer of intrinsic silicon ($300m$) reduces the capacitance of the diode and the serial noise. A small voltage is required to deplete the device completely because the depleted region has a very low concentration of dopants. Another advantage is that the recombination-generation time constant is the longest one in case of undoped materials; this fact allows to have a minimal thermal generation current. The PIN photodiode has no internal gain and this offers an exceptional stability; however a charge sensitive amplifier and a low bandwidth filter amplifier are needed for the detection of low light level signals above the noise caused by the leakage current and the large diode

capacitance. The use of a charge sensitive preamplifier and a filter amplifier makes the signal slow [57].
The main characteristics of the PIN photodiode are summarized below:

- high quantum efficiency ($\approx 80\%$ at $550nm$);
- low capacitance;
- high speed response;
- high stability;
- good energy resolution;

A feature no less important is its cost, which is lower than ULTRA detector ones. This type of detector can be directly used or coupled to small sparkling crystals, especially no hygroscopic and then more suitable to the measurement type to which we are interested.
In this section the tests carried out with different PINs of Hamamatsu are reported. The preliminary tests were made in vacuum with alpha sources, reported in the following table 4.4, using an external electronics composed by preamplifier, amplifier and a multichannel system.

Source	E_α(MeV)	Branching ratio
^{239}Pu	5.156	73.8%
^{239}Pu	5.143	15.2%
^{239}Pu	5.105	10.7%
^{241}Am	5.486	85.2%
^{241}Am	5.443	12.8%
^{241}Am	5.388	1.4%
^{244}Cm	5.805	76.4%
^{244}Cm	5.763	23.6%

Table 4.4: Alpha sources.

4.3.1 Hamamatsu S3590-09

The first tests were performed on PIN S3590-09. It has a sensitivity matching with BGO and CsI(TI) scintillators, a high quantum efficiency and a high speed response. Among its characteristics there are:

- active area$(mm) = 10x10$;

- spectral response range λ (nm) = 340 to 1100;
- depletion layer thickness (mm) = 0.3;
- reverse voltage max (V) = 100;
- unsealed window material;
- ceramic package.

As shown in the plot in the figure 4.16, this detector has a very good energy resolution.

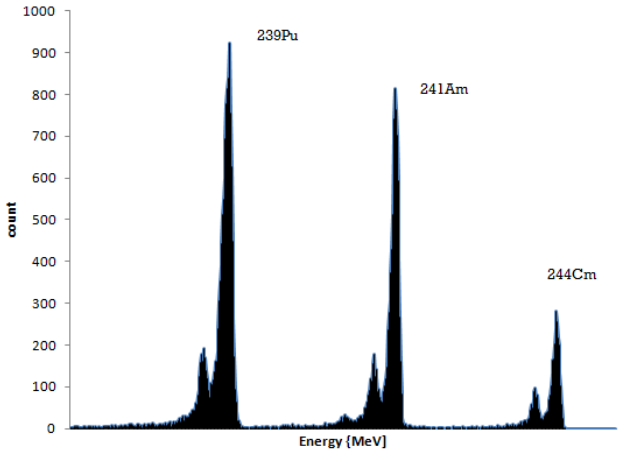

Figure 4.16: Spectrum of a double alpha source with PIN Hamamatsu S3590-09.

The first study was about the PIN behavior as a function of the reverse voltage. As shown in the plot in figure 4.17, the peak position of each source changes with the voltage and the plateaux is immediately reached, around to $20V$.

The relative energetic resolution of this device, in figure 4.18, is quite flat; from this analysis is deduced that a good working point is between $20V$ and $30V$.

Other tests were made as a function of the shaping time of the amplifier and the results are shown in the figures 4.19 and 4.20.

The peak positions of the sources increase a little bit with the shaping time up to reach a plateaux around to 3000 channels. The relative resolution is quite flat for americium and curium sources, while a little less for the plutonium source. However the values are comparable within the error bars,

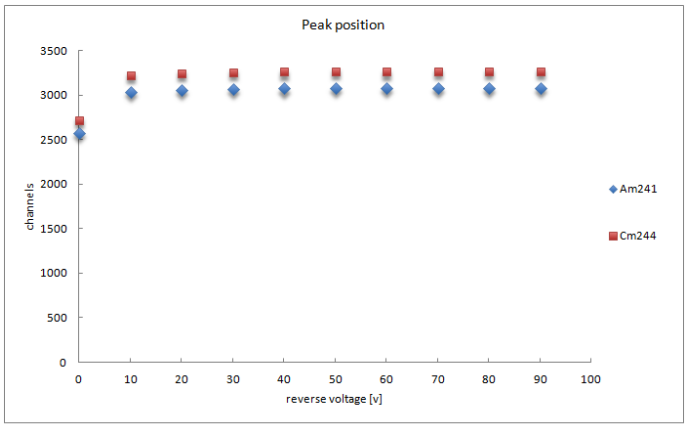

Figure 4.17: Hamamatsu PIN S3590-09. Peaks position of the sources as a function of the reverse voltage.

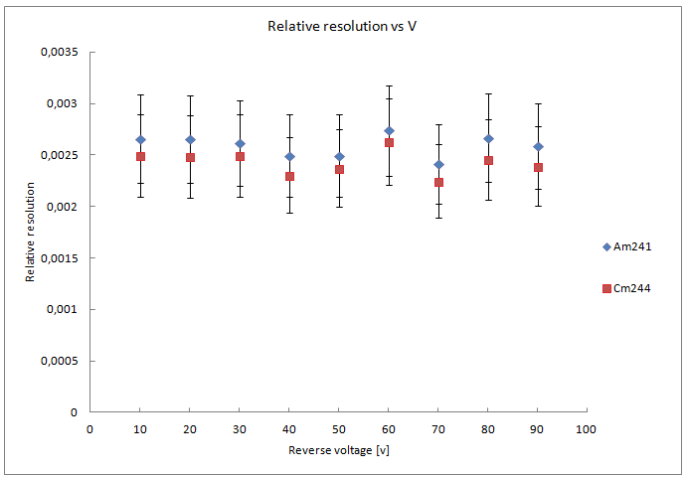

Figure 4.18: Hamamatsu PIN S3590-09. Relative energetic resolution as a function of the reverse voltage.

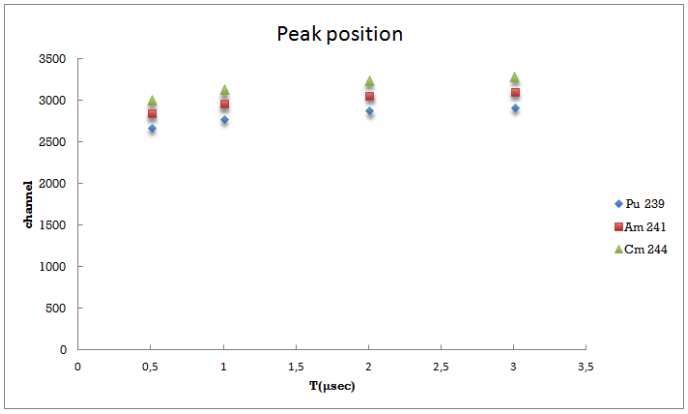

Figure 4.19: Hamamatsu PIN S3590-09. Peaks position of the sources as a function of the shaping time of amplifier.

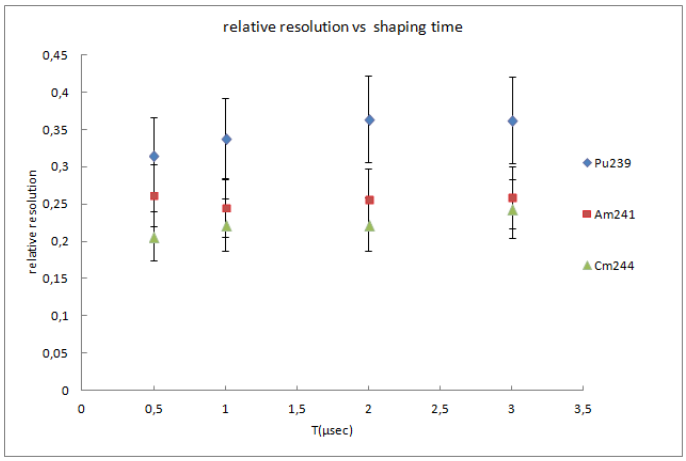

Figure 4.20: Hamamatsu PIN S3590-09. Relative energetic resolution as a function of the shaping time of amplifier.

in particular at $3\mu s$ all the relative energetic resolutions are more similar, so this value is chosen as working point.

4.3.2 Hamamatsu S3590-19

The second tested device is the PIN S3590-19. It has the same type of listed characteristics of the previous device, such as a high quantum efficiency and a high speed response, but it has a better sensitivity matching with blue scintillator, like LSO, GSO, etc..
The same tests performed with the previous detector, were carried out with this PIN. By setting the working point of the amplifier shaping time at value of $3\mu s$, it was studied the PIN behaviour as a function of the reverse voltage. Observing the spectrum of triple alpha source produced by this detector in the figure 4.21, one can note a resolution worse than that achieved with the previous PIN.

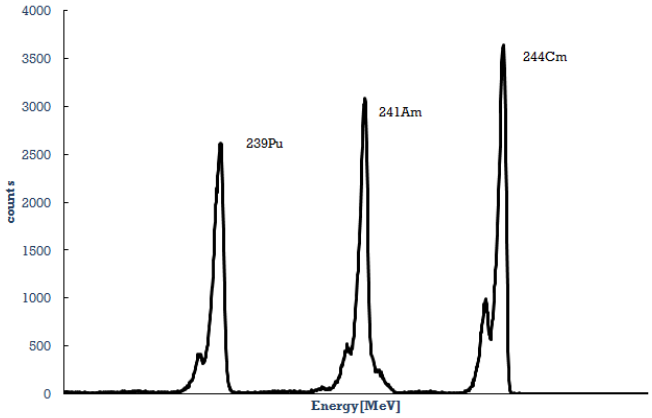

Figure 4.21: Spectrum of a triple alpha source with PIN Hamamatsu S3590-19.

This observation is confirmed by the tests results, shown in figures 4.22 and 4.23.

Also in this case a good working point for the reverse voltage is found to be between $20V$ and $30V$.

4.3.3 Hamamatsu S3204-09

The last tested device is the PIN S3204-09, which has exactly the same characteristics as the first one, also the same sensitivity matching with BGO and CsI(TI) scintillators, but an active area larger, $(18x18)mm^2$. From the

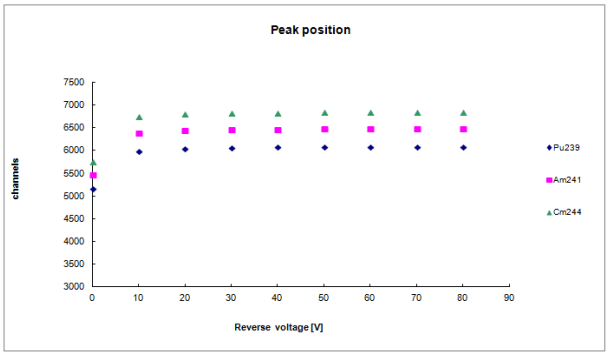

Figure 4.22: Hamamatsu PIN S3590-19. Peaks position of the sources as a function of the reverse voltage.

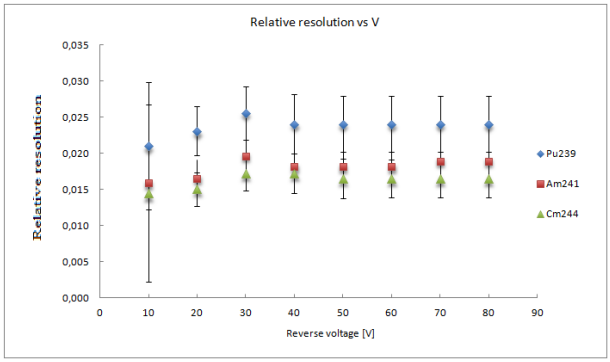

Figure 4.23: Hamamatsu PIN S3590-19. Relative energetic resolution as a function of the reverse voltage.

literature it is known that the noise of large PIN photodiodes increases proportionally to the area, respectively to the diode capacitance.
By performing the same tests as a function of the reverse voltage, reported in the figures 4.24 and 4.25, the working point for this detector is found to be around to $50V$, in agreement with its resolution.

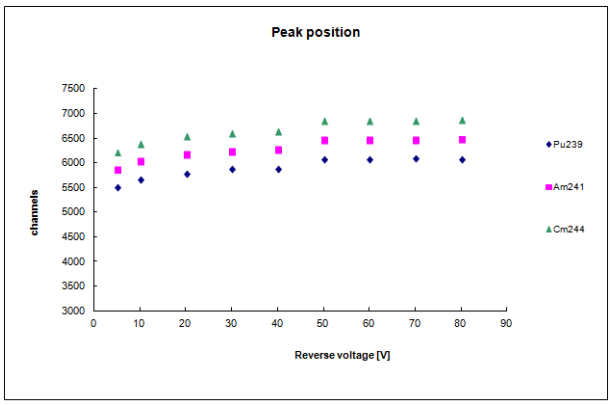

Figure 4.24: Hamamatsu PIN S3204-09. Peaks position of the sources as a function of the reverse voltage.

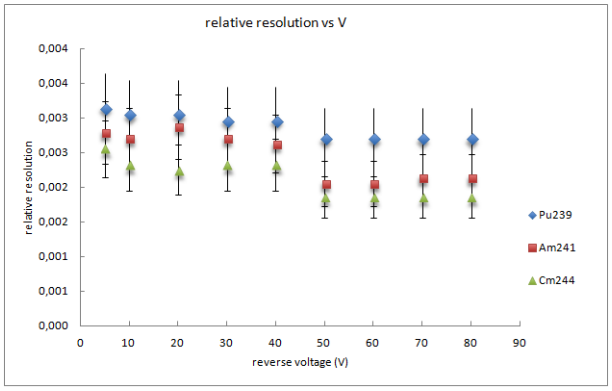

Figure 4.25: Hamamatsu PIN S3204-09. Relative energetic resolution as a function of the reverse voltage.

The relative energetic resolution is comparable with the first tested PIN, also if in the previous case the results are better. In the figure 4.26, the spectrum of a triple alpha source obtained with this device, using the previous set working point, is shown.

From these preliminary studies, the PIN chosen to replace the alpha RAMONA detector is the first one, the PIN S3590-09.

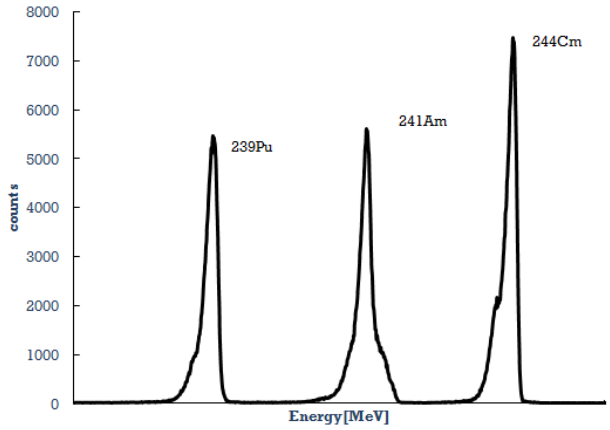

Figure 4.26: Spectrum of a triple alpha source with PIN Hamamatsu S3204-09.

4.3.4 Hamamatsu S3590-09 with RAMONA System

After the choice of the better device among the PIN photodiodes, the detector was implemented in the RAMONA electronic board inside the classical chamber, as shown in figure 4.27.

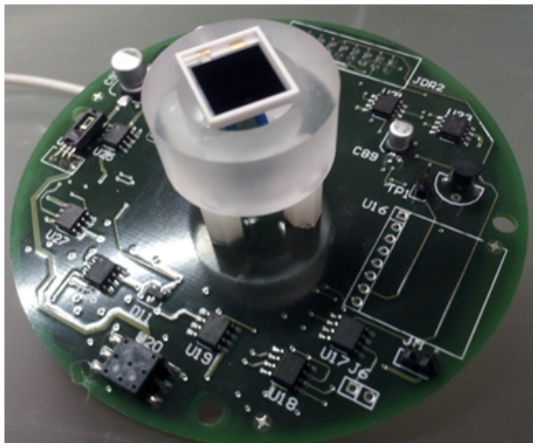

Figure 4.27: Electronic board with a PIN photodiode of Hamamatsu, S3590-09.

Because of a known radon activity, earlier measured through the gamma spectroscopy, the behaviour of this composed system was studied. In particular, the calibration factors for both the radon daughters were evaluated.

As described in the previous chapter, the measured count rate of the polonium isotopes and the known radon activity are related by the relationship that returns the calibration factor value:

$$\epsilon = \frac{cps \cdot V}{A} \tag{4.7}$$

where V is the active volume.

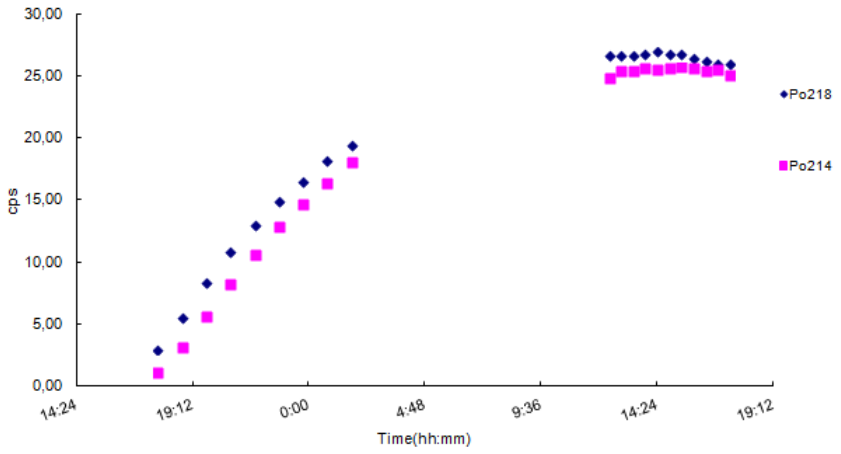

Figure 4.28: Count rate of the polonium isotopes as a function of the time with PIN photodiode detector.

After reached equilibrium between the radon and its decay products, it was possible to calculate these factors, whose results are:

$$\epsilon_{Po218} = (3.19 \pm 0.02) * 10^{-2}\,[cps/(Bq/l)] \tag{4.8}$$

$$\epsilon_{Po214} = (3.02 \pm 0.05) * 10^{-2}\,[cps/(Bq/l)] \tag{4.9}$$

To evaluate the calibration factor related to the thoron decay products, the chamber has been connected to the calibration facility. Inside the two active volumes of both chambers, the same gas atmosphere circulates, controlled by the facility internal monitor. In the picture 4.29 is shown the spectrum acquired with RAMONA system in the new conditions.

From the ^{216}Po count rate, shown in the figure 4.30, and from the monitored thoron activity concentration, the calibration factor of this polonium isotope has been calculated:

$$\epsilon_{Po216} = (0.023 \pm 0.003)\,[cps/(Bq/l)] \tag{4.10}$$

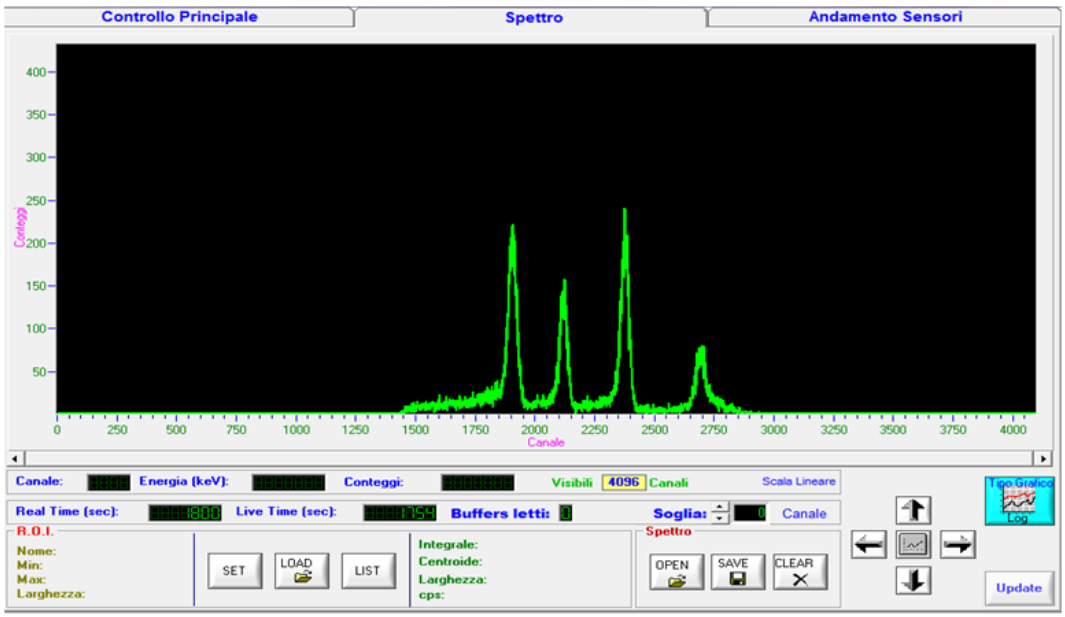

Figure 4.29: Polonium isotopes spectrum acquired by RAMONA system during its calibration with the PIN.

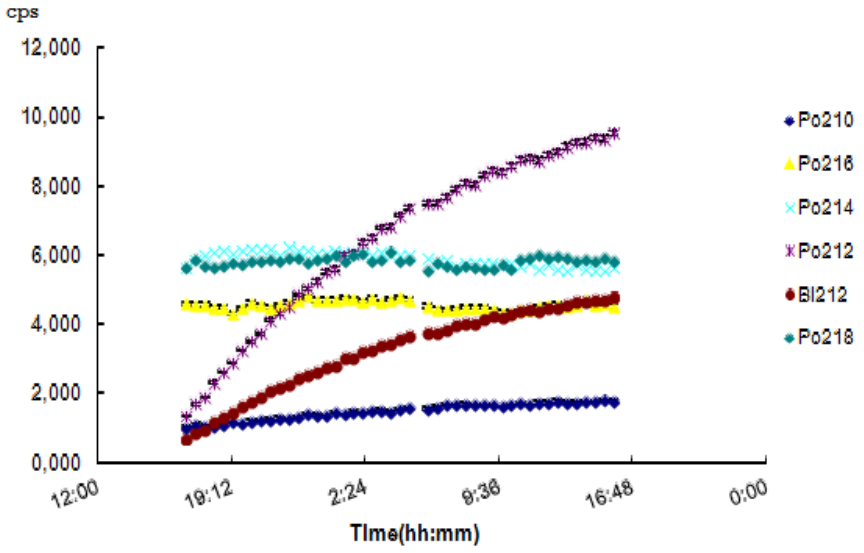

Figure 4.30: Count rate of the polonium isotopes, both of radon and of thoron, as a function of the time, with PIN photodiode detector implemented in the RAMONA electronic board.

Chapter 5

Applications of the RAMONA upgrading

In this last chapter applications of RAMONA device improvements are reported. In particular in the first section, the measurements of the radon concentration in soil gas are analyzed. Furthermore the comparison between the radon concentration measurements obtained, using the classical chamber of RAMONA and the new one, the exhalator, is shown.
The last chapter part is dedicated to the technological RAMONA transfer.

5.1 Continuous radon and thoron measurements in Phlegraean Fields

As already explained in the previous chapters the radon concentration in soil, air and groundwater was often associated to the deep movements along faults or to magmatic activity [58][59][60]. The absence of any orderliness in the identification of a causal relationship, between observed seismic-volcanic phenomena and radon anomalies, has produced the progressive abandonment of radon as geoindicator for these activity types. The insufficient evaluation of the reactive transport of the radium progeny in geological media, the low sampling often reduced at a single point of measure on a large area and the geophysical complexity of the monitored area, containing more of one radon source, are the principal limits in interpreting radon anomalies.
A few years ago, it has been started a collaboration project between the sections of INFN Naples (National Institute of Nuclear Physics) and OV-INGV (Vesuvianus Observatory-National Institute of Geophysics and Volcanology) [63][61]. Its goal is the continuous acquisition of gas radon concentration in conjunction with other geochemical, geophysical and climatic parameters, in

multiple disigned sites in a dense area. The idea is to identify significant correlations useful to check the correspondence between the variations of radon concentration levels and the dynamics of systems under observation. Therefore, in addition to the active radon monitoring of the soil gas, this project required the radiometric characterization of the monitored sites in order to have a correct interpretation of the radon signal.
The analyzed area is the Phlegraean Fields place, a very interesting area of the Campania region. It is a particular seismic-volcanic area, frequently interested by bradysismic events. As indicated in figure 5.1, seven sites have been chosen for this study, but, due to the environmental conditions, the continuous radon measurements were performed only in two sites, Mt.Olibano and Mt.S.Angelo, respectively indicated with abbreviations OLB and MSA.

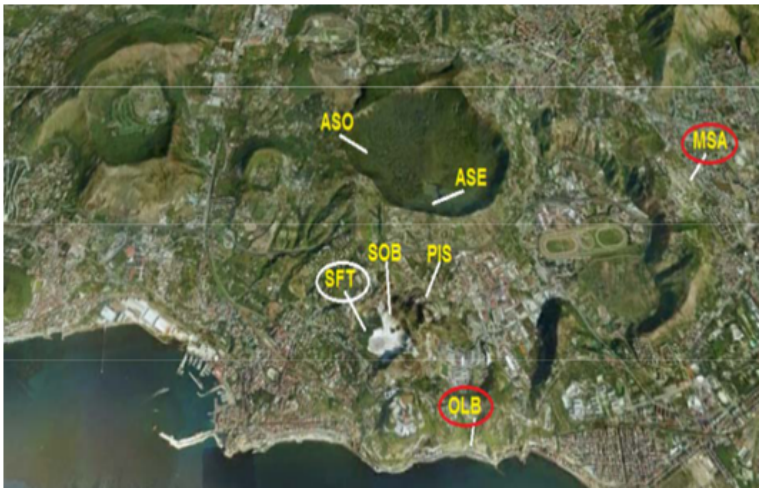

Figure 5.1: Phlegraean Fields area, $\approx 5km^2$, with indication of the interesting points for the network.

These two sites, together with a third one, the Solfatara caldera indicated with SFT, were characterized by the radiometric point of view. However this last site is characterized by the presence of the hot and corrosive gases, very rich in moisture $80 - 90\%$. These conditions have produced, in short working time, serious damages of the RAMONA electronic components, making practically impossible its use.
The MSA site, located on the edge of the studied area, can be considered a test site, while the OLB site is located in the Phlegraean area, under the Mt.Olibano in a disused gallery, and its ground consists mainly of pozzolana. From the data of MSA and OLB reported in the figures 5.2 and 5.3, it is evident that, although the radium content is equivalent in both sites (about

$250 Bqkg^{-1}$), the radon in soil gas at OLB site is higher an order of magnitude than in MSA site.

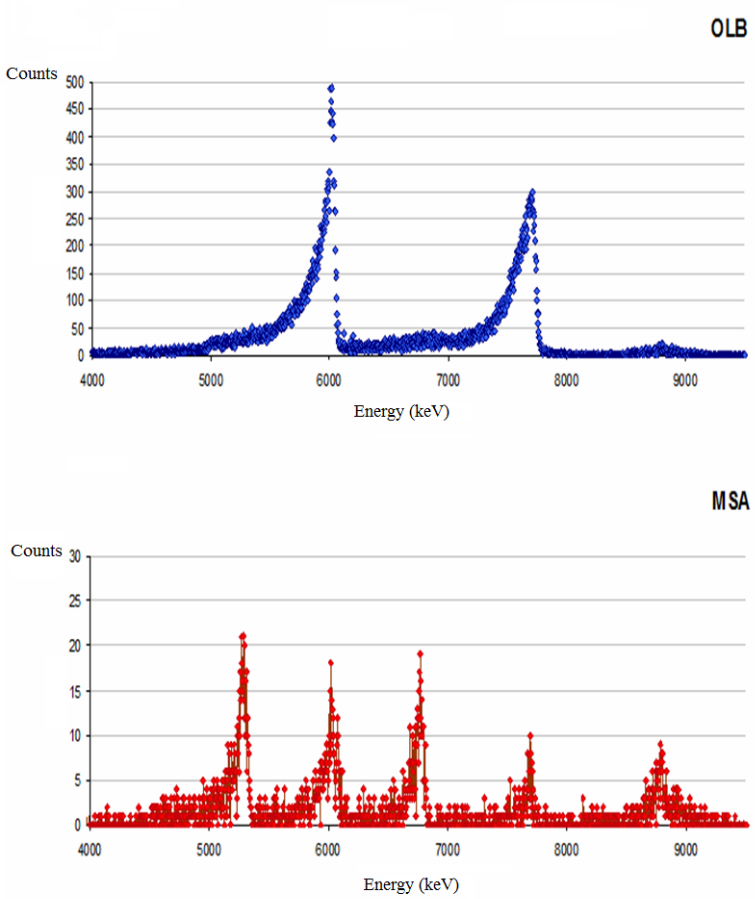

Figure 5.2: Alpha spectra produced by the radon and thoron progenies in Mt.Olibano, in the upper side, and in Mt.S.Angelo, in the lower part. The peaks areas of all polonium isotopes are comparable in MSA, where the local radon concentration has the same magnitude order of the remote one. This does not happen in OLB, where the local radon concentration is ten times lower than the remote one.

This phenomenon can be explained in two ways. On one side, it can be due to the radon emanation coefficients, to the soil porosity and to the radon diffusion velocity, that strongly influence the fraction of the radon produced by radium decay which is present in the soil gas. In particular, the measured value of the radon emanation coefficients in the MSA and OLB sites are (0.023 ± 0.001) and (0.083 ± 0.005) respectively. On the other side, in the soil

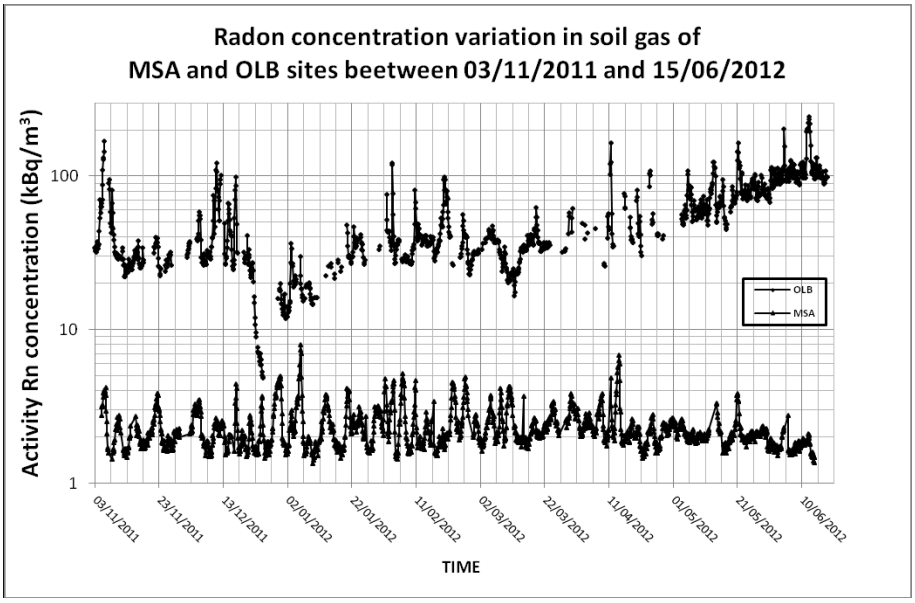

Figure 5.3: Temporal variations of radon concentration in soil gas from November 3, 2011 to June 10, 2012, obtained by continuous monitoring at sites of MSA and OLB [61].

gas the thoron decay products are present both the radon ones, namely locally produced radon and remotely produced one [61]. Usually the interesting observed quantity is the remote one, therefore a technique for the separation of various origins radon activities, such as the alpha spectrometric analysis of the radon daughters offered by the RAMONA device, is needed [62]. The oscillations in the radon concentration are presents in both the measure sites, but the frequency is different, probably due to local reasons. It clear that the long term observation of radon signal in many sites of a seismic-volcanic area could give the area characterization and could also contribute to understand anomalous signals. About this last point, it is basic to observe that the monitoring in different sites is important because all anomalies that are not simultaneously recorded in the measurement sites can be associated to local phenomena, not to the whole area monitored.
In order to realize this analysis on the continuous radon data from the soil gas, a monitoring network able to resolve the problems linked to the measurements in such hostile sites is needed.
In this context the RAMONA improvements are placed. When the environmental conditions are not very hostile, the studied dryer system is sufficient to reduce the gases and humidity into RAMONA chamber, otherwise the exhalator use is more adequate.

5.1.1 Mt.Olibano: comparison between exhaled and in soil activity

The exhalator has been installed at Mt.Olibano in order to test its performances in soil gas measurements. This place is very interesting as test site for two main reasons. The first one is linked to an unusual environmental condition, in fact the humidity value is very high, about 100%. Therefore if the device works in such environment, it should be able to work in very hostile conditions. The second one is that this site is also monitored through the classical RAMONA system, so from the comparison between the two different measurements it is possible to obtain more informations about the behaviour of the new chamber. In the figure 5.4, the two chambers, during the radon monitoring at Mt.Olibano, are shown.

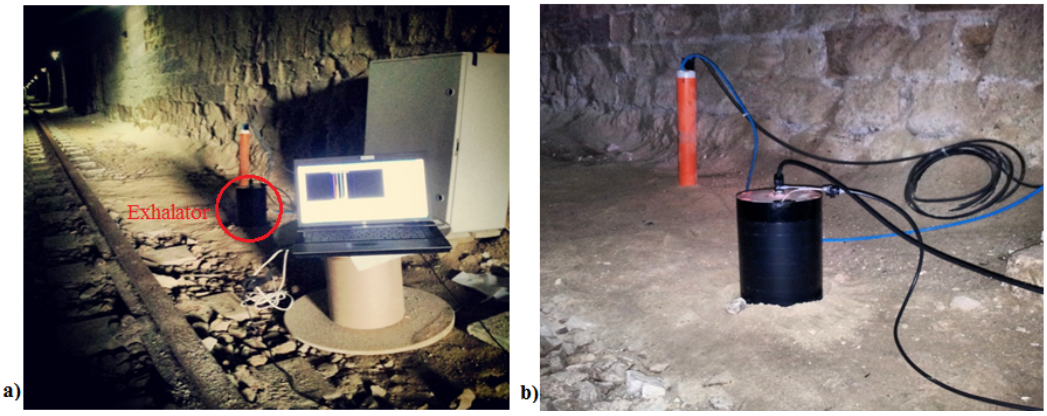

Figure 5.4: **a)** Set Up measurement with both the chambers. The classical chamber is contained in the grey box on the right, while the new one is put on the ground surface; **b)** the sampling points for the radon measurements are very near, about $50cm$.

The test main goal is to verify if it is possible monitor the radon variations of the soil gas, during the time, with the exhalator placed on the ground surface, as well as you do sampling the gas at one meter depth. In order to achieve the better measurement condition, the chosen position for the exhalator chamber is very near to the RAMONA sampling point, about $50cm$. The monitoring carried out by the exhalator, shown in figure 5.5, has been performed thanks to RAMONA acquisition and control unit, described in the second chapter. The sampling time for the alpha spectra construction is three hours; the collection cell and the silicon detector supply voltage are put at $3000V$ and at $20V$ respectively.

In the figure 5.6 the count rates of the radon and thoron decay products

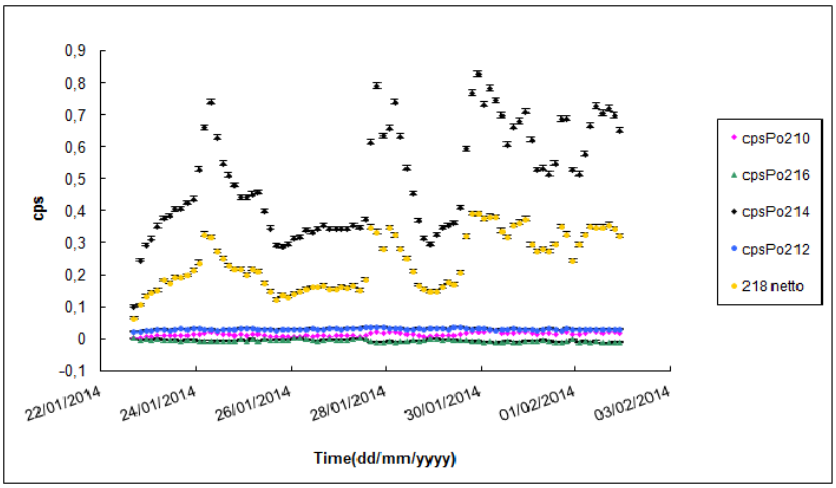

Figure 5.5: The count rates of the radon and thoron daughters as a function of the time, evaluated through the exhalator placed at Mt.Olibano in the Phlegraean Fields.

are reported as a function of the same time of the previous measurements, but using RAMONA chamber.

Although the *cps* values coming from the two measurements are very different, the evaluated radon concentrations are comparable, thanks to their unequal calibration factors. In particular, from the comparison between these two measurements, it is clear that the the cps trends are reproducible; the soft curves coming from the exhalator are due to its sampling time, different from the RAMONA one, that is about one hour.
As well as in the classical measurement from the soil, described before, the exhalator results show a higher radon presence in comparison to the thoron one, namely a strong component of remote radon.
However there is a evident difference in the ratio between ^{218}Po and ^{214}Po evaluated from the two sequences. This ratio is approximately one in the soil gas measurement. This fact means that the most part of ^{218}Po is ionized, then collected on the detector, and it decays giving rise to ^{214}Po. From these arguments the count rate of the two polonium isotopes could be similar, but using the exhalator the situation is different. In this case $R = cps_{214}/cps_{218}$ is equal to 0.48 ± 0.03. This can be explained taking into account that a fraction of not ionized ^{218}Po produces, with its own decay, ionized ^{214}Po ions. This behaviour implies that, in the spectrum, the ^{214}Po intensity peak is higher than ^{218}Po one. In addition, a fraction of ionized ^{218}Po ions can capture an electron; however its decay could in turn produce an ionized daughter

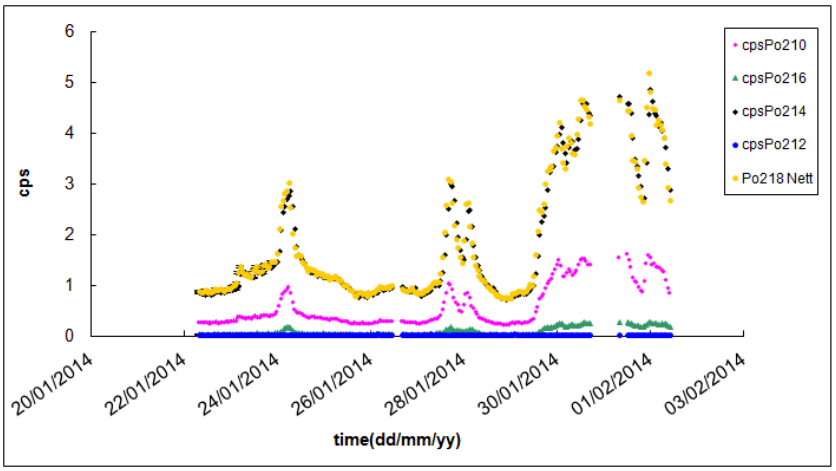

Figure 5.6: The count rates of the radon and thoron daughters as a function of time, evaluated through the RAMONA system installed at Mt.Olibano in the Phlegraean Fields.

that can be collected on the detector surface. These machanisms can explain the different polonium isotopes count rates coming from the two chambers probably due to the different degree of contamination of the gas, in soil and in air, with water, hydrocarbons or other components [53].
The very important thing of this test is that also with this new chamber, it is possible to observe the variations of radon concentration in soil gas. Thanks to this result, a future plan will consider the exhalator tests in Solfatara.

5.2 Tecnological transfer

An industrialized version of RAMONA, more compact and basic, is currently in development by an Italian company under licence of the INFN, owner of the relative patent in Italy and USA. The prototype , whose scheme is shown in figure 5.7, takes into account some results obtained in this work.

In particular, the detector used is the PIN photodiode S3590-09 of Hamamatsu, associated to a new electronic developed by the company researchers. In the spring 2014, the prototypal device is gioing to be tested and calibrated in the calibration facility of the Laboratory of Radioactivity of the Physics Department. The goal of this project is the production of an instrument to be used outside of scientific laboratory, for the human health prevention purpose, in structures as ASL, ARPA, etc..

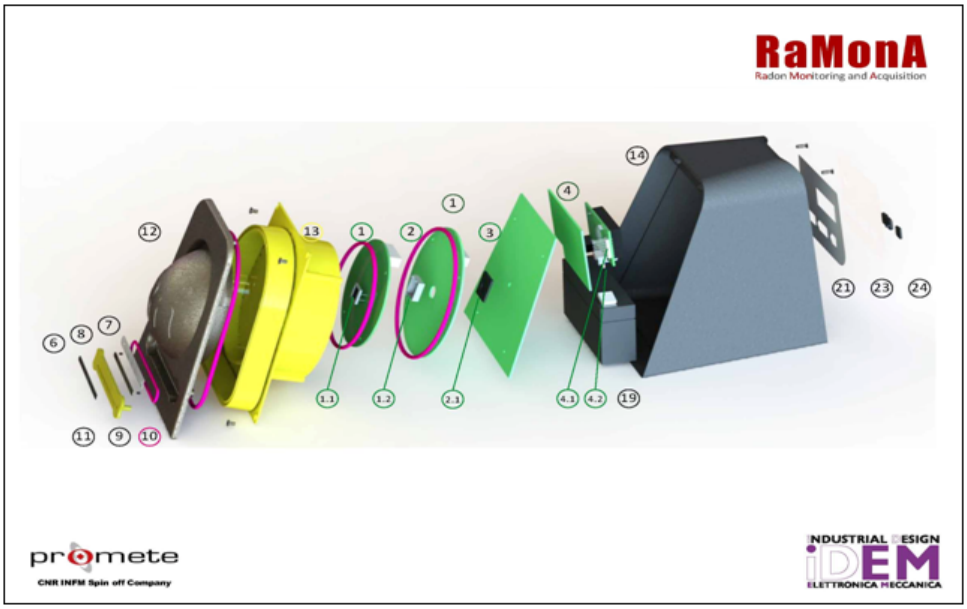

Figure 5.7: Scheme of the disassembled prototype for the RAMONA industrialized version. The different parts that compose the device are indicated with a number: **1)** detector/converter board; **1.1)** PIN photodiode S3590-09; **1.2)** metallic protection cover; **2)** supply board; **2.1)** microblower; **3)** processing board; **4)** interface board; **4.1)** display with selection key; **4.2)** USB connector; **6)** and **7)** metal sheets; **8)** cover in ABS; **9)** Tyvek layer; **10)**, **15)**, **17)** and **18)** o'ring; **11)** supermagnets; **12)** front panel in ABS: collection chamber with volume equal to $130ml$ and whose walls at $1500V$; **13)** closure plan in ABS; **14)** external structure in ABS.

Conclusion

The interest in realizing a detector for the monitoring of radon activity in all cases where both isotopes of this gas are present is the main reason behind the work presented in this thesis. The above objective can be reached only if the spectroscopic analysis of the radon daughter can be performed. Few detectors based on the electrostatic collection of the radon daughters can guarantee this result, which is mandatory for all applications of this measurement linked to the human health prevention and to the study of Earth crust dynamics. The perform in these fields the availability of suitable calibration facilities is necessary and the spectroscopic separation of radon and thoron is a powerful tool. The reported research work fully shows this statement.
The first step was the development of a calibration facility and then the realization of reference sources for both isotopes. A methodology for the creation of thoron atmospheres was developed, while existing and already established procedures for the realization of atmospheres of known radon activity were used. Six thorium sources were realized. By using thorium and radium sources, two traceability chains for the realization of independent internal atmospheres of known specific activity and mixed atmospheres were developed. The calibration facility allows to change and to monitor the gas environmental conditions. The exposure chamber with an internal monitor based on electrostatic collection is the main part of the apparatus. The studies were performed with different specific activities in the range between $(14 \div 665) Bq/l$ of mixed atmospheres and showed stable calibration factors for each radon isotope.
Concerning the RAMONA upgrade, particular attention was given to the development of methods for the reduction of hostile gases and humidity. This reduction is mandatory to achieve good gas conditions into the radon chamber in order to prevent damage to the electronics and detector. In particular, the $Perma\ Pure\ MD^{TM} - Series$ gas drier was tested. The results showed a small loss of radon with this tool, about $\approx 0.005 Bq/h$, which is negligible compared to the usual radon activity.
A hermetic separation between the electronic components and the collection

chamber was realized, putting inside the active volume only the environmental parameters sensors, in order to protect the electronics during the measurements in non-standard conditions.
Within the detector upgrade the reduction of costs becomes an important issue, as the usage of the device in non-standard conditions implies a high probability of detector damage. For this aim, several PIN photodiodes of Hamamatsu were tested. The chosen PIN to replace the alpha RAMONA detector is the S3590-09, for its good energetic resolution. A future improvement will use this photodiode coupled with a hygroscopic sparkling crystal, which becomes the detector and moreover protects the silicon surface.
In addition to the chamber material, now insulating and lighter than before, also its shape has been modified. A new chamber without the bottom was realized to allow the continuous radon monitoring also when the gas from the soil is hot and too rich in corrosive gases and water vapor. After the development of a calibration method, the chamber has been installed in Mt.Olibano, to test its performances in soil gas measurements. This place, sited in Phlegraean Fields, is very interesting for two main reasons. The first one is linked to an unusual environmental condition, in fact the humidity value is very high ($\sim$ 100%); the second one is that this site is also monitored through the classical RAMONA system. The measurement results showed that it is possible to observe the variations of radon concentration in soil gas with the chamber placed on the ground surface. This result is very interesting for the realization of a radon monitoring network in hostile environments. A near-future plan will regard the radon monitoring in the Phlegraean Fields. In the next months, the new chamber will be tested in Solfatara caldera.
Taking into account some of the results obtained in this work, an industrialized version of RAMONA is currently being developed by an italian company under licence of the INFN, owner of the relative patent in Italy and USA. During spring 2014, the prototype will be tested and calibrated with the facility realized and described in this work.

List of Figures

List of Tables

Contents

Bibliography

[1] UNSCEAR, 2000.

[2] M.Doi and S.Kobayashi, *Characterization of Japanese Wooden Houses with Enhanced Radon and Thoron Concentrations*. Health Phys., 66, pp.274-282, 1994.

[3] M.Wakita, Y.Nakamara et al., *Radon anomaly: a possible precursor of the 1978 Izu-Oshima-Kinkai earthquake*, Science, Vol.207, pp.882-884, 1980.

[4] V.I.Ulomov, B.Z.Mavashev, *earthquakes and radon*, Dkl.Akad. SSR 176, 1967.

[5] P.Gasparini, M.S.M.Mantovani, *Fisica della Terra solida*, Galilei, Lausenne, 1984.

[6] C.H.Scholz *The Meccanics earthquakes and faulting*,University of Cambridge, New York, 1990.

[7] G.Sciocchetti et al., *Esposizione alle radiazioni naturali in Italia*, Energia Nucleare, n.1, 1989.

[8] W.W.Nazaroff and A.V.Nero, *Radon and its decay products in indoor air*, 1998.

[9] A.Mogro-Campero, R.L.Fleisher and R.S.Likes, *Changes in subsurface radon concentration associated with earthquakes*, J. Geophysic.Res., Vol.85, pp.3053-3057, 1980.

[10] G. Martinelli, G.Etiope, *Migration carrier and trace gases in the geosphere: an overview*, Physics of Earth and Planetary interiors, Vol.129, pp.185-204, 2002.

[11] G.K.Batchelor, *An introduction to fluid dynamics*, Cambridge University, 1967.

[12] A.Damkjaer and U.Korsbech, *Measuremt of the emanation of radon222 from Danish soils*, The Science Tot.Environ.,Vol.45, pp.343-350.

[13] D.A.W.Bossus, *Emanating power and specific surface area*, Radiation Protection Dosimetry, Vol.7, pp.73-76, 1984.

[14] A.B.Tanner, *Radon migration in the ground: a supplementary review*, Natural Radiation Environ.III, Gesell and Lowder, pp. 5-56, 1980.

[15] D.Iskardar,H.Yamazawa and T.Iida, *Quantification of the dependency of Radon emanation power on soil temperature*, Applied Radiation and Isotopes, Vol.60, pp.971-973, 2004.

[16] L.Morawska, C.R.Phillips, *Determination of the radon surface emanation rate from laboratory emanation data*, The science of the total Environment, Vol.106, pp.253-262, 1980.

[17] G.Martinelli, *Gas geochemistry and ^{222}Rn migration process*, Radiation Protection Dosimetry, Vol.78, pp.77-82, 1993.

[18] R.P.Chauhan and S.K.Chakarvarti, *Radon diffusion through soil and fly ash:effect of compaction*, Radiation measurements, Vol.35, pp.143-146, 2002.

[19] J.N.Andrews, D.F.Wood, *Mechanism of radon relase in rock matrices and entry in groundwater*, Trans.Inst.Min.Met., Vol.81, pp.197-209, 1972.

[20] K.Wattananikorm, *Soil gas radon as an earthquake precursor: some considerations on data improvement*, Rad.Measur., Vol.29,N.6, pp.593-5598, 1998.

[21] Qiuju Guo, Kainan Sun and Jianping Cheng, *Methodology study on evaluation of radon flux from soil in China*,Radiation Protection Dosimetry, 2004.

[22] V.Roca, A.Boiano, A.Esposito et al., *A monitor for continuous and remote control of radon level and enviromental parameters*, 14th Int Workshop on Room Temperature Semiconductor X and Gamma Ray Detectors, Rome, 2004.

[23] S.Agosteo, A.Foglio Para, *The use of silicon devices(diodes,ram,etc.) for alpha particle detection*, Environmental Radioactivity and Earth Sciences, Trieste, 1989.

[24] V.Dankelmann, A.Reineking, J.Porstendorfer *Determination of neutralization rates of* ^{218}Po *ions in air*, Radiation Protection Dosimetry, N.4, pp.353-357, 2001.

[25] K.D.Chu, P.K.Hopke, *Neutralization kinetics for Polonium-218*, Environmental Science and Technology, N.22, pp.711-717, 1988.

[26] J.Porstendorfer, P.Pagelkopf, M.Grundel, *Fraction of the positive 218Po and214Pb clusters in indoor air*, Radiation Protection Dosimetry, 113, N.3, pp. 342-351, 2005.

[27] S.D.Goldstein, P.K.Hopke, *Environmental neutralization of Polonium-218*, Environmental Science and Technology, N.19, pp.146-150, 1985.

[28] A.Busigin, A.Van Der Vooren, J.C.Babcock, C.R.Phillips, *The nature of unattached RaA(218Po) particles*, Health Phys., N.40, pp.333-343, 1981.

[29] B.Shi, P.K.Hopke, *Study of neutralization of 218Po ions by small ion recombination in O2,Ar and N2*, Health Physics, N.61, pp.209-214, 1991.

[30] M.J.Hawrynski , *The theory of clusters. In H. Stocker(ed.), Proc. Int. Conf. on Occupational Radiation and Safety in Mining*, Canadian Nuclear Assoc., Toronto, Canada, p.551.

[31] A.J.Howard, E.Carroll, W.P.Strange, *A simple system for radon in air concentration determinations*, American Journal of Physics, 59(6), 1991.

[32] H.M.Y.Leung, C.R.Phillips, *The electrical and diffusive properties of unattached* ^{218}Po *in argon gas*, Radiation Protection Dosimetry, N.18, pp.311, 1987.

[33] L.M.Chanin, M.A.Biondi, *Temperature dependence of ion mobility in helium, neon and argon*, Physical review, N.106, pp.473479, 1957.

[34] S.De Martino, C.Sabbarese, G.Monetti, *Radon emanation and exhalation rate from soils measured with an electrostatic collector*, Applied Radiation and Isotopes, N.49(4), pp.407-413, 1998.

[35] V.Roca, P.De Felice, A.M.Esposito, M.Pugliese, C.Sabbarese, J.Vaupotich, *The influence of environmental parameters in electrostatic cell radon monitor response*, Applied Radiation and Isotopes, N.61, pp.243-248, 2004.

[36] V.Roca, A.Boiano, A.DOnofrio, M.Pugliese, C.Sabbarese, G.Venoso, *A remote controlled system for continuous radon measurements to realize a monitoring network*, Second European IRPA Congress on Radiation Protection, France, 2006.

[37] G.Venoso, M.Pugliese, V.Roca, C.Sabbarese, *A radon facility at Naples University: Features and rst tests*, Applied Radiation and Isotopes, 67, pp.863866, 2009.

[38] P.De Felice, Xh.Myteberi, *The 222Rn reference measurement system developed at ENEA*, Nucl. Instr. and Meth., A 369, pp.445451, 1996.

[39] I.Kaplan, *Nuclear physics II*, Addison-Wesley, Japan, 1963.

[40] R.Buompane, V.Roca, C.Sabbarese, F.DeCicco, C.Mattone, M. Pugliese, M.Quarto, *Realization and characterization of a ^{220}Rn source for calibration purposes*, Applied Radiation and Isotopes, 81, pp.221225, 2013.

[41] M.C.Lpy e al., *Intercomparison of efficiency transfer software for gamma ray spectrometry*, Applied Radiation and Isotopes, Vol. 55, Issue 4, pp 493-503, 2001.

[42] T.Vidmar, *Efficiency transfer between extended sources*, Applied Radiation and Isotopes, Vol.68, Issue 12, pp.2352-2354, 2010.

[43] E.I.Shabana, K.S.Al-Mogabes, K.N.Al-Najem, M.A.Farouk, *Radioactivity in some gas-ow lantern mantles produced by different manufacturers*, Applied Radiation and Isotopes, 51(6), 609613,1999.

[44] DuPontTM, *Product Handbook for DuPont Tyvek*, 2002.

[45] DuPontTM, *DuPontTM Tyvek Users Manual*, 2004.

[46] P.Kotrappa, J.C.Dempsey, R.W.Ramsey, L.R.Stieff, *A practical E-PERM (Electrect passive environmental radon monitor) system for indoor 222Rn measurement*, Health Physics, 58, pp. 461-467, 1990.

[47] I.Bolognino, C.Cattaneo, E.Giroletti, G.Liguori and P.Salvini, *Background radioactivity in the scaler mode technique of the Argo-YBJ detector*, Astrophysics and Space Sciences Transactions, 7, pp.311-314, 2011.

[48] U.Marseglia, *Caratterizzazione di un'area sismo-vulcanica usando il radon, il toron ed i loro progenitori*, thesis in Physics, University of studies of Naples "FedericoII", 2012.

[49] L.Morawska, *Two ways of determining the ^{222}Rn emanation coefficient*, Health Physics, Vol.57, pp.481-483, 1989.

[50] S.De Martino, C.Sabbarese, *A method for emanation coefficient measurements of ^{222}Rn and ^{220}Rn from soils*, Phys.Chem.Earth, Vol.22, N. 1-2, pp.19-23, 1997.

[51] L.Morawska, C.R.Phillips, *Dependence of the radon emanation coefficient on radium distribution and internal structure of the material*, Geochimica et Cosmochimica Acta, Vol.57, pp.1783-1797, 1993.

[52] Due S.K. et al., *Influence of relative humidity on the charged fraction of decay products of radon and thoron*, Health Physics, Vol.45, pp.152-157, 1983.

[53] J.Kiko, *Detector for ^{222}Rn measurements in air at the $1mBq/m^3$ level*, Nuclear Instruments and Methods in Physics Research, section A 460, pp.272-277, 2001.

[54] E.Choi, M.Komori, K.Takahisa, N.Kudomi, K.kume, K.Hayashi, S.Yoshida, H.Ohsumi, H.Ejiri, T.Kishimoto, K.Matsuoka, S.Tasaka, *Higly sensitive radon monitor and radon emanation rates for detector components*, Nuclear Instruments and Methods in Physics Research, Section A 459, pp.177-181, 2001.

[55] J.L.Gutirrez, M.Garcia-Talavera, V.Pena, J.C.Nalda, M.Voytchev, R.Lopez, *Radon emanation measurements using silicon photodiode detectors*, Applied Radiation and Isotopes, N.60, pp.583-587, 2004.

[56] A.Martin-Martin, J.L.Gutirrez-Villanueva, J.M.Munoz, M.Garcia-Talavera, G.Adamiec, M.P.Iniguez, *Radon measurements with a PIN photodiode*, Applied Radiation and Isotopes, N.64, pp.1287-1290, 2006.

[57] D.Renker, E.Lorenz, *Advances in solid state photon detectors*, Journal of Instrumentation - J INSTRUM , Vol.4, N.04, 2009.

[58] C.Cigolini, F.Salierno, G.Gervino et al., *High-resolution radon monitoring and hydrodynamics at Mount Vesuvius*, Geophysical Research Letters, 28, pp.4035-4038, 2001.

[59] C.Cigolini, G.Gervino, R.Sonetti et al., *Tracking precursors and degassing by radon monitoring durino major eruptions at Stromboli volcano (Aeolian Islands, Italy)*, Geophysical Research Letters, 32, L12308, 2005.

[60] C.Cigolini, M.Laiolo, D.Coppola, *Earthquake-volcano interactions detected from radon degassing at Stromboli (Italy)*, Earth and Planetary Science Letters, 257, pp.511-525, 2007.

[61] F.De Cicco, R.Buompane, U.Marseglia, C.Mattone, M.Pugliese, M.Quarto, V.Roca, C.Sabbarese, F.Giudicepietro, W.De Cesare, I.Aquino, C.Del Gaudio, C.Ricco, *Methods for the characterization of a seismo-volcanic area using radon, thoron and their parents*, 11th international workshop on the geological aspects of radon risk mapping, Czech Republic, September 18nd 20th, 2012.

[62] U.Marseglia, *Caratterizzazione di un'area sismo-vulcanica usando il radon, il thoron ed i loro progenitori*, thesis, University of Studies of Naples "FedericoII", 2012.

[63] W.De Cesare, G.Scarpato, C.Buonocunto, A.Caputo, M.Capello, R.Avino, V.Roca, F.De Cicco, M.Pugliese, C.Sabbarese, F.Giudicepietro, *Installazione di una stazione per la rivelazione continua del radon mediante spettrometria alfa nella Solfatara di Pozzuoli*, Rapporti Tecnici INGV, 206, 2011.